ADDIS ABABA UNIVERSITY
ADDIS ABABA INSTITUTE OF TECHNOLOGY
SCHOOL MULTIDISCIPLINARY ENGINEERING
GRADUATE PROGRAM IN RAILWAY ENGINEERING

EFFECT OF AERODYNAMIC DRAG ON PERFORMANCE OF HIGH SPEED TRAIN

By

Solomon Asmamaw

A Research Thesis submitted to the School of Graduate Studies of Addis Ababa University in partial fulfillment of the requirements for the Degree of Masters of Science in Mechanical Engineering

(Railway Engineering Stream)

Advisor

Dr.-Ing. Demiss Alemu

SCHOOL OF MULTIDISCIPLINARY ENGINEERING

ADDIS ABABA UNIVERSITY

September 7, 2016

DECLARATION

I hereby declare that the work which is being presented in this thesis entitled **''Effect of Aerodynamic Drag on Performance of High Speed Train**" is my original work, has not been presented for a degree in this or other universities. All sources of materials used for this thesis work have been fully acknowledged.

Name: Solomon Asmamaw Signature: _____

Place: Addis Ababa Institute of Technology, Addis Ababa University, Addis Ababa, Ethiopia
Date of Submission: _____

This thesis has been submitted for examination with my approval as a university advisor.

Advisor's Name: Dr.–Ing. Demiss Alemu Signature: _____

Solomon Asmamaw

Addis Ababa

Sept/2016

Addis Ababa Institute of Technology

School of Graduated Studies

Postgraduate Program in Railway Engineering

Addis Ababa University

Effect of Aerodynamic Drag on Performance of High Speed Train

By

Solomon Asmamaw

Approved by Board of Examiners

Dr. Birhanu Beshah	_____	_____
Railway Center Head	Signature	Date
Dr.–Ing. Demiss Alemu	_____	_____
Advisor	Signature	Date
Dr. Yilma Tadesse	_____	_____
Internal Examiner	Signature	Date
Dr. Abdukadir Aman	_____	_____
External Examiner	Signature	Date

DEDICATION

To GOD for his immeasurable mercy, support, encouragement, being hope to me, and patience for my sinfulness!

ACKNOWLEDGMENT

I acknowledge with gratitude, honor, and humanity to Dr.-Ing. Demiss Alemu, for his valuable guidance, proper advice, constant encouragement for choosing reliable research title, developing formal research paper, and his help to bring this present work to this level, also for his excellency willingness for supervision from the start of the proposal of this research thesis.

Secondly I would like to thank AAiT University and all staffs of School of Mechanical and Industrial Engineering for their great support in completing the courses and doing this thesis.

Next I would like to thank Ethiopian Railway Corporation (ERC) for their appreciable financial and technical support.

Also I need to give special thank for AAiT lab stuffs and ERC Center of Excellence staffs for their permission to use the computer lab as a special case.

Then I would like to thank all of my friends for their encouragement, support, and cooperation with different materials and ideas.

Lastly but not the least I would like to thank all of my family for their encouragement, support, and patience.

ABSTRACT

The aerodynamic drag resistance is the main constraint on the performance of high speed rolling stock technology. Its effect increases as speed of train increases and with poor aerodynamic body shape design of high speed train body. Problems such as passenger discomfort, safety conditions reduction, environment disturbance, and more traction power consumptions are main effects of aerodynamic drag resistance. This thesis investigates the effect of aerodynamic drag resistance of passenger rolling stock of two high speed train models with leading car, middle coach, and tail car. The first train model is existing European ICE-2 Regional Train and the second modified train model is called Ehio-HST-250+. The aerodynamic investigation is done using CATIA V5R20 modeling software and ANSYS-Fluent V 17.0 Computational Fluid Dynamics (CFD) simulation software. The numerical method used on Fluent solver is viscous-incompressible steady state Reynolds Average Navier-Stock (RANS) and two equation turbulence model of Realizable k - ε model (RKE) with Non-equilibrium wall function (NWF) of near wall treatment for the simulation of the system in an open air condition. The input data to the CFD software are collected from relevant literatures with consideration of Ethiopian average air temperature of 25°C for input air property variables. The study does not include passenger discomfort, safety conditions (cross wind, tunnel test etc.), pantograph component, and vibration of the vehicle as time and computing material quality limits. Thus using steady RANS CFD method in open air condition, reduction of coefficient of aerodynamic drag percentage amount of 49.01% of enormous aerodynamic drag is reduced and 636.13 kW traction power is saved. This can increase the safe and comfort environment of the system.

Key words: ANSYS-Fluent V 17.0, CATIA V5R20, Computational Fluid Dynamics (CFD), Inter City Express (ICE-2 Train), Reynolds Average Navior-Stock (RANS), Realizable $k - \varepsilon$ model (RKE), Non-equilibrium wall function (NWF).

TABLE OF CONTENTS

DECLARATION I
DEDICATION III
ACKNOWLEDGMENT IV
ABSTRACT V
TABLE OF CONTENTS VI
LIST OF FIGURES VIII
LIST OF TABLES XI
NOMENCLATURES XII
1. CHAPTER ONE: INTRODUCTION 1
1.1 Background of the Study 1
1.2 Statement of the Problem 5
1.3 Basic Research Questions 6
1.4 Hypothesis on the Research 7
1.5 Research Objective 7
1.6 Delimitation and Limitation of the Study 8
1.7 Significance of the Study 10
1.8 Organization of the Research 11
2. CHAPTER TWO: LITERATURE REVIEW 12
2.1 Analysis Methods of Aerodynamic Drag on High-Speed Trains 12
2.2 Analysis Techniques for Aerodynamic Drag on High-Speed Trains 15
2.3 Literatures of Similar Method and Techniques 16
2.4 Formation Mechanism of Train Aerodynamic Drag 23
3. CHAPTER THREE: RESEARCH METHODOLOGY 31
3.1 Research Design Procedure 31
3.2 Method of Analysis (Data Analysis and Interpretation) 31
3.3 ANSYS Fluent setup 43
3.4 Solution Accuracy 49
4. CHAPTER FOUR: RESULT AND DISCUSSION 50
4.1 Results 50
4.2 Discussions 79

5. CHAPTER FIVE: CONCLUSION, RECOMMENDATION, AND FUTURE WORK INDICATIONS 81
5.1 Conclusions 81
5.2 Recommendations 81
5.3 Future Works Indications 82
Reference 83
Appendix 92

LIST OF FIGURES

Figure 1: Research conceptual framework. 11
Figure 2: Experimental analysis photograph [6].....12
Figure 3: CFD computation of flow over ICE-2 train [80].....13
Figure 4: Coordinate definition of train [89]. 24
Figure 5: Pressure contours of fore-body and after-body of train: (a) Fore-body of train; (b) After-body of train [89]. 27
Figure 6: Flow structures in wake of after-body of different shape train: (a) Wake of bluff body train; (b) Wake of streamline shape head train [89]. 28
Figure 7: Procedures for Research Design. 31
Figure 8: 2D of ICE-2 Regional train. 33
Figure 9: 2D of Ethio-HST-250+ train. 33
Figure 10: 3D of ICE-2 Regional train: (a) CATIA right side view, (b) under body with rectangular nose view, (c) common simplified bogie [45]. 34
Figure 11: 3D of Ethio-HST-250+ train: (a) CATIA right side view, (b) bottom, underbody with elliptical nose view. 34
Figure 12: Front view of (a) ICE-2 train and (b) Ethio-HST train. 34
Figure 13: Some geometric consideration for HST modeling [69]. 36
Figure 14: Aerodynamic drag on ICE (the hatching area is the device to smooth the structures underneath train; the right side shows aerodynamic drag components of ICE) [79].....36
Figure 15: Comparison of common numerical viscid Methods [8], [69]. 37
Figure 16: Turbulence Models Available in FLUENT (ANSYS, Inc. Release 13.0). 37
Figure 17: Computational domain of the flow field [84], [102], [103]. 43
Figure 18: Computational symmetric air domain of the flow field. 44
Figure 19: Computational full air domain of the flow field. 44
Figure 20: ICE-2 Regional mesh view. 45
Figure 21: Ethio-HST mesh view. 45
Figure 22: Computational Air domain mesh with colored of symmetry walls and velocity inlet. 48
Figure 23: Computational Air domain mesh with colored of symmetry, rail-road walls, train model, and pressure outlet. 49
Figure 24: Scale residuals convergence of ICE-2 Train. 50

Figure 25: Scale residuals convergence of Ethio-HST Train. 51
Figure 26: Coefficient of drag force convergence history of ICE-2 Regional Train. 52
Figure 27: Coefficient of drag force convergence history of Ethio-HST Train. 52
Figure 28: Coefficient of lift force convergence history of ICE-2 Regional Train. 53
Figure 29: Coefficient of lift force convergence history of Ethio-HST Train. 53
Figure 30: Coefficient of moment convergence history of ICE-2 Regional Train. 54
Figure 31: Coefficient of moment convergence history of Ethio-HST Train. 54
Figure 32: Pressure coefficient plot of ICE-2 Train model. 55
Figure 33: Pressure coefficient plot of Ethio-HST Train model. 56
Figure 34: ICE-2 Regional Train Velocity Magnitude Vector Profile (m/s). 57
Figure 35: ICE-2 Regional Nose Region Velocity Magnitude Vector Profile (m/s). 57
Figure 36: ICE-2 Regional Wake Region Velocity Magnitude Vector Profile (m/s). 58
Figure 37: Ethio-HST-250+ Train Velocity Magnitude Vector Profile (m/s). 58
Figure 38: Ethio-HST-250+ Train Nose Region Velocity Magnitude Vector Profile (m/s). .59
Figure 39: Ethio-HST-250+ Train Wake Region Velocity Magnitude Vector Profile (m/s). 59
Figure 40: ICE-2 Regional Train Velocity Magnitude Contour Profile (m/s). 60
Figure 41: ICE-2 Regional Nose Region Velocity Magnitude Contour Profile (m/s). 60
Figure 42: ICE-2 Regional Wake Region Velocity Magnitude Contour Profile (m/s). 61
Figure 43: Ethio-HST-250+ Train Velocity Magnitude Contour Profile (m/s). 61
Figure 44: Ethio-HST-250+ Train Nose Region Velocity Magnitude Contour Profile (m/s). 62
Figure 45: Ethio-HST-250+ Train Wake Region Velocity Magnitude Contour Profile (m/s). 62
Figure 46: ICE-2 Regional Train Static Pressure Contour (Pascal). 63
Figure 47: ICE-2 Regional Train Nose Region Static Pressure Contour (Pascal). 63
Figure 48: ICE-2 Regional Train Wake Region Static Pressure Contour (Pascal). 64
Figure 49: Ethio-HST-250+ Train Static Pressure Contour (Pascal). 64
Figure 50: Ethio-HST-250+ Train Nose Region Static Pressure Contour (Pascal). 65
Figure 51: Ethio-HST-250+ Train Wake Region Static Pressure Contour (Pascal). 65
Figure 52: The relationship between air flow direction and drag resistance. 69
Figure 53: The turbulent boundary layer. 71
Figure 54: Coefficient of drag force convergence history of ICE-2 Regional Train. 92
Figure 55: Coefficient of drag force convergence history of Ethio-HST Train. 92
Figure 56: Coefficient of lift force convergence history of ICE-2 Regional Train. 93

Figure 57: Coefficient of lift force convergence history of Ethio-HST Train. 93
Figure 58: Coefficient of moment convergence history of ICE-2 Regional Train. 94
Figure 59: Coefficient of moment convergence history of Ethio-HST Train. 94
Figure 60: Key Dimension of ICE-2 model shown in mm (scale: 1/25) [28]. 95
Figure 61: ICE-2 Regional Train real Photograph of an ICE2 train [28], [48]. 96
Figure 62: The improved geometry of under body [46]. 96
Figure 63: The underbelly of the ICE 3 CAD-model [46]. 97
Figure 64: Side view of underbelly of the ICE 3 CAD-model [46]. 97
Figure 65: Rocket head and Sword tail profiles [95]. 98
Figure 66: Improved CRH with new structured headstock and tailstock [91]. 98
Figure 67: Train with bogie fairings [63]. 98
Figure 68: Use of spoiler underbody [70]. 98

LIST OF TABLES

Table 1: Typical drag and friction coefficients for trains [81]. 16
Table 2: Suggested length of streamline shape head at different velocities [89]. 18
Table 3: Dimensional comparisons of ICE-2 Regional and the new model (Ethio-HST-250+). 35
Table 4: Mesh Information (Report) for ICE-2 Regional and for Ethio-HST-250+. 45
Table 5: Domain Physics for ICE 2 Regional and for Ethio HST 250. 47
Table 6: Boundary Physics for ICE 2 Regional and for Ethio HST 250. 47
Table 7: Summary of drag, lift, and moment values. 67
Table 8: Comparisons of parametric values between half (symmetric) and full reference area. 73
Table 9: Summary of the aerodynamic parameters comparison. 80
Table 10: Distribution of aerodynamic forces of the CRH380A train [102]. 99
Table 11: Total aerodynamic drag coefficient of TGV running at 260 km/h [79]. 99

NOMENCLATURES

SYMBOLS

A	Reference Area, Projected Area
a, b, c	Constants determined by the experiment
$a+bv_t$	Mechanical drag
a_{RTL} and b_{RTL}	Coefficients related to the drag of the leading car and the length of the streamline shape
a_{RWL}, b_{RWL}, c_{RWL}	Coefficients related to the drag of the tail car and the length of the streamline shape
c	Speed of Sound
C_L	Coefficient of Lift
C_D	Coefficient of Drag
C_M	Coefficient of Moment
C_p	Coefficient of Pressure
C_q	Specific Heat Capacity
cv_t^2	Aerodynamic drag
C_x	Coefficient of aerodynamic drag
C_{xt}	Drag coefficient of the leading car or locomotive
C_{xw}	Drag of the tail car
$C_{xz}(i)$	Friction coefficient along the train
F_D, F_x	Total Aerodynamic Drag Force
F_L	Lift Force
F_{px}	Pressure Drag

F_R	Total Drag
$F_{\tau x}$	Friction Drag
F_{xt}	Drag of the leading car or locomotive
F_{xw}	Drag of the tail car
$F_{xz}(i)$	Friction along the train
g	Gravity Constant
k-ε	Reynolds stress models in two turbulent parameters to simulate and read turbulent flow
k	Coefficient of Thermal Conductivity
k	Turbulent kinetic energy
L	Characteristics Length
L_d	Length of the streamline shape
M	Moment
Ma	Mach number
p	Pressure
P	Power
P_{bx}	Skin pressure of the train along x axis
q	Dynamic pressure
Re	Reynolds number
Re_x	Reynolds number along a position x
S_F	Area of the train wall surface
S_x	Cross-sectional area of train
t	Time
T	Temperature

U	Train velocity
v_t	Train velocity relative to the ground
ε	Turbulent energy dissipation rate
ρ	Density
τ	Shear Stress
τ_{ix}	Shear stress on the train along *x* axis
μ	Dynamic viscosity
ϑ	Static Viscosity
Φ	Viscose Dissipation

ABBREVIATIONS

AAiT	Addis Ababa Institute of Technology
CFD	Computational Fluid Dynamics
DES	Detached Eddy Simulation
DLES	Dynamic LES
DNS	Direct Numerical Simulation
ERC	Ethiopian Railway Corporation
Ethio-HST-250+	Ethiopian high speed train 250+ (running speed)
ETMT	Evacuated Tube Maglev Trains
ETSC	European Transport Safety Council
EVM	Eddy-Viscosity Models
FEM	Finite Element Method
HST	High Speed Train
ICE	Inter City Express

LBM	Lattice Boltzmann Method
LES	Large Eddy Simulations
NKS	Newton–Krylov–Schwarz
NLAS	Nonlinear Acoustics Solver
NWF	Non-equilibrium wall function
RANS	Reynolds-Averaged Navier-Stokes
RKE	Realizable k - ε model
TGV	Train a Grande Vitesse
UIC	International Union of Railways
URANS	Unsteady Reynolds-Averaged Navier-Stokes

1. CHAPTER ONE: INTRODUCTION

1.1 Background of the Study

Effect of drag force on performance of high speed train is too much valuable. The drag force is a force which resists the forward movement of a body. In railway engineering or rolling stock engineering, this type of phenomenon will be appeared due to forward motion of the rolling stock by its traction force, while drag or reaction force of wind begins to resist this forward motion. Drag can be divided in to static, friction (mechanical dynamics), and aerodynamic (air pressure) types [62], [89]. The concern of this study is on aerodynamic drag reduction scenarios.

The resistance of drag force is the opposition of pressurized air block or wind against the moving high speed rolling stock which tries to stop the motion of the train. The streamlined aerodynamic shape (having a shape which reduces the drag from air moving past) of the rolling stock is major solution of keeping the aerodynamic drag resistance to the minimal level of drag force as much as possible. Because of this concept, it is difficult to let low speed trains run as high speed trains as their aerodynamic (streamlined) shape design do not offer them to run at high speed.

There are other parameters which have greater value than aerodynamic shape for conventional and freight trains. While improving the aerodynamic shape of the train, there may be negative effect on overall load capacity of the rolling stock. Thus, low speed trains are more concerned on body strength with relative to weight reduction and their need of high volumetric capacity to load passengers and freight.

High speed trains are the most aerodynamically concerned type of rolling stock technology which are given exceptional attention regards to streamlined body shape. Their performance is measured due to several parameters such as aerodynamics shape, brake system, suspensions systems, train speed, overall weight, steering system, etc. to get overall efficient performance of the train, these systems should be very efficient enough. Due to the improvement of the aerodynamics shape, train performance can be enhanced by increasing speed and stability of moving high speed train within mind of saved traction power.

Mostly, from the aerodynamic point of view, studies should be on the nose of the locomotive with somewhat less consideration of the remaining part of the rolling stock. This is even done

with no consideration of parts except the nose of the locomotive for computation cost effectiveness. Thus the favor of cost reduction of the study on the locomotive especially on its nose is effective design approximation. But the study of the whole rolling stock of aerodynamic profile, makes the study to approaches to ideal form and will give higher value of worth on simulation accuracy.

The need of study on this topic is needed because of the engineering concept known as optimization. While optimizing of major parameters, designers can vary the efficiency of aerodynamics of the train to get maximum overall efficiency or maximum performance.

Studies have done concerned on aerodynamic drag resistance, until know there is no tip on ideal aerodynamic shape of existing high speed rolling stock technology. It is possible to get required multiple sets of result by varying parameters depending on the major concern of the designer.

The study is going on through considering the Ethiopian weather (concerning on air property for given temperature value) and improving the body shape profile of high speed train with other remaining parameters on ANSYS left default as the existing rail is not designed for high speed trains. Also the existing train itself is low speed of conventional type with maximum speed of passenger train is 160 km/hr. This will limit the study parameters being less constrained or rigid with regarding Ethiopian condition especially with topographic parameters (e.g., rail gradient) with respect to train speed (of high speed train level).

The study has its own part on technology transfer between leading world and Ethiopians in case of CFD study of high speed train aerodynamics. The study tries to implement the high speed trains parameter on Ethiopians special nature based on air property which is related with the effect of aerodynamic drag force which governs the performance of high speed trains in general.

With the increase of the train speed, aerodynamics has become an important key in the rail vehicles field. The study of the aerodynamics of a train can lead to substantial cost savings and more environmental friendly trains. The most studied phenomenon in the realization of a train is the drag generated by the displacement of the train in the air flow. Reducing the drag leads to a reduction of the amount of energy needed. But some others aerodynamic phenomena are of interests, such as the pressure variations while the train is driving in a tunnel, the study of the consequences of a crosswind, the study of the train rollover or the slipstream. A short overview of different aerodynamic phenomena is given below.

When a train runs, a strong head pressure pulse is created at the very front of the train which leads to a change of pressure in the surrounding. A low pressure bubble is also created at the rear part of the train but is less strong than the first one, and is mostly a problem for people or objects standing near to the track.

The pantograph is situated in an area where the flow conditions change a lot. In order to avoid unauthorized large variations of the contact surface it is important that the flow around the pantograph is not too turbulent, which can be enabled by adding some so called fairings.

While entering a tunnel the air at the train nose is compressed this creates an overpressure wave that migrates at the speed of sound. When this wave reaches the end of the tunnel a part of the wave is reflected and goes back as an under-pressure wave. As the train tail enters the tunnel an under pressure wave is created and migrates to the end of the tunnel. The pressure variation is maximum when an under pressure wave meets a reflected overpressure wave. The pressure difference reaches then a peak value. This mostly causes discomfort for the passenger since he/she is subject to a high pressure difference in a short time, for example the legislation in Sweden is 1500 Pa in 4 seconds [33].

The bogies movement is restricted to the tracks. A suspension system connects the train body to the bogies. The trains can then roll, yaw and pitch. A yawing moment can increase in strong crosswinds. This can be very dangerous in case of strong crosswind and particular yaw angle and can lead to overturning.

Aerodynamic noise comes from the pressure fluctuations that occur in the turbulent boundary layer and as the flow separates. Vortices produce also a lot of aerodynamic noise (von Karman vortex during flow separation). It is therefore important to have attached flow since the separation of the boundary layer creates a lot of noise. One can say that the power of external aerodynamic noise grows with about the sixth power [62].

Much energy is lost when overcoming the air drag, and since the drag has a greater impact at higher speeds more research has been performed to reduce the air drag on high-speed trains than on low-speed trains. The high-speed trains therefore usually should have a streamlined design, but the regional and freight-trains used in today are relatively old type and do not have an appropriate aerodynamic design like ICE-2 Regional needs to be aerodynamically improved with respect to its operating speed (250+ m/s). By making some changes in the train effective parts of the geometry, a large drag reduction could be achieved in consideration of train loading capacity and manufacturing coast.

1.1.1 Motivations and Previous Research

External aerodynamics is becoming an important field of study in recent years. This is because of its effectiveness in the study visibility of comfort, stability, and overall performance of the train [62]. Many aerodynamics researches have been done internationally, but in Ethiopia no visible research is done under railway engineering of high speed train trend. About three students has worked on conventional train aerodynamics. The International Union of Railways (UIC) defines that the speed of a high-speed train must be at least 200 km/h for upgraded track and 250 km/h for new track [33], [62]. This condition lets the researcher to study the aerodynamics on high speed train among preliminary researchers in the country.

The increase of energy demand has become inappropriate with available energy source. To decrease the energy usage caused by aerodynamic drag, the improvement of train body profile is essential. By appropriate improvement of vehicles body, it is possible to save 50% of fuel consumption [27], [43].

Many researches have done in different approximation on model designing and numerical method for CFD simulation in different parts of the train. These things make difference on this research from the others. Additionally, it is limited only on open air condition of computational air domain for CFD simulation.

1.1.2 History on Vehicle Aerodynamics and High Speed Trains

As referenced by Mamo N. [62], Studies on aerodynamics have originated from aeronautics and marine applications. At the turn of World War Two, substantial progress on aircraft aerodynamics was obtained due to the amount of research and analysis being done. Study of vehicle aerodynamics first began to surface during the earlier part of the 20th century and has continued up until the present day. During the earlier part of the 20th century, vehicle aerodynamics study is being associated with vehicle performance rather than for vehicle beauties (aesthetics) only. Aerodynamicists during that time carried out vehicle aerodynamics research with an aim to produce vehicles that can achieve a high speed to power ratio. To achieve high vehicle performance, much of the attention focuses on lowering the vehicle drag coefficient (C_D), which accounted to about 75 to 80% of total motion resistance at 100 km/h. However, in the later part of the 20th century, during the oil crisis of 1973-1974, the focus on vehicle aerodynamics study shifted towards lowering the drag coefficient in order to produce vehicles with better fuel economy. The trend shifted again in the early 1990's especially in North America where a low fuel price coupled with the increased popularity of light trucks and

sport-utility vehicles have of which drag coefficient of around 0.45 have reduced the importance the need on research to reduce drag coefficient. Aerodynamicists then shifted their focus towards designing vehicle that provides maximum comfort to its occupants. Vehicle comfort consists of fine-tuning areas such as ventilation, heating, air conditioning and minimizing wind noise inside the vehicle [62].

1.2 Statement of the Problem

Now days, the technology of railway engineering is getting higher and higher, thus it can be competent with airplane transportation by speed and even better on safety conditions [60]. This can be strengthening by the technology of high speed trains up to in vacuum medium despite its disadvantage of abnormal conditions and behavior of passengers' discomfort like annoyance, stir, nausea, vomiting and other similar uncontrolled and urgent abnormality characteristics while in this type of transportation. Similar thing for growth of this technology is magnetic levitation traction system which is capable of train speed to consider as flight state. The annoying conditions and environments described above are common phenomenon in high speed transportation mediums even via airplane.

With consideration of the above problems, the importance of high speed trains technology is undeniable for existing complex world to cover daily tasks timely. But, extreme high speed trains are not fully important not only for the above problem but also for the whole traffic system. As the speed increases the degree of danger of life loss in terms of hazard phenomenon will be magnified. This is because of more uncontrolled and severe behavior of high speed trains while braking and easy to danger for cross wind effects. Other characteristic is when the derailment phenomenon is appeared. It is also difficult to control easily before the whole thing is crashed and goon.

From the above conditions this study is not going further in to extreme high speed scenarios. But goes to on popular or standard high speed level as described on UIC, it is possible to increase the train traction force while reducing drag force with constant traction power in common railway technology rail system. The profile or shape of the whole rolling stock especially the nose or front part of the locomotive leads to the achievement of better high speed. This re-profiling (making streamlined shape with other techniques) of nose or the whole parts of the train is not much expensive than the above two major study areas of high speed train technologies (i.e., on vacuum and maglev). The speed can upgrade valuably in common rail by extensive aerodynamic shape improvement and traction power.

The best design on aerodynamic of the rolling stock, the better will be the optimization or reduction of traction power which dissipated to overcome the aerodynamic drag force of resistance to forward force of motion.

While enhancing train speed and traction power the aerodynamic shape helps to the rolling stock system valuably or incredibly much lees noisy, vibration, and passenger discomfort because of the flood of relative high speed of wind with respect to the train speed is streamlined. The smoothness of aerodynamic shape leads to treat the symptoms of annoyance, stir, and nausea phenomenon in rolling stock transportation. Better aerodynamic shape not only increases the speed of the train with constant traction power but also it enhances health from urgent abnormality of passengers caused from severe conditions of high speed trains. This implies that, despite the reduction of train speed, when aerodynamically poor designed high speed trains are left to run, the extreme conditions such as vibration, noise, and health abnormality will be dominated.

The above things are beyond enough to study on this area with variation of parameters even though it may be studied via many scholars. They may have been studied more accurately, not to make amplifying as they are scholars and source of technologies. But most of researchers' study on their own living area, as it is more appropriate and correct to concern their living area. This is because of the unique behavior of defined area of place in terms of such as environmental parameters for accurate result. These reasons lead the researcher to try to approach to Ethiopian conditions as much as possible to get better accuracy from scholars who studies on their living area despite the knowledge of how to study comes from them.

Finally, the research helps ERC and the country to test the CFD aerodynamic performance of the future high speed rolling stock only using computer and the required train model without any other cost to examine if the required amount of aerodynamic drag and available traction power is economical to buy from particular company of a branded train manufacturer or even to manufacture by its own capacity. Also helps to select the train from manufacturers with required performance and efficiency of the train as the need of the country.

1.3 Basic Research Questions

There are lots of questions according to this study area, but for the sake of indicating the areas where to be solved by this study which reduces the performance of high speed technology, it is essential to list major questions which must be answered directly or indirectly by this study.

- ✓ How much is the effect of aerodynamic drag on the performance (in terms of traction power reduction) of high speed trains for given parameters?
- ✓ How can achieve better aerodynamics shape (streamlined shape with other techniques) that can be used to reduce aerodynamic drag resistance for given parameters and reduce co-existing severe conditions which lead to less passenger comfort (noise, urgent health annoyance), vibration and safety conditions?

1.4 Hypothesis on the Research

Aerodynamic drag resistance is oppositely or indirectly proportional with aerodynamic body shape and traction power of the train. But it is directly proportional with train speed passenger discomfort, wind noise, and vibration etc. The effect of drag resistance on dissipation of traction power will be analyzed in terms of increasing traction force while reducing the aerodynamic drag force with constant traction power. In other terms if forward force or speed is increased by only improving the aerodynamic shape of the train nose and the whole effective parts of rolling stock, this implies that the drag resistance decreased and the traction power used to overcome this resistance is converted to forward traction force in addition to the previous forward traction force magnitude which have been used before shape optimization. If someone wants to save this form of traction power, it is possible to reduce the power which was used to overcome the drag resistance of air with maintained previous speed.

1.5 Research Objective

The objective is the main task which must be done throughout the completion of the research thesis session. Study the effect of aerodynamic drag resistance on the performance of two high speed train models using CATIA V5R20 modeling-software and commercial CFD simulation-software (ANSYS-FLUENT V17.0) with steady RANS numerical method at running speed of 250km/h. Using this cost effective CFD method, this can indicate for ERC to test before manufacturing by itself or selecting future High speed project trains from manufacturers which have less power consumption plus other benefits.

1.5.1 Specific objectives

- ✓ The effect of aerodynamic drag resistance in open air without crosswind, tunnel, and other effects (because of time and computer quality shortage) will be studied with the help of modeling and CFD simulation software and this able the study to figure out the magnitude of the aerodynamic drag on the reduction of longitudinal forward speed of the rolling stock or in general traction power.

- ✓ Estimate or discuss the saved traction power (in terms of speed, and forward force increment or reduced aerodynamic drag percentage). It is possible to reduce the power which was used to overcome the drag resistance of air with maintained previous speed.
- ✓ The study will show difference between existing model or ICE-2 German Regional train and the aerodynamically designed improved shape of high speed train (named as: Ethio-HST). This will magnify the aerodynamic drag magnitude difference of these two different train models.
- ✓ The 3D body profile of both ICE-2 Regional train and improved train will be modeled on CATIA V5R20 software and simulated on ANSYS Fluent V17.0 software. The implementation of steady incompressible RANS model, RKE turbulence two equations model, and NWF wall treatment for CFD numerical method under fluent solver.

1.6 Delimitation and Limitation of the Study

1.6.1 Delimitation of the Study

The territory or the scope of this thesis is to cover the major challenge of aerodynamic drag resistance on the performance or efficiency of trains with high speed range types. But, the nonexistence of high speed project in the country will give freedom of judgment for the researcher to give optimal assumption for the required parameters.

Initially the CFD examination of the aerodynamic drag performance of ICE-2 Regional train (maximum operating speed 280 km/h) which has similar to rectangular shape of train profile and considered as less aerodynamic shape of high speed train. Using commercial CFD-software (ANSYS-FLUENT V17.0) with the operating speed of the train of 250km/h and the simulation of open air will be taking place. The modeling of two locomotives and a single middle coach/wagon by CATA V5R20 is used for the researcher preference. Then the researcher designs and simulates another train model of high speed passenger train aerodynamics and simulate in the same way. Then the researcher decides how to do by comparing the aerodynamic drag value of the two different train body profile after simulation.

The better aerodynamics shape the less drag force as there is no ideal aerodynamic shape which leads to absolute smooth flow of air and results absolute zero drag resistance. But it is possible to design aerodynamics shape body repeatedly which leads to more less drag force resistance as the need of the designer with consideration of other parameters such as volumetric capacity of train body which holds train equipment and passengers and other parameters. So the study will show aerodynamic drag magnitude difference between rectangular train (ICE-2 Regional

train) and more aerodynamically improved body shape of a train model in open air condition with selected numerical method.

Severe conditions which leads to passenger discomfort caused by poor aerodynamic shape are vanished together with aerodynamic drag resistance (caused by impact of train body with wind). The reduction in aerodynamic drag resistance while increasing traction force shows the reduction of passenger discomfort and another similar phenomenon. Thus there will not be any analysis for severe condition except the aerodynamic drag magnitude. But, the reduction of serveries is directly related with aerodynamic drag magnitude reduction and it is obvious. The only justification to their reduction is on the hand of aerodynamic drag reduction for this research.

The only visible method in this thesis is, showing reduction in drag resistance and suggests the reduction in severe conditions. Because the main concern of the study is to investigate the effect of drag resistance towards high speed trains in terms of power maintain through reduced aerodynamic drag percentage. Other results of aerodynamics effects are optional except the aerodynamic drag resistance parameters which are the target task and goal of the study.

1.6.2 Limitation of the Study

To study all challenges of aerodynamic effects of drag resistance on high speed trains performance, it needs more time and research material. Thus the overall performance is not being covered all in all under this thesis. Because some topics like vibration of train components, passenger discomfort, noise, and other similar topics are not covered under this methodology part as they broad the study within the given period of time. Thus, only aerodynamic drag resistance reduction will be analyzed. Other effects such as passenger discomfort (acoustic noise, vibration, symptoms of annoyance, stir, and nausea phenomenon), vibration of train, and others will be commented and discussed as these things are correlated in terms of one time (synchronously existence) phenomenon but are indirect relationship type with aerodynamic drag force. So their effect will be justified in terms of the effect of aerodynamic drag resistance as it is the only burden to this thesis.

The other thing which will not cover under this study is the static and dynamic friction drag of mechanical components of the rolling stock. Also the researcher does not cover the safety conditions such as cross wind (maximum effect of perpendicular direction of wind to the train motion) and train passing through tunnel aerodynamics effects and other basic safety concerns. Transient state condition of the flow will not cover (only studied by steady state condition) on

this study. Despite the recommendations of transient condition for high speed train, the method is still valuable as cross wind is not considered. But the steady state condition is the CFD flow analysis method to simplify the study with cost effective result. All these things are coming from the scared of time and computation materials limitation.

1.7 Significance of the Study

This topic deals with the issues of reliability and validity of the study. The study of aerodynamic drag resistance may seem to be luxury when compared to other main train systems such as braking system, steering system, and suspension systems etc. which may lead to the loss of whole system. Even though despite its enormous list of functions, even someone may think work with this topic is a worthless compared to its gain. To give attention to this topic the following major values may be arise as function of this study for the purpose of visualization of the use the issued topic.

Traction power is the energy source of the whole rolling stock system. To extract minimal of power from the power source of rolling stock, some of designers thought the reduction of overall weight may be the only key to save loss of traction power. It is real and the most effective way to gain excess power from the initial power input when reasonable overall weight optimization is done. In similar sense the drag resistance is the force component which has similar effect with train weight in terms of power reduction. Thus when the aerodynamic drag is reduced, the traction power will be gained. Too much reduction of overall train weight may lead to the use of less strong, tough, and harder material. This may decrease the overall performance and life time of the train. Another reason is as the train weight gets lighter and the train speed gets higher, the lift force increases, then the danger of derailment and over through of the train gets higher with the existence of cross wind effect. To remove this scare, someone needs to design optimal weight of train and implement best aerodynamic shape for the train, thus traction power can be saved without any drawback with consideration of volumetric capacity of the train. The aerodynamic drag of a road vehicle is responsible for a large part of the vehicle's fuel consumption and it can contribute to as much as 50% of the total vehicle fuel consumption at highway speeds [27], [43].

While reducing the drag force, caused by better aerodynamic shape of significant surfaces of train body, severe conditions which is most connected with passengers' health and was written several times under previous topics repeatedly will be gets vanished.

This also can help to lengthen the life time of rolling stock body within (if the designer needs to include) reasonable and optimal soft and light weight material type to improve high speed train performance, then the cause of continual impact and stress of air block with train body surface profile especially at frontal areas will be too much diminished with the drag resistance. This worthiness is not relevant only for high speeds trains but also have countable effect on conventional (low speed trains). The criticalness of this effect increases as train speed increases with given aerodynamic shape and traction power.

The better the aerodynamics shape the better the aesthetics view also being achieved. Most of high speed train designs are attractive caused by higher order of aerodynamic shape modifying techniques with large streamlined head.

Under train modeling, the train body of the improved model (Ethio-HST) is more cylindrical than the ICE-2 train model, with this shape the cross wind effect is expected to be reduced for the improved train.

1.8 Organization of the Research

The organization the research is based on chronological sequence of the study. In general, the procedures used for completion of this research will be depicted on the following figure. The flow of the research organization being logical order is indication of its scientific procedure. The major processes which will be done progressively are described as follows:

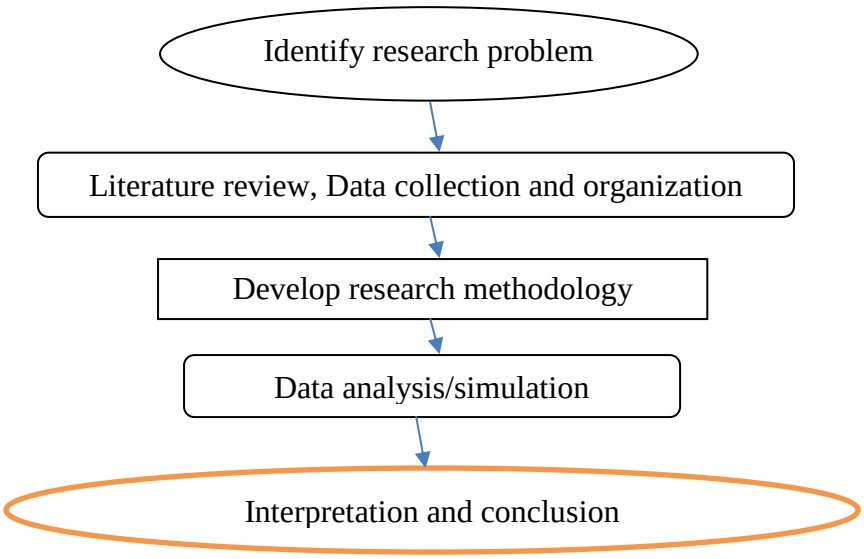

Figure 1: Research conceptual framework.

2. CHAPTER TWO: LITERATURE REVIEW

2.1 Analysis Methods of Aerodynamic Drag on High-Speed Trains

Researchers are using many methods to study aerodynamic effect on their train model. There are two major divisions to study the aerodynamic effects. These experimental and numerical methods as described below.

2.1.1 Experimental Analysis Method

This type of analysis is proceeding with the real body test and environment condition (but the size may be mostly reduced for large bodies and sometimes enlarged for small bodies if necessary). Measuring devices are used to know the value of the required parameter.

Figure 2: Experimental analysis photograph [6].

As shown on the above picture this type of analysis is the most real and accurate. Because all things are real except if size scale (i.e., not full scale) is used.

2.1.2 Numerical Analysis Method

This type of analysis as the name indicates the analysis of the real world using numerals and formulas. This method approximates the solution by using several formula approximation methods. Based on their approximation and accuracy, list of some methods using software of CFD method in general are given below as an example.

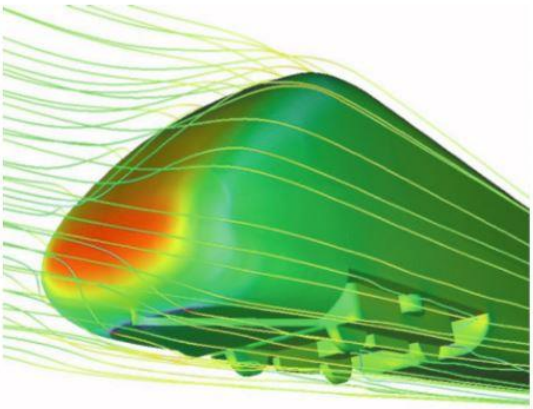

Figure 3: CFD computation of flow over ICE-2 train [80].

- Lattice Boltzmann Method (LBM)
- Large-Eddy Simulation (LES)
- Dynamic LES (DLES
  - Spatially Filtered Navier-Stokes equation
  - Turbulence Model for Sub Grid Scale
- Direct Numerical Simulation (DNS)
  - Complete Navier-Stokes equation
  - No Turbulence Model Required
- Newton–Krylov–Schwarz (NKS)
- Eddy-Viscosity Models (EVM)
- Nonlinear Acoustics Solver (NLAS)
- Detached Eddy Simulation (DES)
  - LES in well Resolved Regions
  - RANS Near Walls and Coarse Grid Regions
- Reynolds-Averaged Navier-Stokes (RANS)

This method of Time Averaged Navier-Stokes Equations Lead to New Terms Called Reynolds Stresses which are then Modeled Eddy Viscosity Models (e.g. k-ε model) can be divided into:

- ✓ Steady State Reynolds-Average Navier-Stokes (RANS), and
- ✓ Unsteady Reynolds-Average Navier-Stokes RANS (URANS)

The first method deals on the constant time or steady state condition while the second method is on unsteady or transient (varying time) conditions. For justification, on the next sub topic the discussion will be on the Reynolds-Average Navier-Stokes (RANS) numerical methods which will be the CFD method used for this study.

2.1.2.1 Reynolds-Average Navier-Stokes (RANS)

CFD or Computational fluid dynamics is a branch of fluid mechanics that is used to compute fluid flow variables with the help of computers and software such as ANSYS Fluent to solve and analyze problems involving fluid flows. Computers are used to carry out calculations using CFD software to solve the value of parameters in an iterative procedure where the solution accuracy is improved for each completion of iterations. The equations that are solved in CFD problems are the Navier-Stokes equations. In the laminar regime, the flow of the fluid can be completely predicted by solving the steady-state Navier-Stokes equations, which predict the velocity and the pressure fields. As the flow begins its transition to turbulence, it is no longer possible to assume that the flow is invariant with time. In this case, it is necessary to solve the problem in the time domain. As the Reynolds number increases, the flow field exhibits small eddies, and the timescales of the oscillations become so short that it is computationally unfeasible to solve the Navier-Stokes equations. In this flow regime, a Reynolds Averaged Navier-Stokes formulation can be used, which is based on the observation that the flow field over time contains small, local oscillations that can be treated in a time-averaged sense [75].

The Reynolds Averaged Navier-Stokes equations (also known as RANS equations) are equations used to predict the fluid flow using a time averaged formulation. The primary concept applied is Reynolds decomposition which involves decomposing an instantaneous quantity into its time averaged and fluctuating quantities. The time averaged nature of its equations makes it an attractive choice while simulating turbulent flows. Considering certain approximations based on the knowledge of properties of turbulent flows, these equations can be used to give time averaged solutions to the Navier-Stokes equations [75].

The k-epsilon model is one of the most commonly used turbulence models. It is a two equation model that employs two extra transport equations to represent the turbulent properties of the flow. This allows a two equation model to account for history effects like convection and diffusion of turbulent energy. This model, however, does not perform well in cases of large adverse pressure gradients [75].

The realizable k-epsilon model addresses the well-known deficiencies of the traditional k-epsilon model by incorporating: A new eddy-viscosity formula involving a variable Cμ originally proposed by Reynolds, and A new model equation for dissipation based on the dynamic equation of the mean square velocity fluctuation [75].

For high Reynolds number flows, such as in external flow around vehicles, resolving the near wall region down to the wall is not practical. To overcome this, wall functions are used. Non-equilibrium walls function (NWF) takes into account the effects of local variation in the thickness of the viscous sub layer, when computing the turbulent kinetic energy budget in wall adjacent cells. Besides this, NWF is also sensitized to adverse pressure gradients which are common in flow around vehicles. Compared to traditional wall functions, NWF provide more realistic predictions of the behavior of the turbulent boundary layers, including flow separation, and they do so without a significant increase in either CPU time or dynamic memory [75].

2.2 Analysis Techniques for Aerodynamic Drag on High-Speed Trains

There are number of analysis techniques or scenarios used for simulation of a train model through CFD software and Experimental analysis. These techniques are used for the issue of overall safety and within the main goal of aerodynamic drag resistance reduction. Some of techniques are listed below.

- Longitudinal, Axial Wind Drag Effect on the Whole Rolling Stock (on open air)
- Longitudinal, Axial Wind Drag Effect on Train Nose only (the Locomotive)
- Transverse, Cross Wind Drag Effect on the Rolling Stock
- Wind Drag Train Passing through The Tunnel
- Drag on Pantograph of the Train
- Drag Underneath, Bottom of the Train
- Slipstream, side way Drag of the Train
- Study of Train under Wake condition
- Study of Train on Embankment
- Study of Train on Bridge
- Longitudinal, Axial Wind Drag Effect on the representative parts of Rolling Stock (on open air)

Among these techniques, this study is going on the Longitudinal, Axial Wind Drag Effect on the representative parts of Rolling Stock, full scale (on open air). As this is the concern of the researcher, some details are given as the following sub topic.

2.2.1 Effect of Aerodynamic Drag on the Opposite Direction of the Motion of the High Speed Train

This research will be done based on the major and common technique under operation of open air condition, that is, no consideration of the tunnel effect, and the effect of cross wind will not

be covered. The importance of tunnel and cross wind effects are very valuable specially the cross wind for safety and the tunnel test for reduction of pressure boom which leads to passenger discomfort. Aerodynamic performance should include drag force, side force, lift force, roll moment, pitch moment, yaw moment, and velocity distribution [69], [70]. With considerations of these points in mind, the study of train aerodynamics through open air environment is too much valuable and enough to cover more than the half parameters of the above points. This can afford the optimization of wind drag towards input traction power. And this is not only to save power losses by air drag resistance, but also it can help to predict the level of passenger discomfort with respect to the degree of reduced drag level. Throughout doing this safety measures caused by lift force and moment can be indicated on this technique. The model only has three parts (locomotive or lead car, middle coach, and tail or end car) and these can represent the whole rolling stock (full scale, i.e., 1:1 scale or ratio) as researches reported that, extrapolation of model-scale (e.g., mostly a popular scale or a ratio of 1:25) or laboratory results to full-scale vehicles can lead to 30% errors in Coefficient of drag [81]. The following typical values of parameters of tabular data can show the effect of drag resistance for ICE Train and other train models under open air without considering crosswind, tunnel and other effects. The coefficient of drag value will help the study as validation criterion.

Table 1: Typical drag and friction coefficients for trains [81].

Train type[b]	$C_D(0)$	A_T (m^2)	l_T	l_L[c]	C_B[c]	C_{DL}[c]	λ_T	Reference
APT-P	2.05	8.05	300	13.0	0.11*	0.2*	0.0172	Gawthorpe 1978
HST	2.11	9.12	300	17.4	0.11*	0.2*	0.0192	Gawthorpe 1978
Conventional passenger train MKII	2.75	8.8	300	20*	0.11*	0.3*	0.0248	Gawthorpe 1978
Container 80% loaded	6.5	8.8	300	20*	0.11*	0.5*	0.0624	Gawthorpe 1978
Shinkansen 200	1.52	13.3	300	24.5	0.11	0.2	0.0160	Maeda et al 1989
ICE	0.69	10.2	115	20.9	0.12	0.2	0.0125	Peters 1990b

[a]From Sockel 1996.
[b]APT-P, advanced passenger train; HST, high-speed train; ICE, InterCity Express.
[c]Asterisk indicates estimated values.

2.3 Literatures of Similar Method and Techniques

As the speed of trains go higher and higher, the aerodynamic drag is one of key issues to be solved under high speed train performance. This aerodynamic drag is known to be proportional to the square of train speed, and the required traction power is proportional to the third power

of the train velocity [89]. Fairings can reduce the drag by∼50%, and telescoping (reducing size) the pantographs can reduce the drag by∼90% [81]. To increase the speed of the train, aerodynamic drag plays an important role for high speed train. Thus, the reduction of aerodynamic drag and energy consumption of high speed train is one of the essential issues for the development of the desirable train system. Aerodynamic drag on the traveling train is divided in to pressure drag and friction drag. Pressure drag of train is the force caused by the pressure distribution on the train along the reverse running direction. Friction drag of train is the sum of shear stress, which is the reverse direction of train running direction. In order to reduce aerodynamic drag, adopting streamlined shape of train is the most effective measure. Note that, for train body shape profile, streamlined profile is used instead of airfoil profile which is implemented mostly to increase the lift and decrease the drag like airplane wing. But for train and other ground vehicles, lift force should have limit for the vehicle safety such as the disaster caused by cross wind. Thus streamlined shape is the most concerned body profile for drag reduction of ground vehicles. The velocity of the train is also related to its length and shape [89].

If the design of train is done by outer wind shields, the train air drag will be reduced up to 15%. Also at the same time, the train with bottom cover can reduce the air drag by about 50%, compared with the train without bottom plate or skirt structure [89]. It is reported that the drag caused by the bogies can be reduced by ≤20% by aggressive application of deflectors under the nose, skirts and underbelly fairings, fairings over the bogies, and non-protruding bogies [81].

Train drag is divided into the aerodynamic drag, the sliding force between the wheel and rails, and the friction force caused by the pantograph system [89]. According to the results of several full scale tests, for the bluff shape train running at a speed of 120 km/h, the aerodynamic drag is about 40% of the total drag, which climbs up to 75% when the speed reaches 160 km/h. For the train with the length of streamline shape more than 5 m (train body mount system and a skirt system to smooth the structures underneath the train), the aerodynamic drag is about 75% of the total drag when the speed of train is 200 km/h. For the train with the length of streamline shape up to 10 m, the aerodynamic drag is about 75% of the total drag when the speed is 300 km/h [89]. Therefore, aerodynamic drag plays an important role for the high-speed train. In order to reduce the drag of train and the energy consumption, detailed understanding on the aerodynamic drag and its precise evaluation are of great importance. Also for streamlined trains at speeds of∼250–300 km/h, 75–80% of the total resistance is caused by external aerodynamic drag [81]. About 30% of this external aerodynamic drag is caused by skin friction, about 8–

13% by nose and tail pressure drag, 38–47% by bogie and associated interference drag, and 8–20% by pantograph and roof equipment drags [81]. For this research thesis the effect of pantograph aerodynamic drag is not considered because of the limit of available computation materials and time. Thus the percentage drag of pantograph and roof equipment of 8–20% in general will be shifted to the roof profile only. From the above references [81], the percentage of aerodynamics drag is good if it is around or less than 80%.

According to researches results, in order to design the shape of the train, the desirable length values of streamline shape train head can be obtained at different running velocities [89]. Table 2 lists the suggested length values of streamline shape head.

Table 2: Suggested length of streamline shape head at different velocities [89].

Velocity/(km·h−1)	200	250	300	350
Length of streamline shape/m	4	＞5	＞6	＞9

Researchers suggests the following points for the model of aerodynamically shaped train simulations: Under the condition without cross wind, air drag of the leading car is the smallest with ellipsoid shaped head and is the largest with flat-wide shaped head, while the air drag of tail car is the smallest with flat- shuttle shaped head and is the largest with convex-wide shaped head. Because of the interaction between the train speed and the cross wind speed that affect the air drag clearly, the air drag of ellipsoid shaped head will exceed that of the flat-wide shaped head under crosswind condition. That is to say, the air resistance of flat-wide shaped head with crosswind is smaller, while the ellipsoid shaped head is larger [89].

With the reference of the above points in consideration, for train of speed 250 km/h with the streamline shape length of 5.5 m, the expectation will be greater than or equal to 75% of drag percentage. From the reference cited above [89], the aerodynamic optimization includes elliptical head, minimal streamlined head of 5.5 m, outer wind shields, bottom cover, bogie fairing, spoilers, chamfering, and bottom plate or skirt structures are almost included on the improved model of the high speed train. It is reported that the drag caused by the bogies can be reduced by ≤ 20% by aggressive application of deflectors under the nose, skirts and underbelly fairings, fairings over the bogies, and non-protruding bogies [81]. The detail and dimensions of the reference model (i.e., ICE-2 Regional Train) is shown on the figure under the appendix.

Literatures which have similar numerical method and simulation with this thesis will be discussed under the next paragraphs and are reviewed as follows:

Yang G.W., et al., "Aerodynamic design for China new high-speed trains" [99], as high-speed trains have very complex running environments, the paper contain single-train running in open air, two-trains passing by in open air, single-train running in tunnel and two-trains passing by in tunnel. When the environment wind appears, cross- wind effects must be considered. Aerodynamic design of high-speed trains mainly aims at the drag, lift, moment, impulse pressure waves, aerodynamic noise, etc. at typical running conditions. In the paper, the aerodynamic design processes of CRH380A and 380B are introduced and the aerodynamic performances of different designs are analyzed and compared. Wind tunnel experiments and running tests indicate that the new generations of high-speed trains have excellent aerodynamic performances. In the open air without any cross-wind effects, the aerodynamic drag and lift coefficients were analyzed with numerical simulation for all of the twenty design models. The massive parallel hybrid grid Navier-Stokes solver with k-ω -SST turbulence models was used for the numerical simulation. The calculations were carried out for these models with train-head, train-tail and one train-middle-car at a train speed of 350 km/h. The drag and lift coefficients for the five models are presented [99].

Asress M.B., and Svorcan J., "Numerical investigation on the aerodynamic characteristics of high-speed train under turbulent crosswind" [5], Increasing velocity combined with decreasing mass of modern high-speed trains poses a question about the influence of strong crosswinds on its aerodynamics. Strong crosswinds may affect the running stability of high speed trains via the amplified aerodynamic forces and moments. In this study, a simulation of turbulent crosswind flows over the leading and end cars of ICE-2 high-speed train was performed at different yaw angles in static and moving ground case scenarios. Since the train aerodynamic problems are closely associated with the flows occurring around train, the flow around the train was considered as incompressible and was obtained by solving the incompressible form of the unsteady Reynolds-averaged Navier– Stokes (RANS) equations combined with the realizable k-epsilon turbulence model. Important aerodynamic coefficients such as the side force and rolling moment coefficients were calculated [5].

Mamo N., "Aerodynamic Characteristics and Aerodynamic Shape Optimization of Ethiopian National Train, Case Study on Addis Ababa Dire Dawa Passenger Train" [62], the aim of this study is to study and improve the aerodynamic performance (drag coefficient, lift coefficient, etc.), to reduce the energy consumption and checking the operational safety of the train against

cross wind. The area of the study mainly concentrated on the frontal aerodynamic drag analysis and related characteristics of Ethiopian National Train (ENT). In particular Addis Ababa Dire Dawa 120 km/hr. speed passenger train is used for the analysis. The computational fluid dynamics (CFD) analysis simulation method is used for the study. To improve aerodynamic drag performance shape optimization of train head is done using multi-objective approximation integrated with computational fluid dynamics and response surface methodology. For the CFD full scale analysis ANSYS fluent 12.0 using steady RANS method is used. Results shows that the train has poor aerodynamic performance at this speed and shape which has around 0.93 drag coefficient. Also has poor performance against cross wind, hence care must be taken especially on the curves and embankment. After shape optimization drag coefficient of around 0.79 is obtained which is close to minimum recommended result (0.5). This result in reduction of more than 15% drag coefficient and this shows reduction in energy consumption [62].

Kwon H.B., Hong J.S., "Aerodynamic Drag Reduction on High-performance EMU Train by Streamlined Shape Modification" [54], the effect of modifying the shape of a high-performance EMU train on the aerodynamic drag is studied here using Computational Fluid Dynamics (CFD) based on three dimensional Steady-state Navier-Stokes equation and two equation turbulence modeling. FLUENT 12 and Gambit 2.4.6 are employed for a numerical simulation of the aerodynamic drag of a streamlined-shape train as well as a proto type train. The characteristics of the aerodynamic drag of trains in tunnels are analyzed in a comparison with these characteristics in an open space. The contribution of the aerodynamic drag of each case is also investigated to establish principal pertaining to drag reduction for urban trains in tunnels. The aerodynamic drag of a streamlined train was reduced to 18% relative to a proto-type train with a blunt nose and a protruding roof facility and underbody shape: the running resistance is expected to be reduced by as much as 4% at a running speed of 80km/h under open space or air [54].

Tian H.Q., et al, "Flow structure around high-speed train in open air" [90], according to the analysis of the turbulent intensity level around the high-speed train, the maximum turbulent intensity is ranges from 0.2 to 0.5 which belongs to high turbulent flow. The flow field distribution law was studied and eight types of flow regions were proposed. They are high pressure with air stagnant region, pressure decreasing with air accelerating region, low pressure with high air flow velocity region I, turbulent region, steady flow region, low pressure with high air flow velocity region II, and pressure increasing with air decelerating region and wake region. The analysis of the vortex structure around the train shows that the vortex is mainly

induced by structures with complex mutation and large curvature change. The head and rear of train, the underbody structure, the carriage connection section and the wake region are the main vortex generating sources while the train body with even cross-section has rare vortexes. The wake structure development law studied lays foundation for the train drag reduction [90].

Tian H.Q., "Formation mechanisms of aerodynamic drag of high-speed train and some reduction measures" [89], Aerodynamic drag is proportional to the square of speed. With the increase of the speed of train, aerodynamic drag plays an important role for high-speed train. Thus, the reduction of aerodynamic drag and energy consumption of high-speed train is one of the essential issues for the development of the desirable train system. Aerodynamic drag on the traveling train is divided into pressure drag and friction one. Pressure drag of train is the force caused by the pressure distribution on the train along the reverse running direction. Friction drag of train is the sum of shear stress, which is the reverse direction of train running direction. In order to reduce the aerodynamic drag, adopting streamline shape of train is the most effective measure. The velocity of the train is related to its length and shape. The outer wind shields can reduce train's air drag by about 15%. At the same time, the train with bottom cover can reduce the air drag by about 50%, compared with the train without bottom plate or skirt structure [89].

Krajnović S., "Improvement of aerodynamic properties of high-speed trains by shape optimization and flow control" [52], Increase in speed of new high-speed trains has led to new requirements for improvement of their aerodynamic properties. Aerodynamic properties such as drag, crosswind stability, aero acoustics noise and upraise of ballast due to flow have to be treated simultaneously in a multi objective optimization procedure. This paper demonstrates an efficient optimization procedure that uses Meta models in form of polynomial response surfaces as a basis for search for optimal designs. Such simple models of objective functions make it possible to use genetic algorithms to explore design space. As a result of the suggested optimization procedure a set of so called Pareto-optimal solutions was obtained that helps exploration of extreme designs and finding tradeoffs between design objectives. Two examples are demonstrated for the purpose of the validation of the optimization procedure: optimization of a front of a train for the cross-wind stability and the optimization of passive flow devices (so called vortex generators) for drag reduction. Influence of turbulence models used in computer experiments on optimization procedure is explored. It was found that the choice of turbulence model influences the shape of the train with minimal lift force. Usage of Reynolds Stress (RSM) and RNG $\varepsilon - k$ model was found to produce noisy data that prevented construction of response surface models [52].

Abel D., "Stability of trains under aerodynamic excitation for Addis Ababa Light Railway Transit (A.A.L.R.T)" [1], Railway train aerodynamic problems is closely associated with the flows occurring around train. This work is based on numerical model using Computational Fluid Dynamics (CFD) approach to obtain the impact of air flow around a train operating in selected scenarios. These scenarios are train passing each other and train passing through the tunnel. The model of generic passenger train was developed using CatiaV5 and generated the wind tunnel and applied the boundary conditions in ANSYS workbench 13.0. The simulation work of the test vehicle and grid system is constructed by ANSYS-13.0. Steady RANS the Realizable k-e turbulence model with non-equilibrium wall function is selected to analyze the flow over the generic passenger car model [1].

Hillina A., "Analysis of Aerodynamic Brakes in Mainline of Ethiopia Railway Corporation (ERC)" [39], Aerodynamic brakes are used as auxiliary braking system in rolling stock. The aerodynamic brake is defined as a stiffened plate subjected to lateral pressure load considering buckling behavior. This research is prepared for the computational fluid analysis (CFD) of aerodynamic braking plate by using Finite Element Method to improve arrangement of braking plate and analyze for Ethiopian National Train (ENT). Through the research the current speed of ENT is taken (120km/h) and also assumed future speed of 300km/h is also considered. The analysis is done using the parameters of the rolling stock to be used by Ethiopian Railway Corporation. The assembly of the train body and braking plate area was modeled by using CATIA software. After modeling, analysis for determination of brake force is used by ANSYS Fluent and steady state RANS numerical method and realizable k-ε non equilibrium wall function model is used [39].

Li Y.F., et al, "Aerodynamic drag analysis of double-deck container vehicles with different structures" [60], To study the aerodynamic performance of a new six-axis X2K double-deck container vehicle, numerical simulation was done based on three-dimensional, steady Navier-Stokes equations and k−ε turbulence model. The results show that the pressure on the front surface of vehicle is positive, and others are negative. The maximum negative one appears as a “gate” shape on front surfaces. The pressure on vehicle increases with train speed, and pressure on vehicles with cross-loaded structure is smaller than that without it. The airflow around vehicles is symmetrical about train vertical axis, and the flow velocity decreases gradually along the axis to ground. Airflow around vehicles with cross-loaded structure is weaker than that without the structure. The aerodynamic drag increases linearly with the train speed, and it is minimum for the mid-vehicle. The linear coefficient for mid-vehicle without

cross-loaded structure is 29.75, nearly one time larger than that with the structure valued as 15.425. So, from the view-point of aerodynamic drag, the cross-loaded structure is more reasonable for the six-axis X2K double-deck container vehicle [60].

Chen X., et al, "Aerodynamic simulation of evacuated tube maglev trains with different streamlined designs" [21], Based on the Navier-Stokes (N-S) equations of incompressible viscous fluids and the standard k-ε turbulence model with assumptions of steady state and two dimensional conditions, a simulation of the aerodynamic drag on a maglev train in an evacuated tube was made with ANSYS/FLOTRAN software under different vacuum pressures, blockage ratios, and shapes of train head and tail. The pressure flow fields of the evacuated tube maglev train under different vacuum pressures were analyzed, and then compared under the same blockage ratio condition. The results show that the environmental pressure of 1 000 Pa in the tube is the best to achieve the effect of aerodynamic drag reduction, and there are no obvious differences in the aerodynamic drag reduction among different streamline head shapes. Overall, the blunt-shape tail and the blockage ratio of 0.25 are more efficient for drag reduction of the train at the tube pressure of 1 000 Pa. The ETMT is assumed to run at a speed of 300 m/s with a Mach number of 0.88. As the Reynolds number of the flow field is greater than 10^5, the flow field is considered turbulent, and the k-ε two-equation turbulence model is used to simulate the flow field. The standard k-ε turbulence model of the two dimensional viscous, steady and incompressible turbulent flow fields is adopted to simulate the flow field of the ETMT [21].

From literatures referred above Abel D., Mamo N., Hilina A., have done the same numerical method which is used for this research paper.

2.4 Formation Mechanism of Train Aerodynamic Drag

In the open air condition, the aerodynamic drag of the train is the sum of the tangential forces (skin friction drag) and the normal forces (pressure drag), both of which are parallel to the opposition direction of vehicle's velocity vector of positive *x*-axis direction. The pressure drag comes from the integral of the skin pressure of the train [89].

The direction of drag is along the negative direction of *x*-axis, as shown in the next figure. But as ANSYS Fluent result shows nothing is changed because of the use of negative *x*-direction of the drag. Thus the sign of the *x*-axis will be considered as positive direction or sign. The friction drag can be obtained by the integral of the tangential forces.

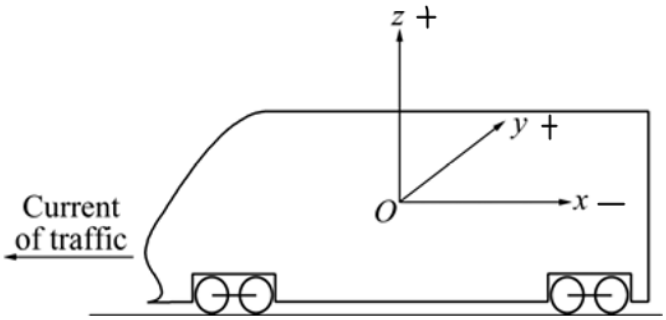

Figure 4: Coordinate definition of train [89].

The drag formula for the train in the open air can be expressed as:

$$F_x = F_{px} + F_{\tau x} \ldots\ldots\ldots\ldots\ldots\ldots\ldots\ldots\ldots\ldots\ldots\ldots\ldots\ldots\ldots\ldots\ldots\ldots\ldots\ldots\ldots\ldots (1)$$

Where F_x is the aerodynamic drag, F_{px} is the pressure drag, and $F_{\tau x}$ is the friction drag. Therefore, the aerodynamic drag on the traveling train is divided into pressure drag and friction drag. That is, in real both pressure drag and friction drag are in the same direction, the sign of positive and negative does not have change for the value of total aerodynamic drag. The formation mechanism of the aerodynamic drag will be discussed in the following part.

2.4.1 Composition of Aerodynamic Drag

The train drag is divided into the aerodynamic drag, the sliding force between the wheel and rails, and the friction force caused by the pantograph system. The total drag of train was composed of the sum of each carriage drag [89].

2.4.1.1 Relationship between Aerodynamic Drag and Total Drag of Train

In the open air condition without any cross-wind effect, the total drag on the traveling train can be expressed by Davis experience formula [89]:

$$F_R = a + bv_t + cv_t{}^2 \ldots\ldots\ldots\ldots\ldots\ldots\ldots\ldots\ldots\ldots\ldots\ldots\ldots\ldots\ldots\ldots\ldots\ldots\ldots\ldots\ldots\ldots (2)$$

Where F_R is the total drag, a, b and c are the constants determined by the experiment, and v_t is the train velocity relative to the ground [89]

In general, in Eqn. (2), the total drag can be divided into two contributions*:* $a+bv_t$ is the mechanical drag which includes the sliding drag between rails and train wheels, and the rotating

drag of the wheels; and cv_t^2 is the aerodynamic drag. So the aerodynamic drag can be expressed as [89].

$$F_x = cv_t^2 \quad \ldots\ldots (3)$$

The coefficient of aerodynamic drag (C_x) can be described as:

$$C_x = \frac{F_x}{qS_x} \quad \ldots\ldots (4)$$

$$q = \frac{1}{2}\rho v_t^2 \quad \ldots\ldots (4.1)$$

Where q is the dynamic pressure and S_x is the cross-sectional area of train. Therefore, the aerodynamic drag can be written as:

$$F_x = qS_X C_x = \frac{1}{2}\rho S_x C_x v_t^2 \quad \ldots\ldots (5)$$

Compared with Eqns. (3) and (4), the coefficient (c) can be expressed as:

$$C = \frac{1}{2}\rho S_x C_x \quad \ldots\ldots (5.1)$$

The aerodynamic drag is proportional to the square of speed of the train, while the mechanical drag is proportional to the speed of the train. Compared with the mechanical drag, the portion of the aerodynamic drag becomes larger as the train speed increases [89].

2.4.1.2 Relationship between Aerodynamic Drag and Each Carriage Drag of Train

The aerodynamic drag of the train is composed of the drag of each carriage. The drag force can be written as [89]:

$$F_x = F_{xt} + \sum_{i=1}^{n} F_{xz}(i) + F_{xw} \quad \ldots\ldots (6)$$

Where F_x is the total aerodynamic drag; F_{xt} is the drag of the leading car or locomotive; F_{xw} is the drag of the tail car; $F_{xz}(i)$ is the friction along the train, which includes the bogies, wheels, interference, and bottom structure of the train; and n is the number of middle carriages [89]. The coefficient (C_x) can be written as:

$$C_x = C_{xt} + \sum_{1}^{n} C_{xz}(i) + C_{xw} \dots\dots\dots\dots\dots\dots\dots\dots\dots\dots\dots\dots\dots\dots\dots\dots\dots\dots (7)$$

Where C_{xt} is the drag coefficient of the leading car or locomotive; C_{xw} is the drag of the tail car; and $C_{xz}(i)$ is the friction coefficient along the train, respectively.

2.4.1.3 Formation Mechanism of Pressure Drag

When the train runs at high speed, there will be a stagnation region with high pressure on the windward face of the train nose, and the flow speed will decrease. At the same time, the flow moves at high velocity along the tail car and the pressure decreases. The pressure drag stems from the pressures due to the abrupt change in the cross-sectional area of the train. The pressure drag can be obtained by integrating along the whole car [89]:

$$F_{px} = \oint_{S_F} P_{bx} dS_F \dots\dots\dots\dots\dots\dots\dots\dots\dots\dots\dots\dots\dots\dots\dots\dots\dots\dots (8)$$

Where P_{bx} is the skin pressure of the train along x axis, and S_F is the area of the train wall surface. For the high-speed train, the pressure drag comes from the pressure due to the shape of fore-body and after-body of the train, the connecting parts between trains, the train wall surfaces, the pantograph system, the bogie, and underneath structure of the train.

The mechanism of forming pressure drag is given as follows: there is a stagnation region in the leading car nose and air guide sleeve. The flow velocity of air is almost equal to zero, when the pressure reaches the largest in these regions. The flow around the pantograph system and bogie can also cause the increase of the skin pressure and the decrease of speed. And there are large pressure changes in the connecting parts between trains. When the air flow along the train reaches the end car, the flow speed will increase and the pressure will decrease. Air flow separation occurs at the nose of the end car. This results in a great change in the pressure distribution at the end car, leading to the pressure drag.

2.4.1.4 Formation Mechanism of Friction Drag

Due to the viscosity of the air, boundary layer occurs on the wall of train when the air flows along the train surface [89]. The height of boundary layer is equal to zero at the nose of the train, and becomes larger at the leeward. The speed of flow increases from zero to running velocity of the train along the boundary layer normal direction. The tangential forces are caused

by the difference of the velocity in the boundary layer normal direction, which is shear stress on the train surface [89].

Friction drag of the train is the sum of shear stress, which is in the reverse direction of the train running direction. Friction drag can be obtained by integrating along the whole train:

$$F_{\tau x} = \int_{S_F} \tau_{ix} dS_F \ldots\ldots\ldots\ldots\ldots\ldots\ldots\ldots\ldots\ldots\ldots\ldots (9)$$

Where: τ_{ix} is the shear stress on the train along x axis.

The shear stress is proportional to the viscosity of the air (μ) and the velocity gradient. The velocity is related to the height of boundary layer. However, the boundary is closely related to the shape of the train, the smooth of the train wall, the running velocity and the ambient surround. Therefore, the friction drag is relevant to the shape of the train, the smooth of train surface, the running velocity and the ambient surround.

2.4.1.5 Measures of Reduction of Aerodynamic Drag

The shape of the fore-body and after-body of the train can significantly influence the aerodynamic characteristics [89]. Fig.5 shows the pressure distribution of for-body and after-body of the train. When air flows around the fore-body of bluff train, the flow velocity becomes slower, and the pressure becomes larger. From Fig.5, the whole fore-body of train is almost in positive pressure region except the top of the fore-body. This is because the bluff body generates the biggest stagnation region on the fore-body of the train. However, for the flow around the streamline shape of the train, the velocity of flow becomes faster and skin pressure becomes smaller. The negative pressure acts on the large part region of the fore-body of the train except that the pressure is almost equal to zero in the region of fore-window. The positive pressure acts on the nose of train and air guide sleeve [89]

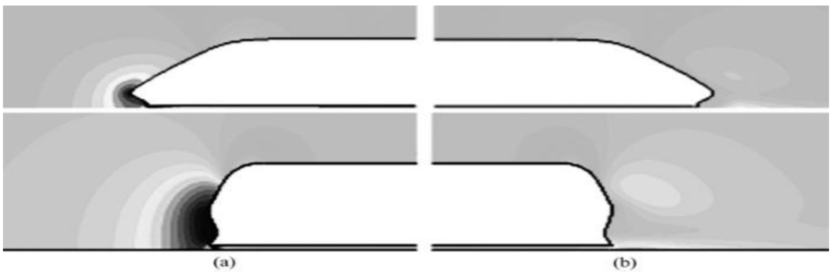

Figure 5: Pressure contours of fore-body and after-body of train: (a) Fore-body of train; (b) After-body of train [89].

The wake structure of train is schematically shown in Fig.6, for the blunt body of the train, there are two asymmetry vortices in the wake of train, which makes the flow velocity become faster. However, there is not vortex in the wake of streamlined after-body of the train. Therefore, the flow velocity is slower and the skin pressure is larger compared with those of the bluff body train. From Fig.6, there is large positive pressure in the wake of bluff body.

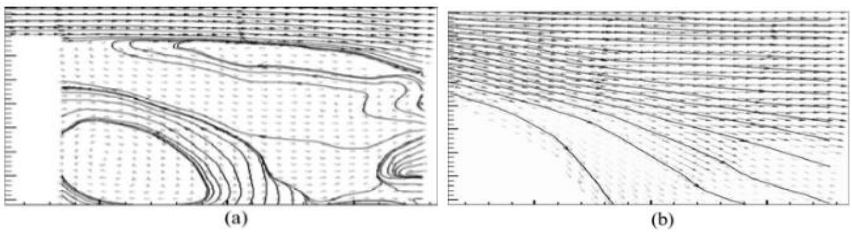

Figure 6: Flow structures in wake of after-body of different shape train: (a) Wake of bluff body train; (b) Wake of streamline shape head train [89].

According to the above figures, some concepts can be obtained. For the bluff body train, there is larger pressure drag due to the greater pressure in the fore-body and less pressure in the after-body of the train. However, for the streamline shape of the train, pressure drag is small due to lower pressure in the fore-body and higher pressure in the after-body of the train. Therefore, adopting streamline shape for fore-body and after-body of the train can reduce the pressure drag significantly [89].

The conductor parameters and control parameters of streamline shape of the train have a great influence on the aerodynamic drag of the train. The control parameters include the length, the height and the width of the streamline shape. The conductor parameters include the maximum control conductor along the longitudinal direction, the horizontal direction, and the cross-section of the train body section.

Research results show that the longer the streamline shape of train, the lower the pressure drag of leading car and tail car. With the increase of the length of the streamline shape, the aerodynamic drag coefficient decreases linearly. The relationship between the length of the streamline shape and the drag coefficient can be expressed as [89]:

$$C_{xt} = |a_{RTL}| - |b_{RTL}|L_d \quad \ldots\ldots\ldots\ldots\ldots\ldots\ldots\ldots\ldots\ldots\ldots\ldots\ldots\ldots\ldots\ldots\ldots\ldots (10)$$

The drag coefficient of the tail car is proportional to the exponential of the streamline shape reciprocal.

$$C_{xw} = |a_{RWL}| \exp\left(\frac{|b_{RWL}|}{L_d}\right) + C_{RWL} \quad \ldots\ldots\ldots\ldots\ldots\ldots\ldots\ldots\ldots\ldots\ldots\ldots\ldots\ldots (11)$$

Where L_d is the length of the streamline shape, a_{RTL} and b_{RTL} are the coefficients related to the drag of the leading car and the length of streamline shape, and a_{RWL}, b_{RWL} and c_{RWL} are the coefficients which are related to the drag of the tail car and the length of the streamline shape. According to other research results, in order to design the shape of the train, the desirable length values of streamline shape head can be obtained at different running velocities. Table 2 lists the suggested length values of streamline shape head.

2.4.1.6 Flow Structure's Change in Connection Place of Adjacent Cars

For the train with inner wind shield but without outer wind shield at the connecting parts between adjacent cars, there are a series of grooves at the connecting positions. On the windward side of the connecting positions, air flow directly scours the end wall's surface of grooves, which results in the free stagnation flow. The air flow moves slowly, which induces much higher positive pressure. On the leeward side of the connecting positions, air flow separates at the grooves, which makes the flow field more complicated. At the same time, irregular vortex is formed, which makes most of the end wall surface negative pressure zones and locally positive zones. Without outer wind shield, the superposition of the positive pressure of the windward and the negative pressure of the leeward side will cause much higher air pressure difference.

When the outer wind shield is set between adjacent cars, it will extend the outer surface of the car body's connection by flexible wind shield, which makes the distance between two cars body's outer surfaces shorter. During the train's running, the space formed by the inner wind shield, outer wind shield and car body works as a static pressure chamber. The flow speed inside static pressure chamber is quite low, on which the pressure distribution is much even and stable. Full scale test and wind tunnel test results show that: under the same train speed, no matter windward side or leeward side, the pressure on the end wall's surface is positive. And the measured pressure differences between different measure points are very small, which means that the pressure distribution on the end wall is stable. Therefore, when the outer wind shield is designed, the positive pressure of the windward offsets the positive pressure of the leeward side, which makes the pressure difference much smaller [89].

Adopting the outer wind shield will change the flow structure of the connecting position, which reduces air resistance with dramatic effects. According to wind tunnel test results, the outer wind shields can lower train's air resistance by 15% or so [89].

2.4.1.7 Improvement of Flow Structure of Car Bottom and Other Position

Generally, there are not bottom covers and skirt plates at the bottom of medium and the low speed rolling stocks. That is, all the equipment at the bottom of the train is exposed. It is normal for high-speed train setting bottom cover at the bottom of the vehicle. That is, all the equipment at the bottom of car between the two bogies and both sides of the two bogies will be covered, so that the bottom of the car except bogies has smooth surface. For simplicity, apron plates are usually set at the bottom of the high speed train. The exterior siding that seems as skirt piece is installed under the side beam of the frame. The bottom equipment has been blocked between the two skirt pieces.

There is a variety of hanging equipment at the bottom of the train. Due to an effect of the rough surface of the uneven equipment on air flow, flow field at the bottom of train is so complicated and flow around is so disturbed. There are a series of local small-scale positive and negative pressure zones along the longitudinal direction of the train, which can induce the friction resistance and increase the air resistance. When the bottom cover is set at the bottom of the train, the outer surface at the bottom is smooth. It is very difficult to form a vortex, thus the disturbance to air flow from the bottom equipment is reduced. The aerodynamic frictional drag and pressure drag of the train are greatly reduced. When the apron plate of the train is set at the bottom of the train, the side outer surface is smooth and the vortex formed between the two bottom apron plates will change the air flow without bottom cover and apron plate at the train bottom, which is an effective way to reduce air resistance of train.

The results of wind tunnel test show that the train with bottom covers can reduce the air resistance by about 50% compared with the train without bottom plate or apron plate. The air resistance is reduced by about 30% on the head car, about 50% on the middle car and about 25% on the end car. The car body with skirt plate at the bottom can reduce the air resistance by about 25%. The air resistance is reduced by about 28% on the head car, about 25% on the middle car, and about 18% on the end car [89].

At the same time, the whole train set should adopt the same cross-section shape to reduce the air pressure drag. Train’s surface should be smooth to reduce train’s air frictional drag. The top of the train except pantograph position should be smooth as much as possible. Dome can be designed for the pantograph base to make the air flow transit more smoothly. Drum-shaped wall should be designed on the side wall to reduce the additional air drag.

3. CHAPTER THREE: RESEARCH METHODOLOGY

The method is a part of a research thesis which connects the research problem and with its solution on the study area; this is done by data collection form relevant sources (reviewed literatures). After data collection modeling trains is done by CATIA software. Then on the analysis and simulation part those relevant data are organized and feed into the ANSYS Fluent software then the output will be coming on this CFD software on post process stage.

3.1 Research Design Procedure

The methodology to solve the given problem is depicted as follows:

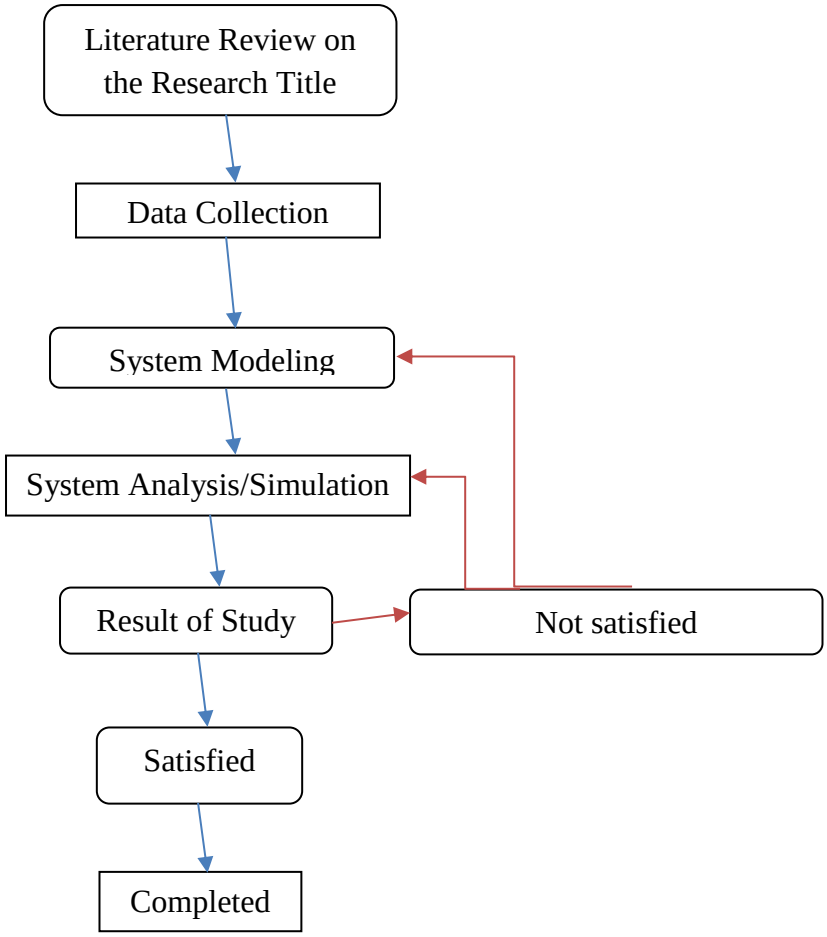

Figure 7: Procedures for Research Design.

3.2 Method of Analysis (Data Analysis and Interpretation)

The analysis is done using computational fluid dynamics (CFD) method of ANSYS Fluent simulation software and the physical modeling is developed on collected data from standards and papers. These data feed into the CATIA modeling system then these conditions affect the

pre-conditions of the aerodynamic system. Then the changes on the system by simulation are the result of the analysis. Those results will be interpreted as quantitative (magnitude) and qualitative (rank) form. So the effect of aerodynamic drag resistance on the performance of high speed train will be determined and predicted.

3.2.1 Input Data Sources

The Data sources which are the input data feed in to the CFD software will be collected from literatures. For example, the temperature of the ANSYS fluent is 288.153 K (15℃) and this condition is most preferable for the home place (U.S.A) of ANSYS software and other similar places may be like Europe and Asia can take this value as default. But in Ethiopia 298.153 K (25°C) [62] is a common room temperature. Thus 25℃ is taken for environmental condition of temperature input by the researcher in consideration of the temperature variation on the country. Some ANSYS Fluent variables are filled based on a guiding paper of titled "Best practice guidelines for handling Automotive External Aerodynamics with Fluent." [55].

Data for modeling (2D or 3D) of the train bodies are gathered from standards and other similar materials such as the e-books, magazines, journals, and relevant literatures. For the ICE-2 Regional train the dimensional data is taken from another research and it is cited under the appendix. This data is not full but it can give way for the researcher to fill other minor dimensional criterions. The modified model is done from the base of ICE-2 dimensions and common features of other high speed trains.

3.2.2 Physical Modeling of Trains

The model of the designed train includes: the locomotive, the rare end tail of the train and single middle coach (also can called carriage, wagon, and railcar) was generated by popular Modeling and designing software CATIA V5R20 by the researcher with the help of standards of high speed trains of streamlined aerodynamic shape and other aerodynamic shape improving technique. In similar way the ICE-2 Regional passenger train will be modeled from its available source. It is necessary to design the flow structure of the fore-body and after-body of the train on its body. It is an effective measure to decrease the aerodynamic drag by adopting streamline shape head. The velocity of the train is related to the length and shape of the train [89]. To get better high-speed train with less aerodynamic drag resistance, the ICE-2 Regional train needs visible profile change of the model. Thus the researcher plays important role on modifying this train model with consideration of manufacturing preferably and cost. The following figures

depicts the difference on models of ICE-2 Regional train and the modified one, the researcher gives its name as Ethio-HST-250+.

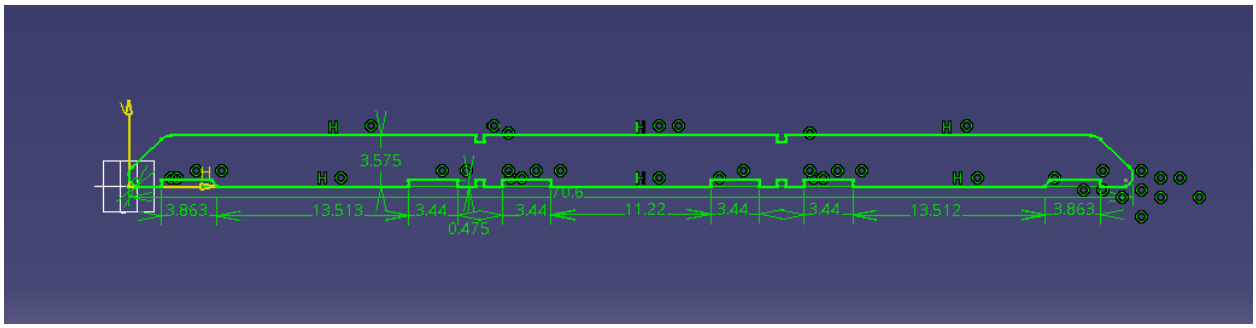

Figure 8: 2D of ICE-2 Regional train.

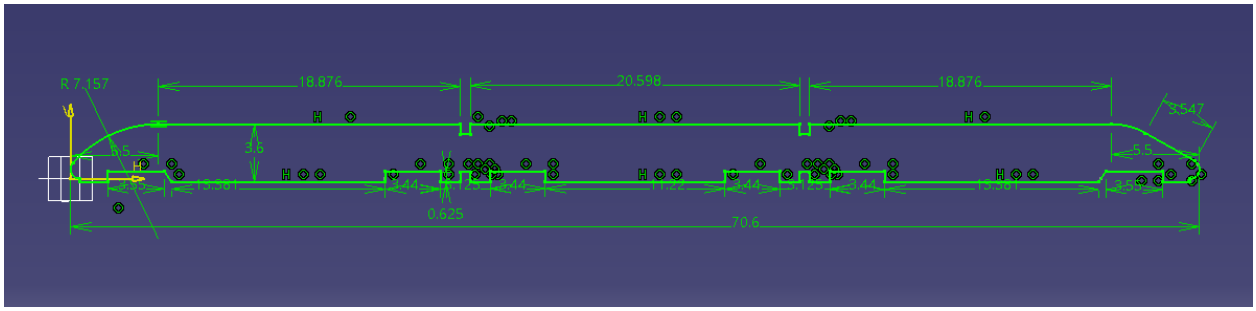

Figure 9: 2D of Ethio-HST-250+ train.

From these two dimensional models the generated 3D model is as shown below.

(a)

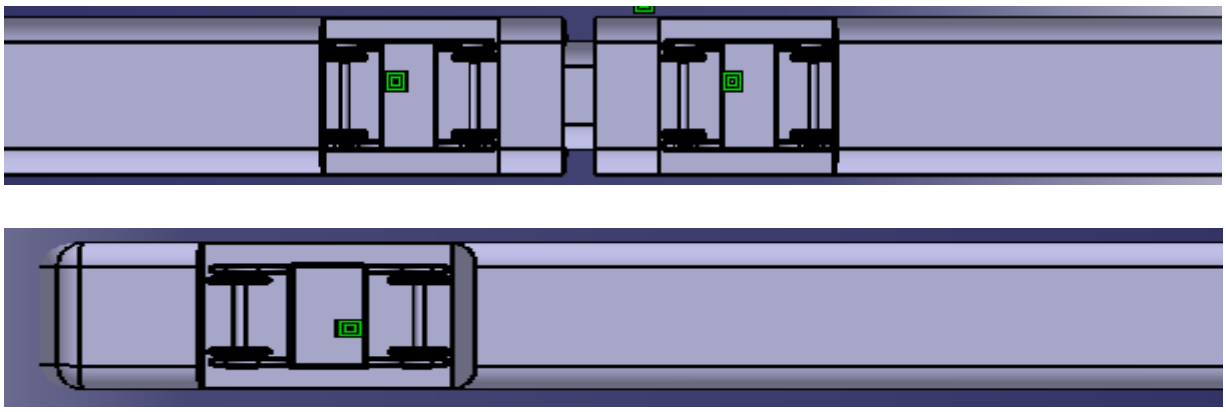

(b)

(c)

Figure 10: 3D of ICE-2 Regional train: (a) CATIA right side view, (b) under body with rectangular nose view, (c) common simplified bogie [45].

(a)

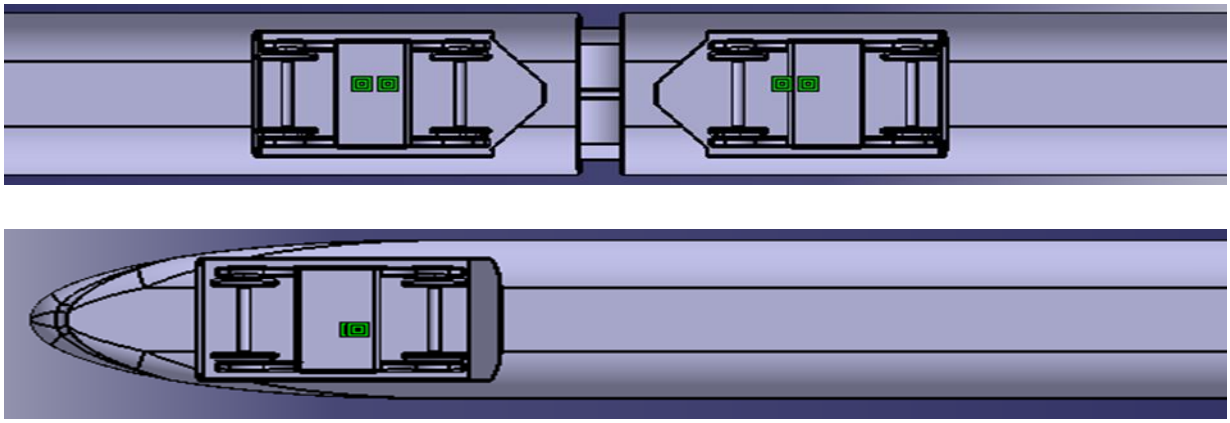

(b)

Figure 11: 3D of Ethio-HST-250+ train: (a) CATIA right side view, (b) bottom, underbody with elliptical nose view.

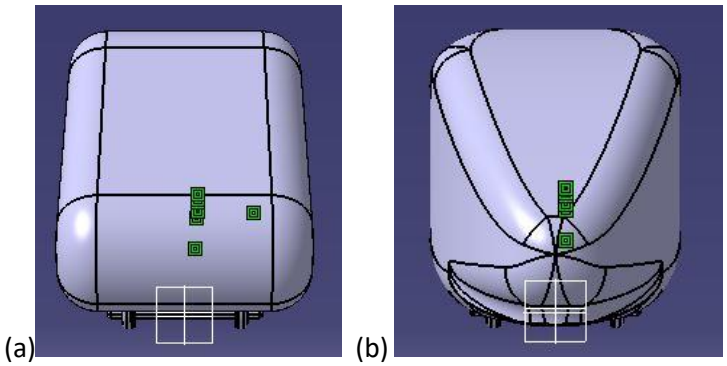

(a) (b)

Figure 12: Front view of (a) ICE-2 train and (b) Ethio-HST train.

For easiness of better comparisons of these two train models table 3 is shown below. This table can show major design variations between the two models.

Table 3: Dimensional comparisons of ICE-2 Regional and the new model (Ethio-HST-250+).

No	Design Variables	ICE-2 Regional train	Ethio-HST-250+ train
1	Nose elliptical profile	No	Yes
2	Nose streamline length	3 m	5.5 m
3	Track gauge	1.435m	1.435m
4	No of bogies	6	6
5	Locomotive length	24.375 m	24.375 m
6	Coach length	20.6 m	20.6 m
7	Tail length	24.375 m	24.375 m
8	Train height	3.575 m	3.6 m [58]
9	Train width	3.075 m	3.3 m [58]
10	Under body cover plate or skirt	No	Yes
11	Bogie fairing	No	Yes
12	Spoiler geometry	No	Yes
13	Chamfering	Yes	Yes
14	Under body design	No	Yes
15	Coupling distance	0.625 m	0.625 m
16	Minimal fillet radius	0.010 m	0.010 m
17	Maximal fillet radius	0.500 m	1.000 m

Some variables which need to be considered for high speed train (HST) geometrical modeling are depicted on the figure below.

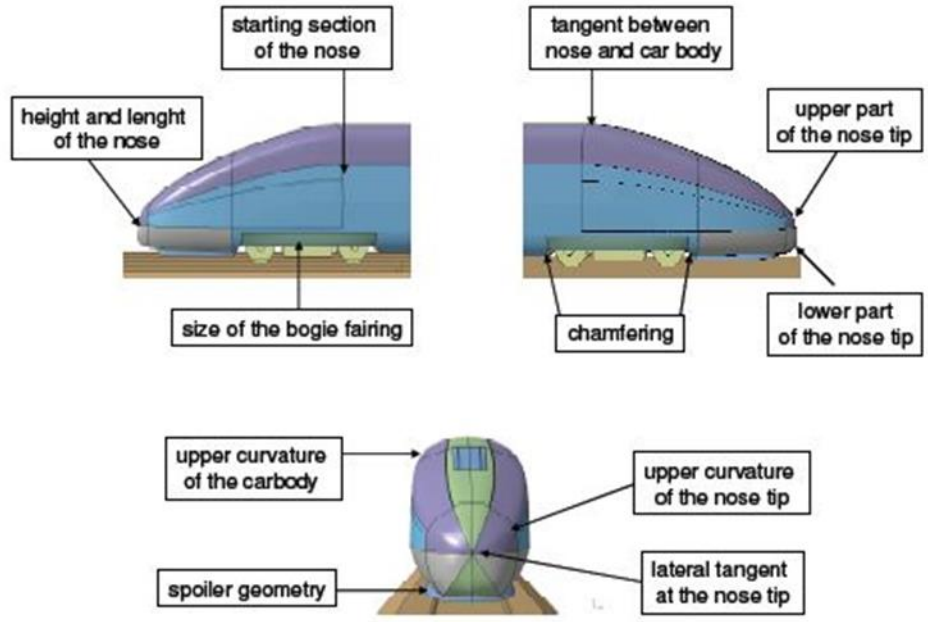

Figure 13: Some geometric consideration for HST modeling [69].

The gain of aerodynamic drag reduction by using these methods is also shown below.

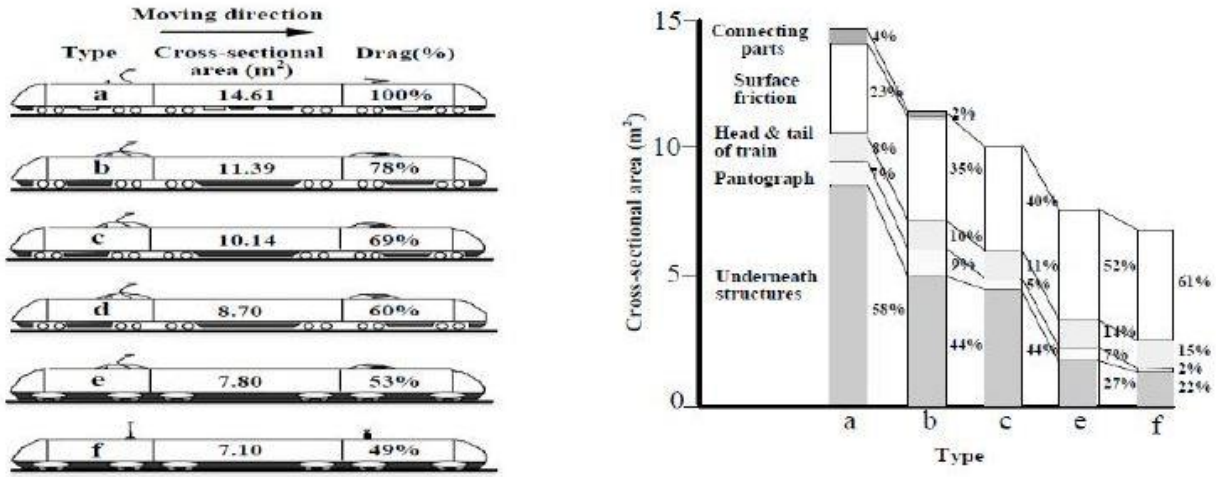

Figure 14: Aerodynamic drag on ICE (the hatching area is the device to smooth the structures underneath train; the right side shows aerodynamic drag components of ICE) [79].

3.2.3 Numerical Modeling on RANS

Computation Fluid Dynamics (CFD) is the use of computer simulations to compute and analyze the dynamics of a fluid and the method is used in various areas such as ventilation, internal combustion engines, and vehicle aerodynamics as in this study. CFD simulations are carried out by dividing the physical domain into small finite volume elements and numerically solved by the governing equations that describe the behavior of the flow. The governing equations are

derived from the laws of conservation, which become very complex, almost impossible to solve analytically and therefore requires numerical simulations. There are many advantages with CFD, such as reduction of cost and lead time when developing new design and is a widely used method in the industry, however due to the complexity of the physics, there still are difficulties. Large and trustworthy results need a high amount of computer capacity and are only as good as the operator and the physics embedded. This section describes some general clues about time averaged steady state (without time change) RANS simulation methods. To do that assessing other methods may help for evaluation of RANS. To squeeze the discussion topics which are only in the solver ANSYS Fluent will be discussed. Note that Direct Numerical Simulation (DNS) is not available under fluent solver. The diagrams listed below shows the general description of each method.

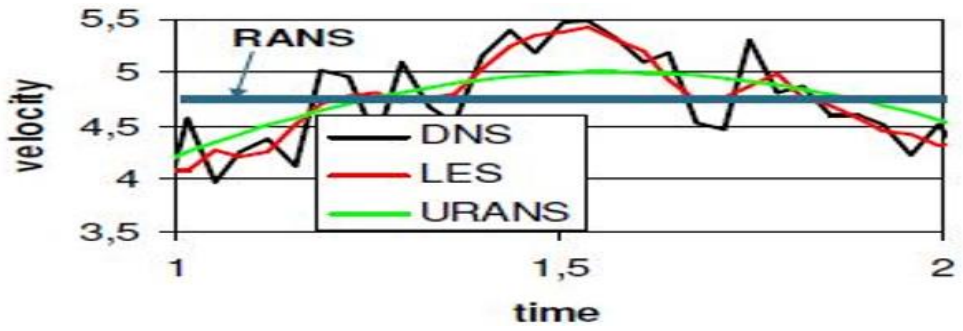

Figure 15: Comparison of common numerical viscid Methods [8], [69].

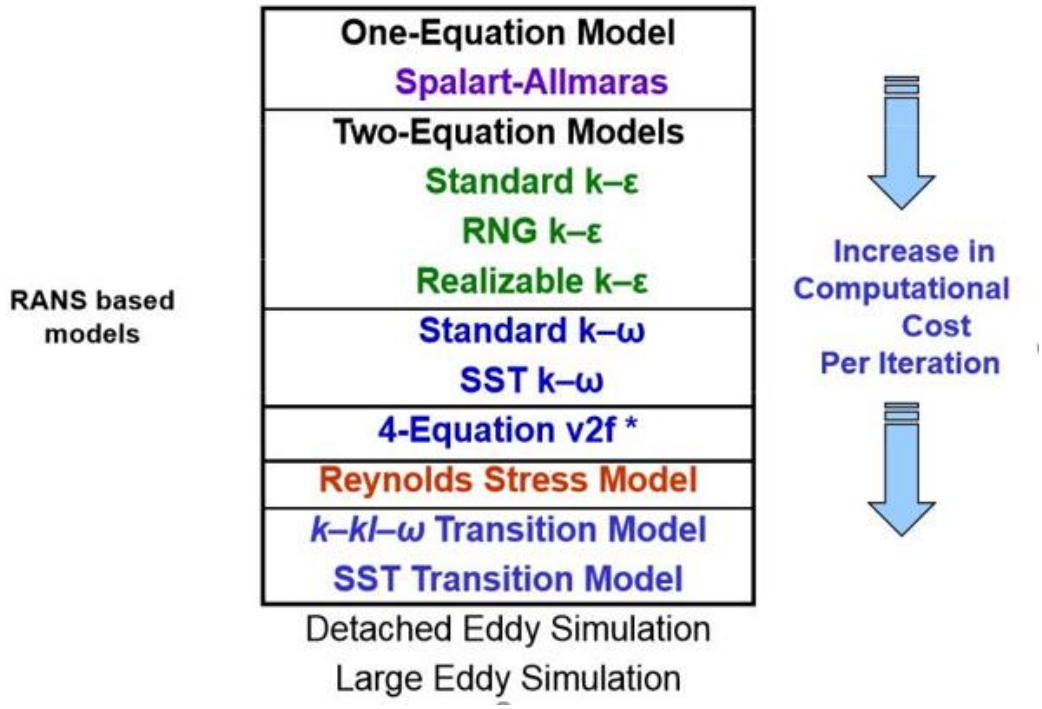

Figure 16: Turbulence Models Available in FLUENT (ANSYS, Inc. Release 13.0).

Reynolds Number: The Reynolds number is defined as

$Re_L = \frac{\rho UL}{\mu}; L = x, d, d_h, etc.$ [60], [67].

For external flow:

$Re_x \geq 500{,}000, along\ a surface;$

$Re_d \geq 20{,}000, around\ an\ obstacle.$

Turbulent flows occur at large Reynolds numbers thus for air/train velocity of 250 km/h (Around 70 m/s with difference of 0.556 m/s), the characteristic length L is can be the height of the train, to be more accurate, the characteristic length will be the hydraulic diameter of the cross section of each trains. air density of ρ = 1.185 kg/m^3, and the dynamic viscosity μ = 1.831e-05 kg/ (m-s) for 298.16 K (25°c) of temperature value [100]. The hydraulic diameter is calculated as follows:

$$D_h = \frac{4A}{P}$$

Where; D_h = Hydraulic Diameter, A = train cross sectional area, and P = Perimeter of the cross section.

The cross sectional area is computed from fluent and the perimeter is calculated manually with approximate dimensions. Thus, the cross sectional area and the perimeter of ICE-2 train is 12.350142 m^2 and 13.242 m respectively. Then the cross sectional area and the perimeter of Ethio-HST train is 12.5895002 m^2 and 12.483 m respectively. The hydraulic diameter (characteristics length) of ICE-2 train and Ethio-HST train models will be computed respectively as follows.

$$D_{h,ICE-2} = \frac{4A_{ICE-2}}{P_{ICE-2}}$$

$$= \frac{4 * 12.350142}{13.242}$$

$$= \frac{49.400568}{13.242}$$

$$= 3.730597190756683$$

$$\cong 3.731m$$

$$D_{h,Ethio-HST} = \frac{4A_{Ethio-HST}}{P_{Ethio-HST}}$$

$$= \frac{4 * 12.5895002}{12.483}$$

$$= \frac{50.3580008}{12.483}$$

$$= 4.03412647600737$$

$$\cong 4.034\ m$$

For ICE-2 Regional Train the Reynolds number will be as follows:

$$Re_x = \frac{\rho UL}{\mu} = \frac{1.185\ * 70 * 3.731}{1.831 * 10^{-05}}$$

$$= \frac{309.48645}{1.831 * 10^{-05}}$$

$$= 16902591.480065537957400327689787$$

$$\cong 16902591.48$$

$$\cong 1.69 * 10^{-07}$$

In similar way, for the Ethio-HST train model:

$$Re_x = \frac{1.185\ * 70 * 4.034}{1.831 * 10^{-05}}$$

$$= \frac{334.6203}{1.831 * 10^{-05}}$$

$$= 18275275.805570726379027853631895$$

$$\cong 18275275.81$$

$$\cong 1.83 * 10^{-07}$$

Thus, the higher amount Reynolds number indicates that the possibility to study external aerodynamics of turbulent flow of air over a rigid body. To simulate external aerodynamics at this much amount of Reynolds number, it is important to consider turbulence flow of the fluid.

The Mach number, Ma $<$ 0.3 indicates incompressible and subsonic flow. The value of Mach number like Reynolds number is to know possibility of assumption of weather the flow of the fluid (air) is compressible or incompressible.

$$Ma = \frac{U}{c} \dots\dots\dots\dots\dots\dots\dots [67]$$

$$= \frac{70}{340.29} = 0.21$$

Where, c = speed of sound at sea level = 340.29 m / s and U = the air speed = 70 m/s.

After finding of Reynolds number and Mach number, the assumption on the numerical method approximation which will be discussed next is become meaningful. As fluid dynamics is the study of fluids in motion, such as airflow around a vehicle, and the physics can be described by the conservation laws of mass, momentum and energy. Conservation of mass is expressed by the continuity equation, which states that the amount of mass flow that enters a control volume must be equal to the amount leaving it. It uses the finite-volume method to solve the governing Navier-Stokes equations for a fluid which are derived from the conservation mass equation (a), the conservation of momentum (b) and the conservation of energy (c) equations [62]. Thus the next formula is called continuity equation.

$$\frac{\partial u}{\partial x} + \frac{\partial v}{\partial y} + \frac{\partial w}{\partial z} = 0 \dots\dots\dots\dots\dots\dots\dots\dots\dots\dots\dots\dots\dots\dots\dots\dots\dots\dots\dots\dots\dots\dots\dots\dots\dots\dots\dots\dots\dots\dots\dots\dots .. (a)$$

The difficulty arises from the fact that the conservation of mass, momentum and energy are coupled and non-linear set of differential equations making them practically impossible to solve analytically for practical engineering problems. Hence CFD software such as Fluent is utilized to provide very reasonable approximation upon solving the specified governing equations [62]. Conservation of momentum (Newton's Second Law of Motion) is expressed by the Navier Stokes equations and is used to obtain a relation between pressure, momentum and viscous forces for a Newtonian fluid. The conservation of momentum equation:

$$\rho g_x - \frac{\partial p}{\partial x} + \vartheta\left(\frac{\partial}{\partial x^2} + \frac{\partial}{\partial y^2} + \frac{\partial}{\partial z^2}\right) = \rho\frac{\partial u}{\partial x}$$

$$\rho g_y - \frac{\partial p}{\partial y} + \vartheta\left(\frac{\partial}{\partial x^2} + \frac{\partial}{\partial y^2} + \frac{\partial}{\partial z^2}\right) = \rho\frac{\partial v}{\partial x}$$

$$\rho g_z - \frac{\partial p}{\partial z} + \vartheta\left(\frac{\partial}{\partial x^2} + \frac{\partial}{\partial y^2} + \frac{\partial}{\partial z^2}\right) = \rho\frac{\partial w}{\partial x}$$

$$\dots\dots\dots\dots\dots\dots\dots\dots\dots\dots\dots\dots\dots\dots\dots\dots\dots\dots\dots\dots\dots\dots\dots\dots\dots\dots\dots\dots\dots\dots\dots\dots\dots.\dots\dots\dots (b)$$

Conservation of energy (First Law of Thermodynamics) is expressed by the energy equation stating that the total amount of energy within a system stays constant:

$$\rho C_p \frac{dT}{dt} = \mathrm{k}\nabla^2 T + \Phi \dots\dots\dots\dots\dots\dots\dots\dots\dots\dots\dots\dots\dots\dots\dots\dots\dots\dots\dots\dots\dots\dots\dots\dots..(C)$$

As mentioned above, the governing equations become very complex. In order to numerically solve them, the differential equations are discretized into large system of algebraic equations in order to solve them. The general approach is to assume incompressible and isothermal flow where the Mach number under 0.3 (for this case Ma = 0.21) and a constant temperature since vehicles travel at a relatively low speed. The governing equations are therefore simplified and the energy equation can be neglected.

Furthermore, since stochastic, three-dimensional and time dependent, fluid flows are almost always turbulent and will experience fluctuations and therefore Reynolds decomposition method is used. The velocity and pressure are split into two parts, an average and a fluctuating part stated as:

$$\overline{u} = \frac{1}{T}\int_0^T u dt \dots\dots\dots\dots\dots\dots\dots\dots\dots\dots\dots\dots\dots\dots\dots\dots\dots\dots\dots\dots\dots\dots\dots\dots\dots\dots..(d)$$

$$p = \overline{p} + p', u = \overline{u} + u', v = \overline{v} + v',\ w = \overline{w} + w' \dots\dots\dots.\dots\dots\dots\dots\dots\dots\dots\dots..(e)$$

This is called Reynolds-Averaged Navier-Stokes (RANS) equations where the additional terms are included in the continuity and momentum equations and time averaged.

$$\frac{\partial\overline{u}}{\partial x} + \frac{\partial\overline{v}}{\partial y} + \frac{\partial\overline{w}}{\partial z} = 0 \dots\dots\dots\dots\dots\dots\dots\dots\dots\dots\dots\dots\dots\dots\dots\dots\dots\dots\dots\dots\dots\dots\dots\dots\dots\dots\dots.(f)$$

$$\rho g_x - \frac{\partial\overline{p}}{\partial x} + \frac{\partial}{\partial x}\left(\vartheta\frac{\partial\overline{u}}{\partial x} - \rho\overline{u'^2}\right) + \frac{\partial}{\partial x}\left(\vartheta\frac{\partial\overline{u}}{\partial x} - \rho\overline{u'v'}\right) + \frac{\partial}{\partial x}\left(\vartheta\frac{\partial\overline{u}}{\partial x} - \rho\overline{u'w'}\right) = \rho\frac{du}{dt} \dots (g)$$

For the above formulas use; ρ = density, t = time, p = pressure, ϑ = static viscosity, g = gravity constant, C_q = specific heat capacity, T = temperature, k = coefficient of thermal conductivity, and Φ = viscose dissipation.

Turbulent flows are characterized by large, nearly random fluctuations in velocity and pressure in both space and time. These fluctuations arise from instabilities that eventually are dissipated (into heat) by the action of viscosity. Turbulent flows occur in the opposite limit of high Reynolds numbers. The two approaches to solving the flow equations for turbulent flow field can be roughly divided into two classes, direct numerical simulations and *k*-*ε*. Direct numerical simulation numerically integrates the Navier-Stokes equations, resolving all of the spatial and temporal fluctuations without resorting to modeling. *k*-*ε*, models Reynolds stress in two turbulent parameters, the turbulent kinetic energy (*k*) and the turbulent energy dissipation rate (ε) defined below by Equations (*h*) and (*i*) respectively [62].

$$k \equiv \frac{1}{2}(\overline{u'^2} + \overline{v'^2} + \overline{w'^2}) \ldots \ldots \ldots \ldots \ldots \ldots \ldots \ldots \ldots \ldots \ldots \ldots \ldots \ldots \ldots \ldots \ldots \ldots \ldots \ldots (h)$$

$$\varepsilon \equiv u\left[\left(\frac{\partial u'}{\partial x}\right)^2 + \left(\frac{\partial u'}{\partial y}\right)^2 + \left(\frac{\partial u'}{\partial z}\right)^2 + \left(\frac{\partial v'}{\partial x}\right)^2 + \left(\frac{\partial v'}{\partial y}\right)^2 + \left(\frac{\partial v'}{\partial z}\right)^2 + \left(\frac{\partial w'}{\partial x}\right)^2 + \left(\frac{\partial w'}{\partial y}\right)^2 + \left(\frac{\partial w'}{\partial z}\right)^2\right] \ldots \ldots \ldots \ldots \ldots \ldots \ldots \ldots \ldots \ldots \ldots \ldots \ldots \ldots \ldots \ldots \ldots \ldots \ldots (i)$$

3.2.4 Parameterization

The major things which affect the HST system will be assigned as parameters for this research. Those major parameters are wind (speed, direction, pressure, force) conditions and train (speed, direction, longitudinal force, aerodynamic shape (active area which impact with air)) have major place for the analysis. In other words, those things govern the operability of HST scenarios.

3.2.5 Discussion on Method

The method planned to use on the study by simulation of real world into CFD system by RANS is efficient to predict and evaluate the required parameters as Mamo [62], and other referred simulations have done with similar method. For bluff bodies, such as trains, the method Large Eddy Simulations (LES) has proven to be a method that gives good results [62]. When improving the energy efficiency of vehicles, the lowering of the aerodynamic drag is an important aspect. Drag reduction of a high speed passenger train can lead to both environmental and economic benefits as the noise sever and the energy consumption is lowered. Using LES and some other methods as shown on fig.16 are more accurate than the RANS. But RANS method is pretty much enough to predict the values of the aerodynamic effects for these two

HST models. So the result would be expected to be similar as the real world conditions. RANS is the main tool used by engineers (ANSYS, Inc. Release 13.0).

3.3 ANSYS Fluent setup

For modeling the geometry, 3D modeling CATIA V5R20 software was used (see figures from fig.8 – fig.12). Before importing its IGES form to ANSYS Workbench. Under Design Modeler freezing is done not to permit the merging behavior of component parts. Then in order to simulate the air flow around the vehicle, a fluid volume needs to be created which will encompass the vehicle. This was done by creating an enclosure around the vehicle and then the Boolean operation of subtracting the vehicle body from the enclosure (air domain). This enclosure acts as the air domain. To reduce the overall computational cost and time, the vehicle was considered symmetric laterally, divided into two halves longitudinally [75]. The size of the rectangular enclosure was taken to be the multiple of the rolling stock length (70.6 m) to 0.5 times for its height, 1 for its width, 1times from train head for its length plus train length and plus 2 times from train end. Thus, width of 70.6 m, height of 35.3 m, and length of 282.4 m will be the dimension of the enclosure [62]. Then Boolean of subtraction of the train from the created fluid enclosure is done to leave only the air domain, as the study is only aerodynamic, not include structural study. The figures shown below, shows how the enclosure exactly locks like with the first referred air domain:

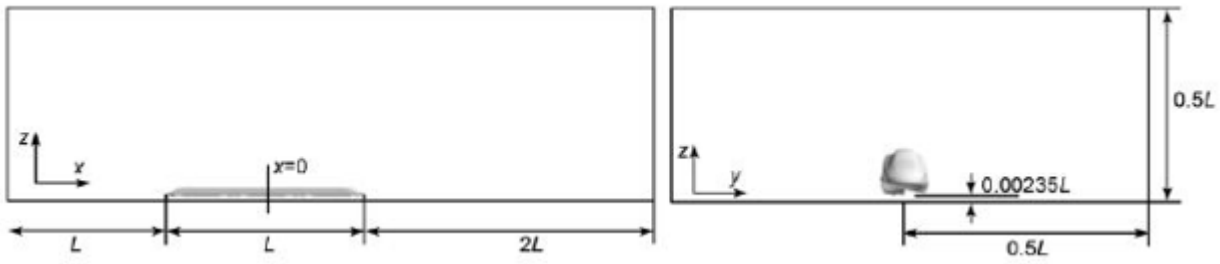

Figure 17: Computational domain of the flow field [84], [102], [103].

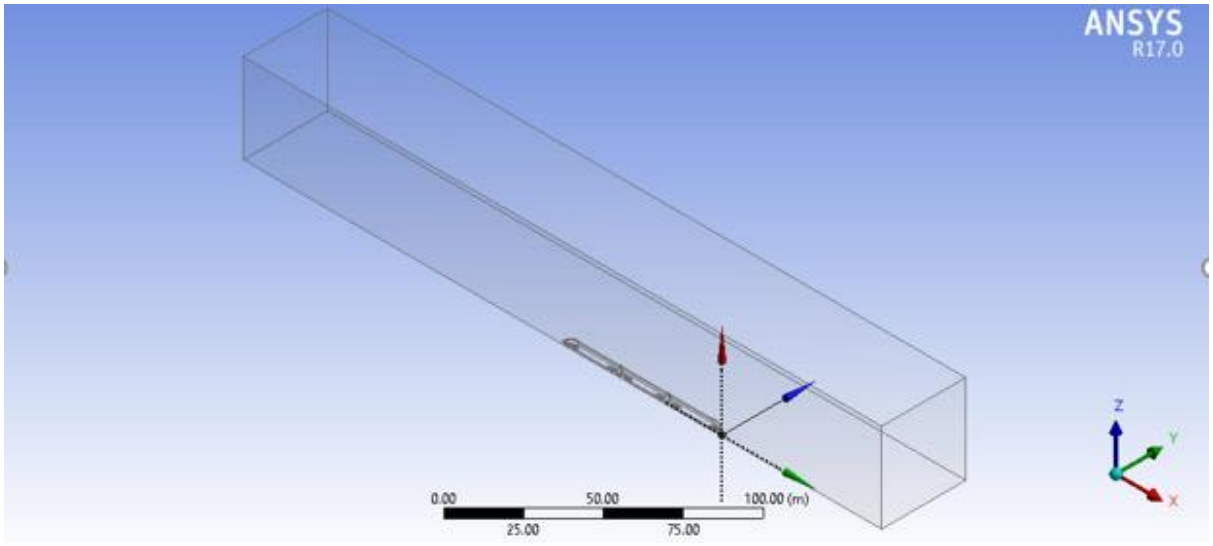

Figure 18: Computational symmetric air domain of the flow field.

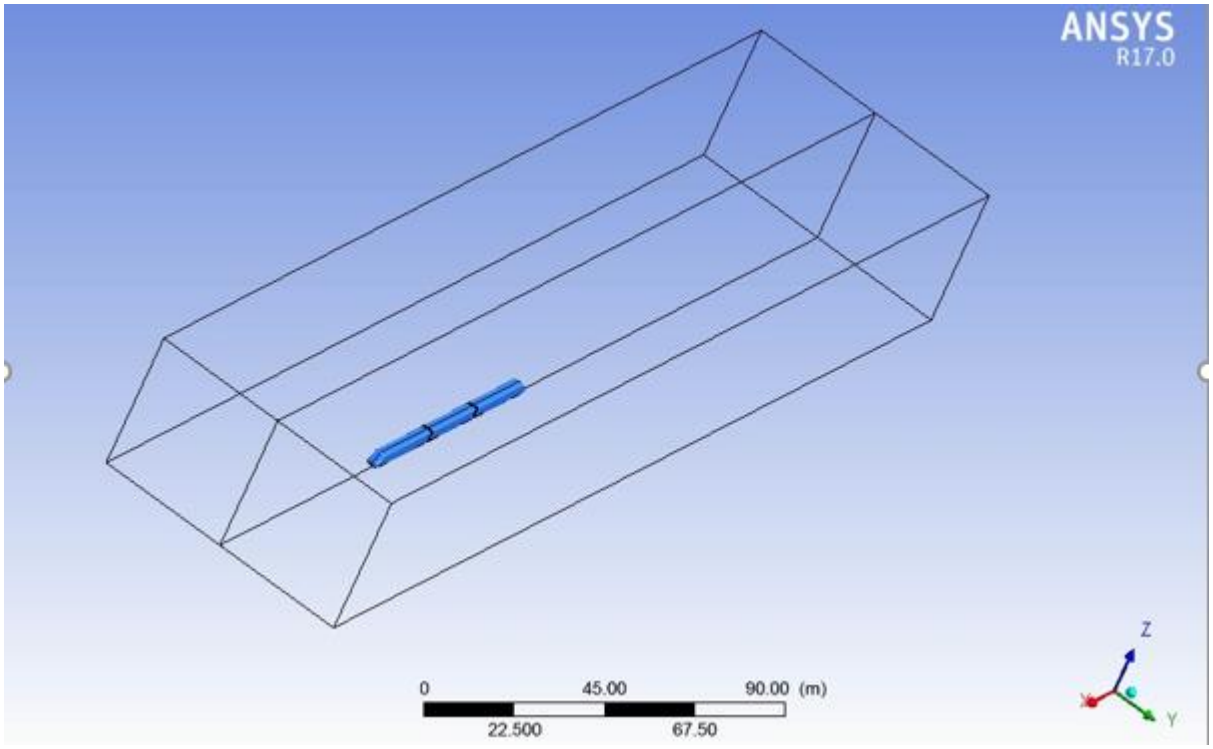

Figure 19: Computational full air domain of the flow field.

Note that, performing numerical simulation for a complete train with a length of more than 70.6 m to include the entire car by turbulent method requires more advanced computational resources than those available [62]. Thus this much length is enough to predict the air flow parameters.

While generating the fine mesh, face sizing were used wherever necessary in order to obtain accurate drag and lift parameters. Since boundary layer separation has a significant effect on drag, five layers of inflation were added to the vehicle surface to properly resolve the boundary

layer [75]. The total number of elements obtained was 2627903 (of 824444 thousand nodes) million for ICE-2 Regional train and 3900464 (of 1252011 million nodes) million for Ethio-HST-250+ train. Note that, these numeral values are for the half values of each train models because of the use of symmetric analysis method. The following figures show the final mesh for the two train models.

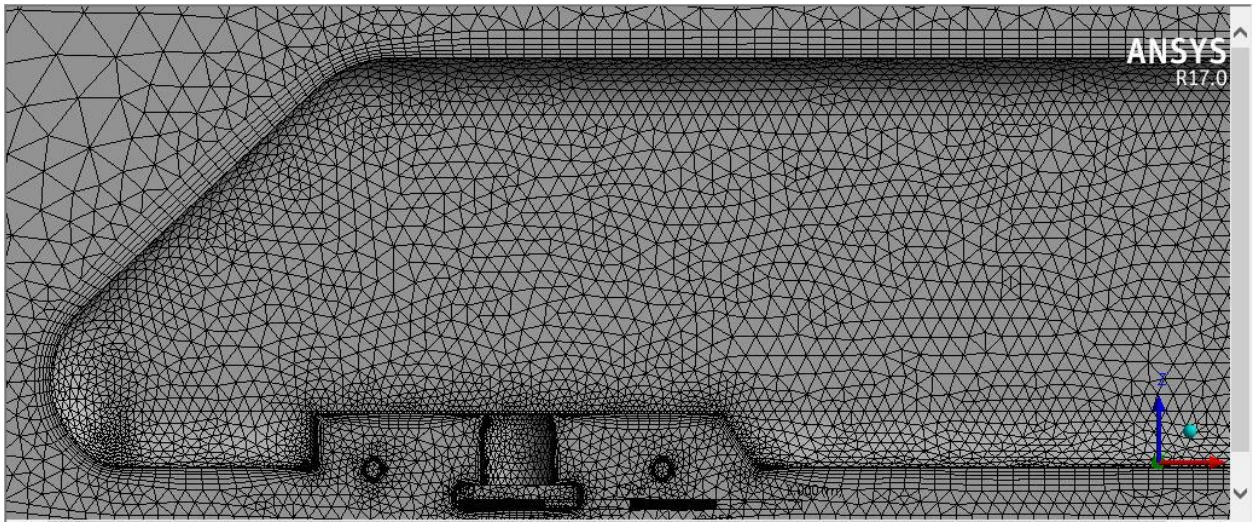

Figure 20: ICE-2 Regional mesh view.

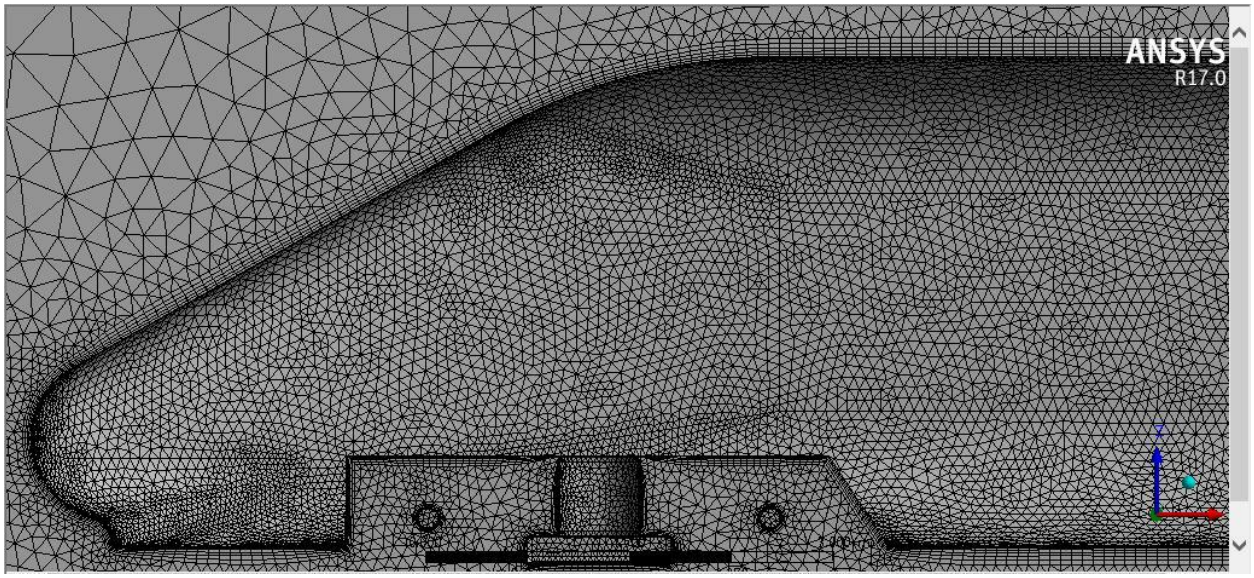

Figure 21: Ethio-HST mesh view.

Table 4: Mesh Information (Report) for ICE-2 Regional and for Ethio-HST-250+.

Domain	ICE 2 Regional		Ethio HST 250	
Air	Nodes	Elements	Nodes	Elements
	824444	2627903	1252011	3900464

3.3.1 Boundary Conditions

The enclosure inlet plane was named "velocity-inlet". Air coming through the inlet was given a velocity of 250 km/h which approximated to 70 m/s. The rail road and the vehicle body were both made walls. The surrounding enclosure surfaces, being imaginary surfaces, were all named symmetry planes having a "no slip" condition. The outlet was named a "pressure-outlet" with its pressure set zero and the operating pressure equal to constant atmospheric pressure. Some detail descriptions are listed below.

CFD Solver Fluent Settings Summary

Domain Settings:

Simulation Type: Steady State

Fluid Flow: Incompressible (viscous) Flow

Domain Pressure: 0.1 MPa (1 bar), default

Fluid (Air) properties:

Boundary Conditions:

Inlet Condition: Velocity Inlet: U = -70 m/s (250 km/h)

Outlet Condition: Pressure Boundary: Static, P = 0 Pa, default

Walls Condition: No-slip, Standard Roughness

Viscous Model:

Turbulence Model: High-Re Realizable quadratic k-ε model

Model Constants: Default

Wall Condition: Non equilibrium wall function

Discretization: Second Order Upwind

Solution Procedure: Coupled

Run Precision: Double

Processing: Parallel processing

Table 5: Domain Physics for ICE 2 Regional and for Ethio HST 250.

Domain	Type
Air	Cell

Table 6: Boundary Physics for ICE 2 Regional and for Ethio HST 250.

Domain	ICE 2 Regional Boundaries		Ethio HST 250 Boundaries	
Air	Boundary - ice 2_regional		Boundary - ethio hst 250	
	Type	WALL	Type	WALL
	Boundary - pressure outlet		Boundary - pressure outlet	
	Type	PRESSURE-OUTLET	Type	PRESSURE-OUTLET
	Boundary - rail road		Boundary - rail road	
	Type	WALL	Type	WALL
	Boundary – symmetry		Boundary – symmetry	
	Type	SYMMETRY	Type	SYMMETRY
	Boundary - symmetry side		Boundary - symmetry side	
	Type	SYMMETRY	Type	SYMMETRY
	Boundary - symmetry top		Boundary - symmetry top	
	Type	SYMMETRY	Type	SYMMETRY
	Boundary - velocity inlet		Boundary - velocity inlet	
	Type	VELOCITY-INLET	Type	VELOCITY-INLET

3.3.2 Fluent Solver

For this analysis, a pressure based steady state solver was used. The solution methods, equations used along with the input data are listed below:

- Pressure based steady state solver,
- Realizable k- epsilon model with non-equilibrium wall functions,
- Air velocity at inlet: 250 km/h or 70 m/s,
- Reference area to determine drag and lift coefficients – Frontal Area (of fluent projected area to the axial flow direction): 6.175071 m^2 for ICE-2 Train and 6.2947501 m^2 for Ethio-HST. Note that, these cross sectional area values are half values because of symmetric analysis. Then for full model the reference area will be doubled for each

models, thus 12.350142 m^2 for ICE-2 train and 12.5895002 m^2 for Ethio-HST train respectively.

- The final solution was obtained by performing the iterations in two stages. With each progressive stage, the solver accuracy was raised by employing higher order equations. In the first stage, first order equations were used to prevent the solution from the possibility of divergence. Once sufficient convergence was achieved, the equation order was raised to second order equations. The iterations were carried up to the point where the change in the value of drag coefficient was found negligible.

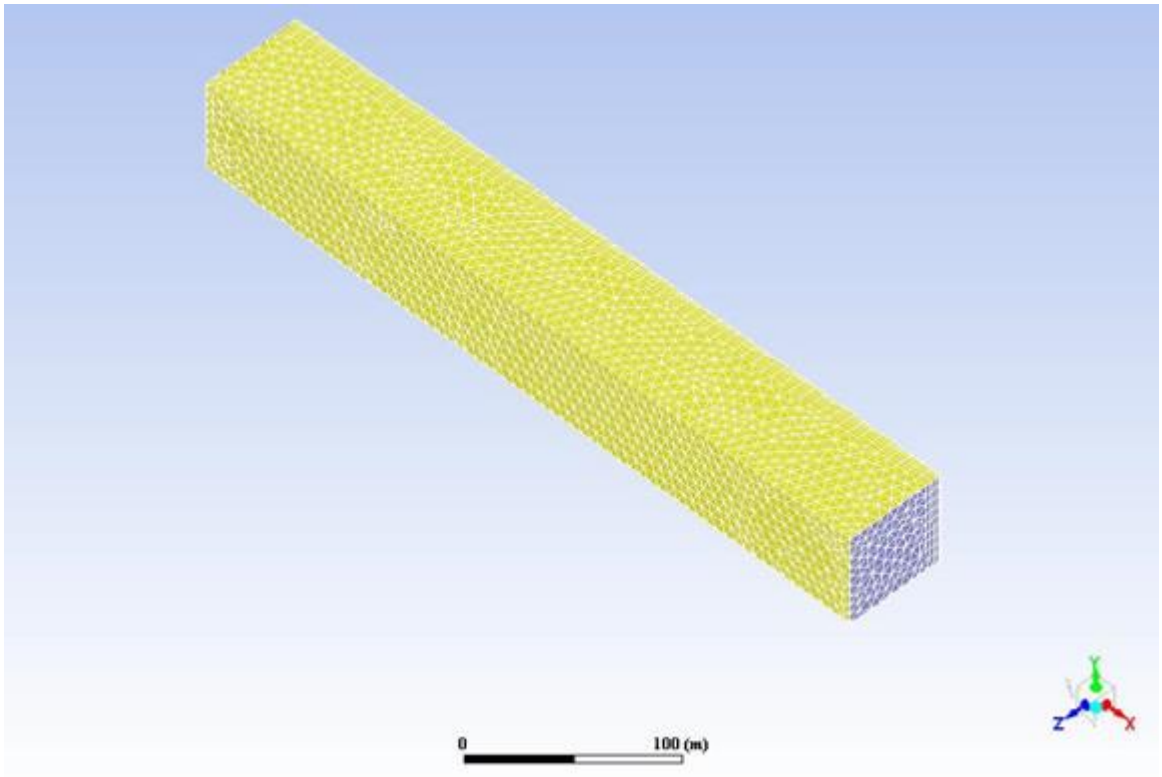

Figure 22: Computational Air domain mesh with colored of symmetry walls and velocity inlet.

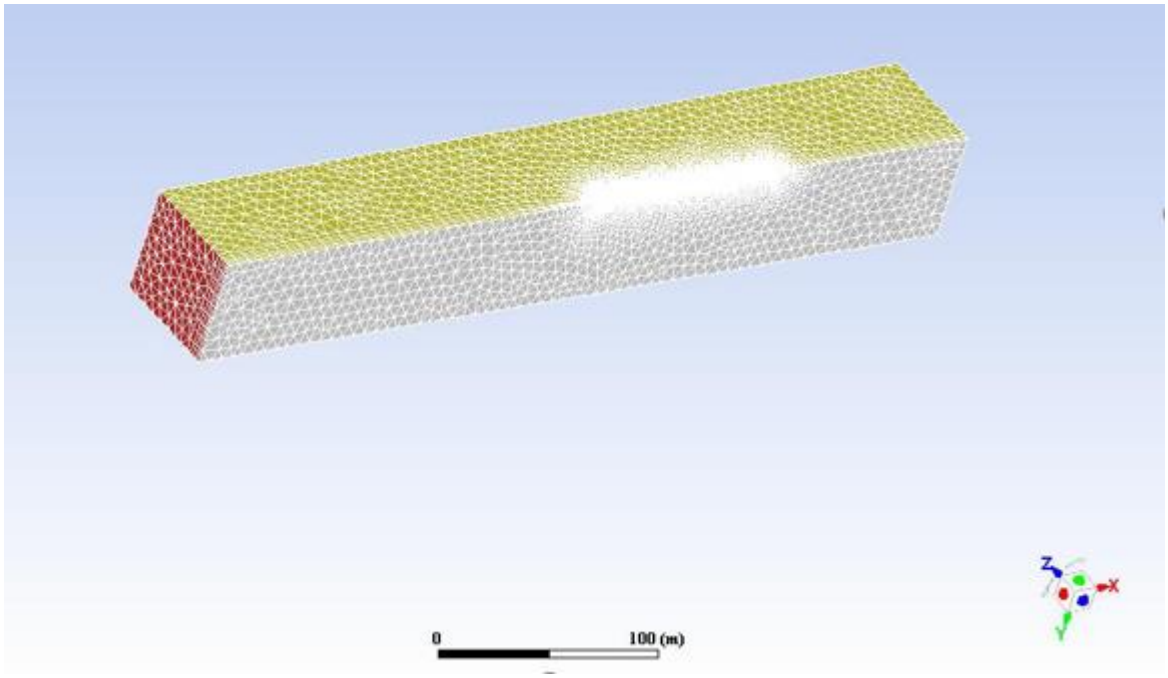

Figure 23: Computational Air domain mesh with colored of symmetry, rail-road walls, train model, and pressure outlet.

3.4 Solution Accuracy

The ICE-2 train from another work shown under Table 1 the coefficient of drag value is 0.69. Using this value, first the accuracy of the CFD simulation will be analyzed with this result for ICE-2 train. Thus the modified train model has identical CFD setup, and then its accuracy will be judged by this. Then compute the percentage of aerodynamic drag within the given accuracy. The simulation of the pantograph system is not included, the percentage of aerodynamic drag of 8–20% is the value shared between pantograph and roof equipment drag [81] will be considered for both the ICE-2 and Ethio-HST models. Thus the value of aerodynamic drag for ICE-2 Train at least should be less than 0.69. If so the accuracy drag coefficient of the other train model (Ethio-HST) will be evaluated in the same manner.

Note that, the train model is not exactly similar with the ICE-2 Train model used in this study. The name ICE-2 trains have some different types but their general external body shape is similar. Thus there is no much effect for external aerodynamic study to use as reference value as the author of the reference also used it as a general ICE. Also the air property and the numerical method used will result difference on parameters. Consideration of their reference area also should be in mind thus the reference area for ICE-2 train of cited document is 10.2 m^2 and for ICE-2 train of this thesis is 12.35 m^2. This much amount of reference area difference is coming from the difference on the models caused by different dimensional approximation as no full dimension is used for the train modeled on this research.

4. CHAPTER FOUR: RESULT AND DISCUSSION

4.1 Results

The output of the simulations parameters described on chapter three can be described possibly in terms of figure, graph, and table and as a summary. The convergence of the simulation is measured by the scaled residuals and the simulation parameters such as coefficient of drag, coefficient of lift and coefficient of moment. Fig. 24 and Fig. 25 shows the convergence of the ICE-2 train and Ethio-HST respectively.

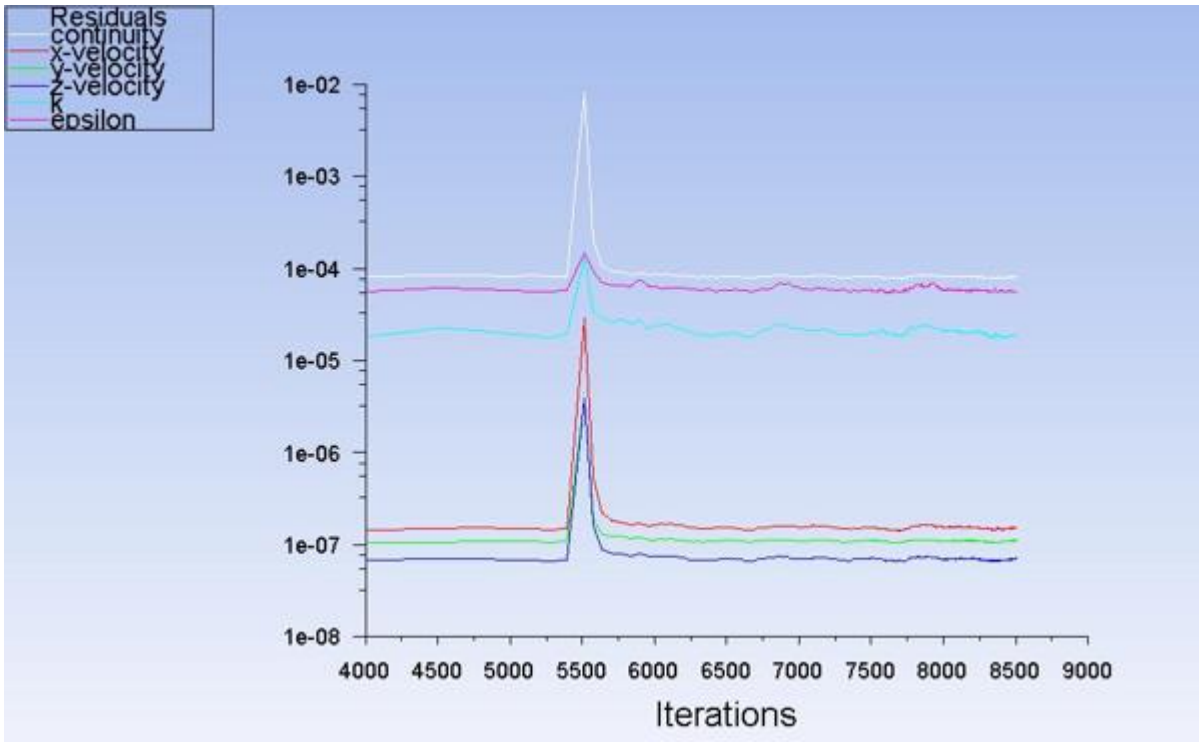

Figure 24: Scale residuals convergence of ICE-2 Train.

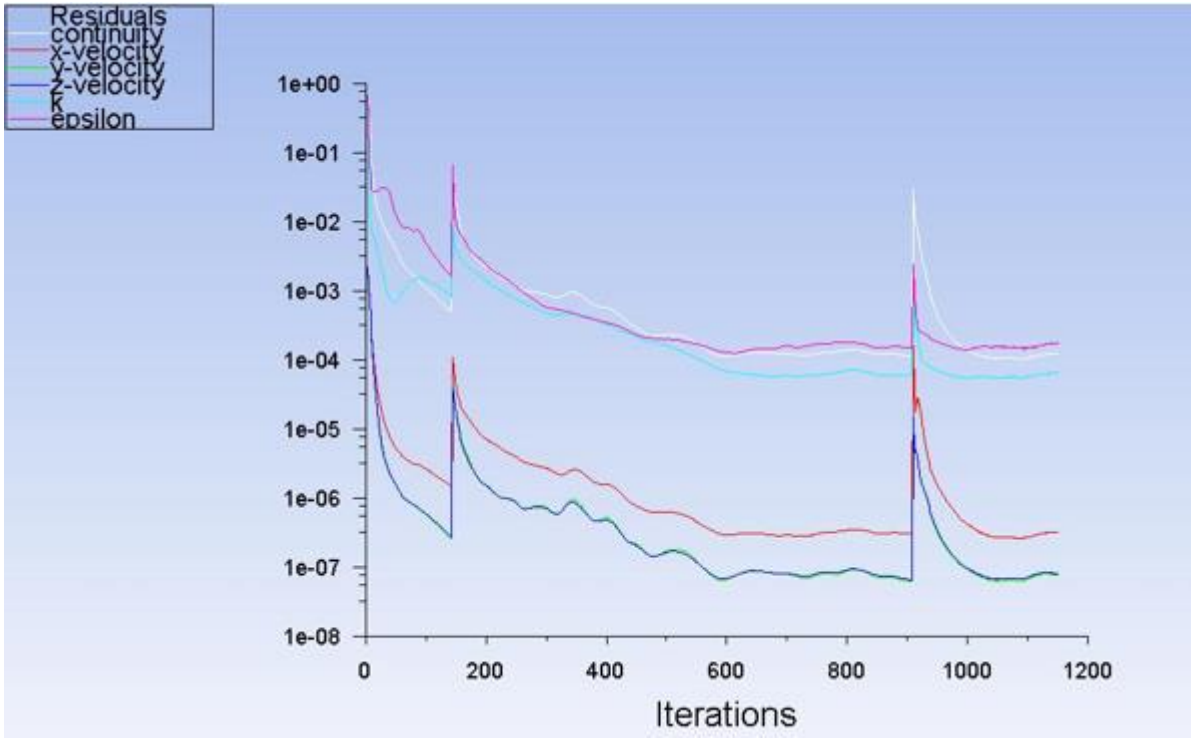

Figure 25: Scale residuals convergence of Ethio-HST Train.

From the above two figures, the convergence for the continuity for ICE-2 train is at the start of the accuracy of 10^{-5} and the beginning of 10^{-4} for Ethio-HST. The fluent default accuracy for continuity residuals is 10^{-3}, thus these convergence iterations for both simulations are enough from engineering respective and computation time cost.

The variation of the graph in the middle way for the two scaled residual graphs is the change of air property values from 15°c to 25°c.Then the iteration from air property at 25°c converges faster than the iteration used for air property of 15°c. because it starts from more converged instant than from starting from the scratch or at the beginning.

The plots of coefficient of drag force, lift force, and moment are plotted using Microsoft excel of line chart type. The data is taken form fluent text (.txt) file results. Note that, almost all parametric values are higher for ICE-2 train than the modified train (Ethio-HST train).

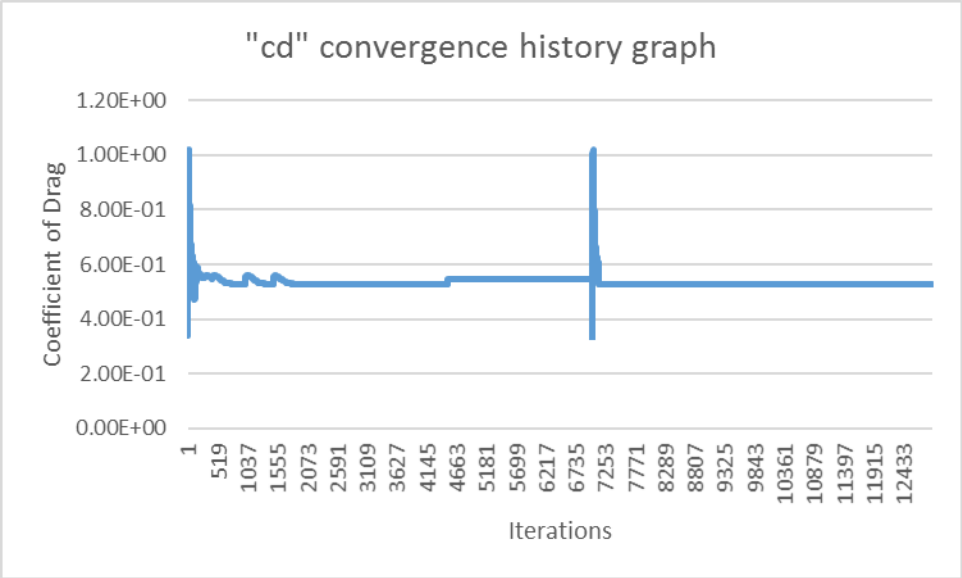

Figure 26: Coefficient of drag force convergence history of ICE-2 Regional Train.

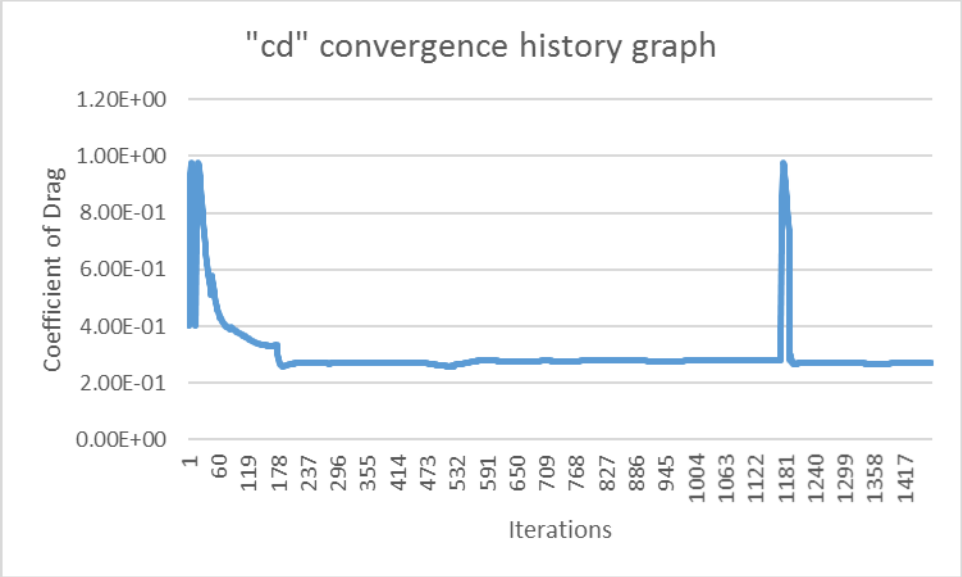

Figure 27: Coefficient of drag force convergence history of Ethio-HST Train.

These two figures of coefficient of drag convergence for both the ICE-2 and the Ethio-HST train models shows the stable state of the coefficient of drag values. Coefficients are parameters which are the one and the major parts of the simulation to evaluate the convergent criterions. The disturbance of the graph is caused by the air property change as discussed on the above paragraphs.

The iteration values of coefficients are not identical with the scaled residuals which is caused by the difference between codes which fluent and excel understands. But excel shows better convergence view. For cross reference the convergence of coefficients plots of fluent will be shown under the appendix.

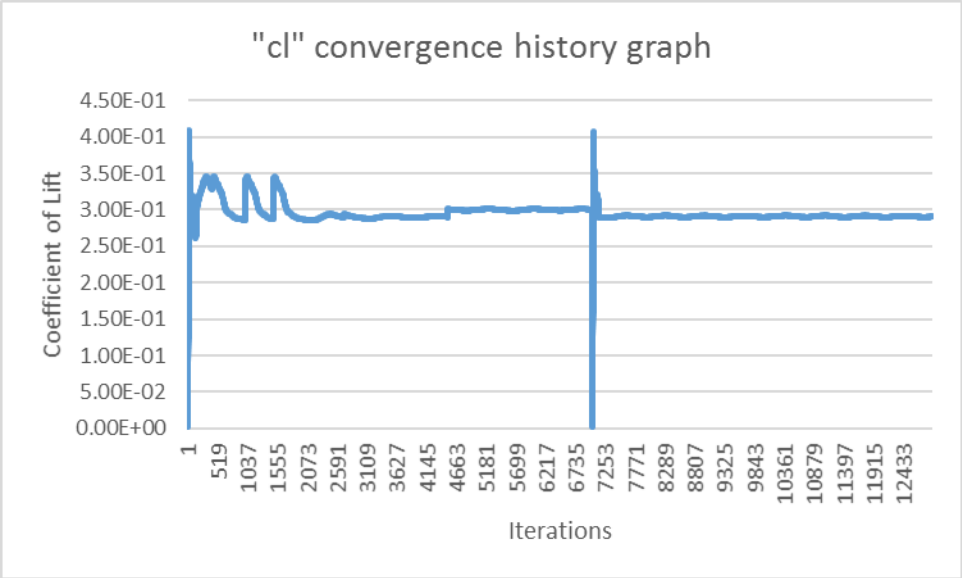

Figure 28: Coefficient of lift force convergence history of ICE-2 Regional Train.

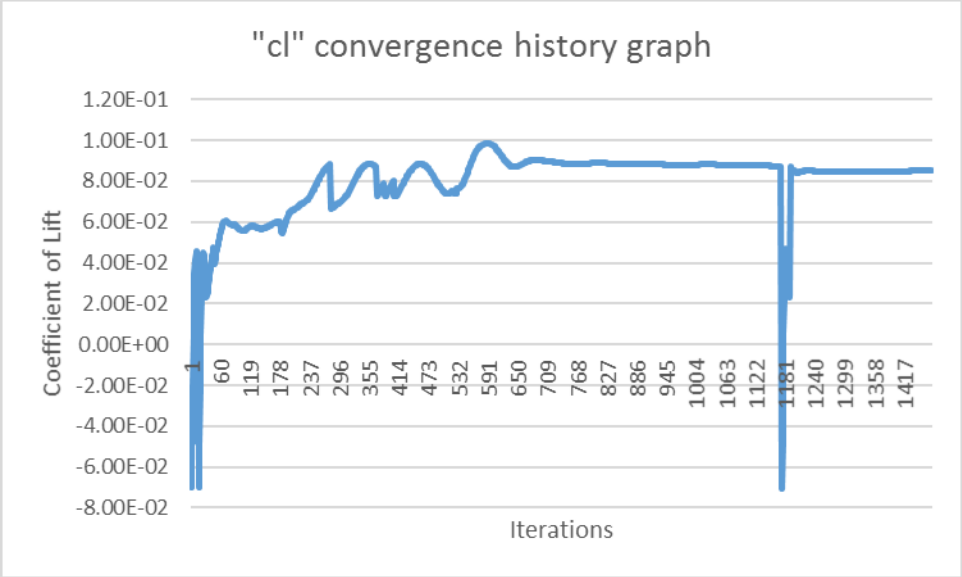

Figure 29: Coefficient of lift force convergence history of Ethio-HST Train.

The coefficient of lift for the ICE-2 train is visibly greater than the Ethio-HST train coefficient of lift. This will afford the stability, safety and comfort of the modified train.

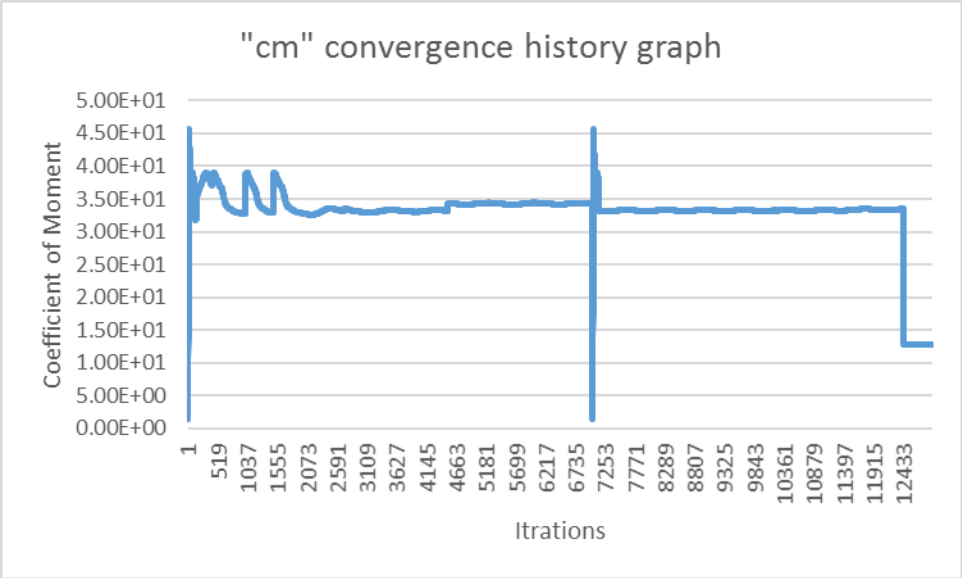

Figure 30: Coefficient of moment convergence history of ICE-2 Regional Train.

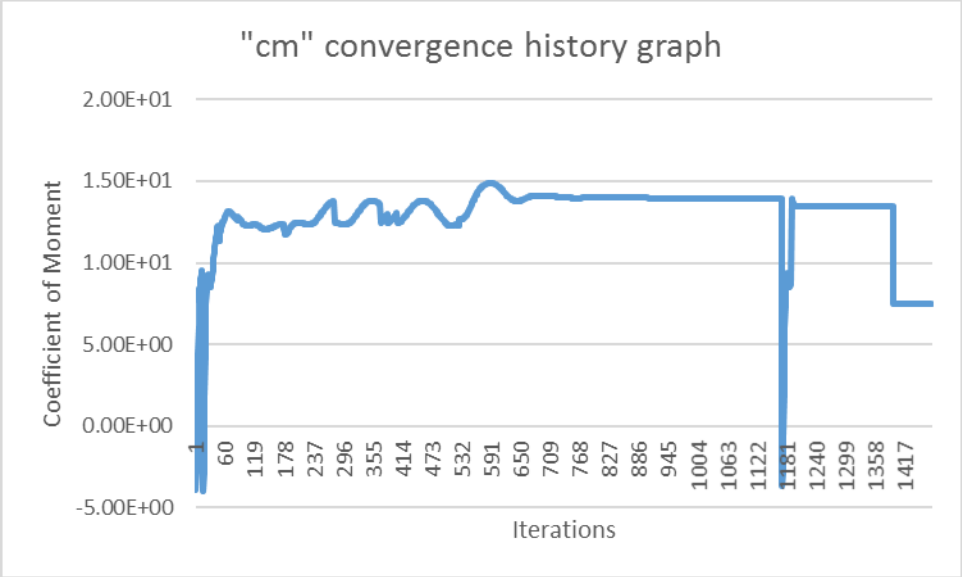

Figure 31: Coefficient of moment convergence history of Ethio-HST Train.

The coefficient of moment on the lateral axis will lead pitching effect. Thus the ICE-2 train have higher coefficient of moment than the Ethio-HST and it would have higher pitching moment. This can lead vibration, passenger discomfort and became cause of derailment as the contact of rail and wheel becomes interrupted. Note that, in addition to air property change, the moment center change to the center of the train leads to the change in coefficient of moment to the last of moment convergence history for both train models.

The following graph depicts pressure coefficient for the two train models. The general profile is the same form the train head to train tail for both models, but the variation for ICE-2 train is higher than the Ethio-HST train.

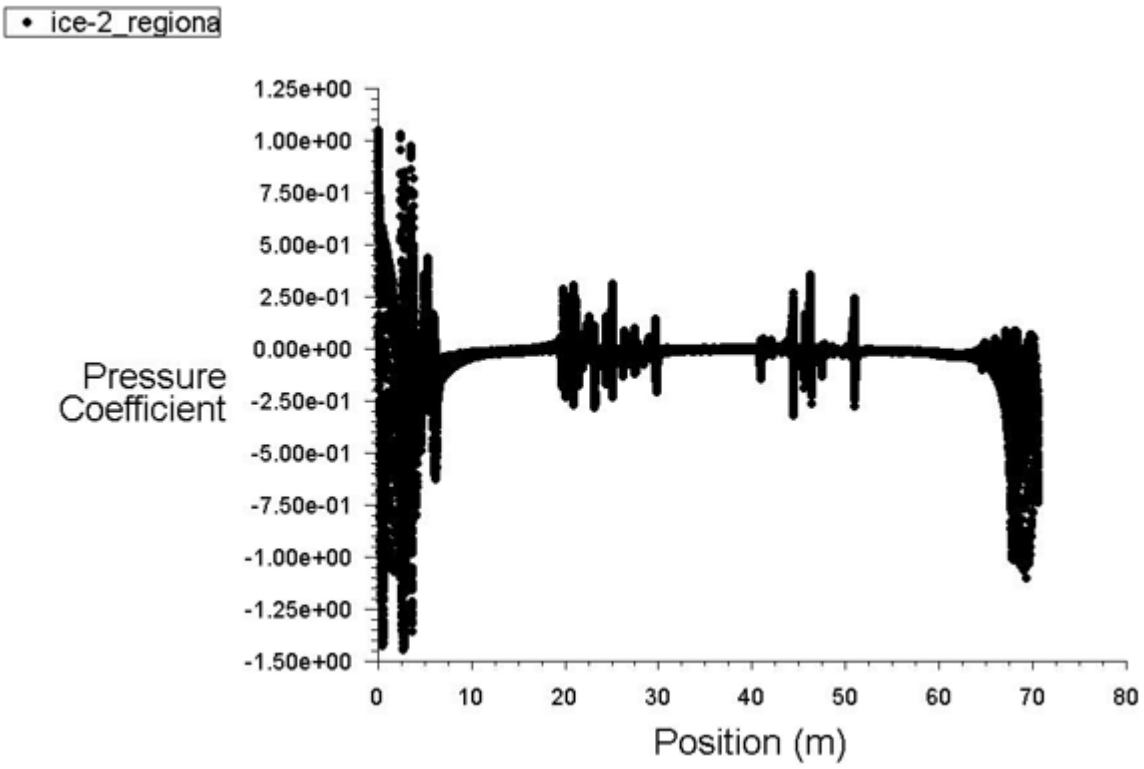

Figure 32: Pressure coefficient plot of ICE-2 Train model.

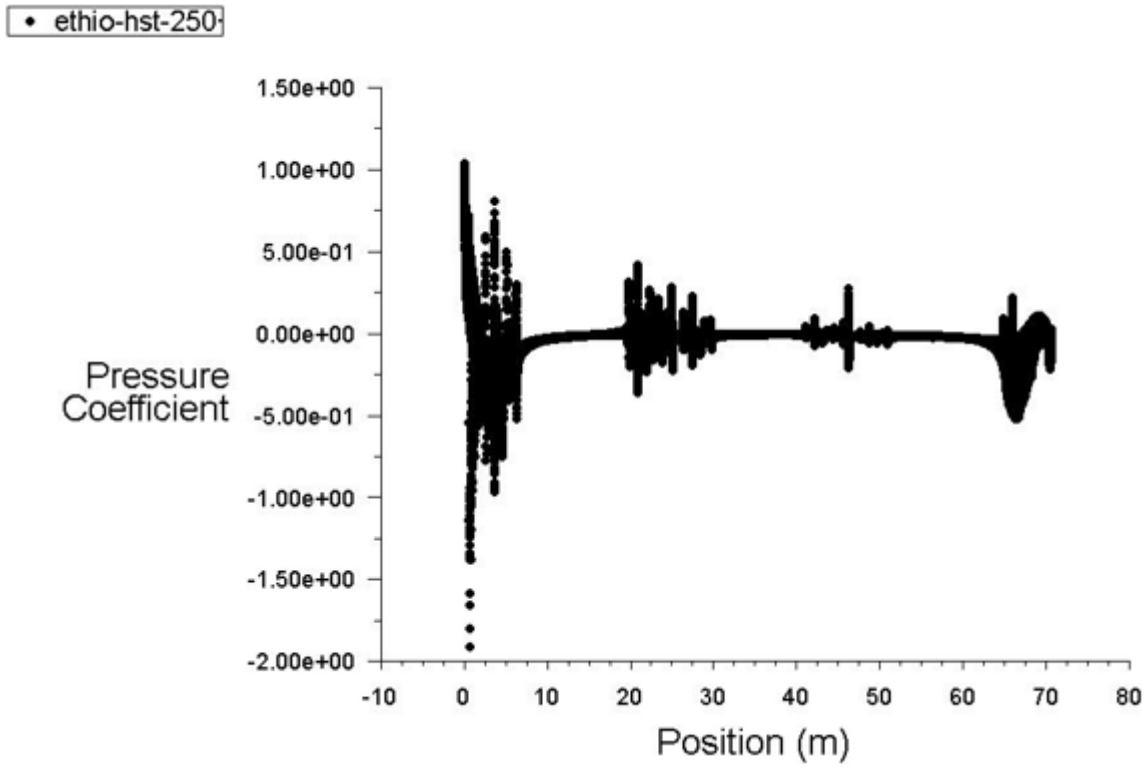

Figure 33: Pressure coefficient plot of Ethio-HST Train model.

The graphs of vectors and contours of velocity magnitude and contours static pressure of both train models will be plotted in full page for each pictures shown below. The general description will be after the plot of these pictures for the convenience of effective page use.

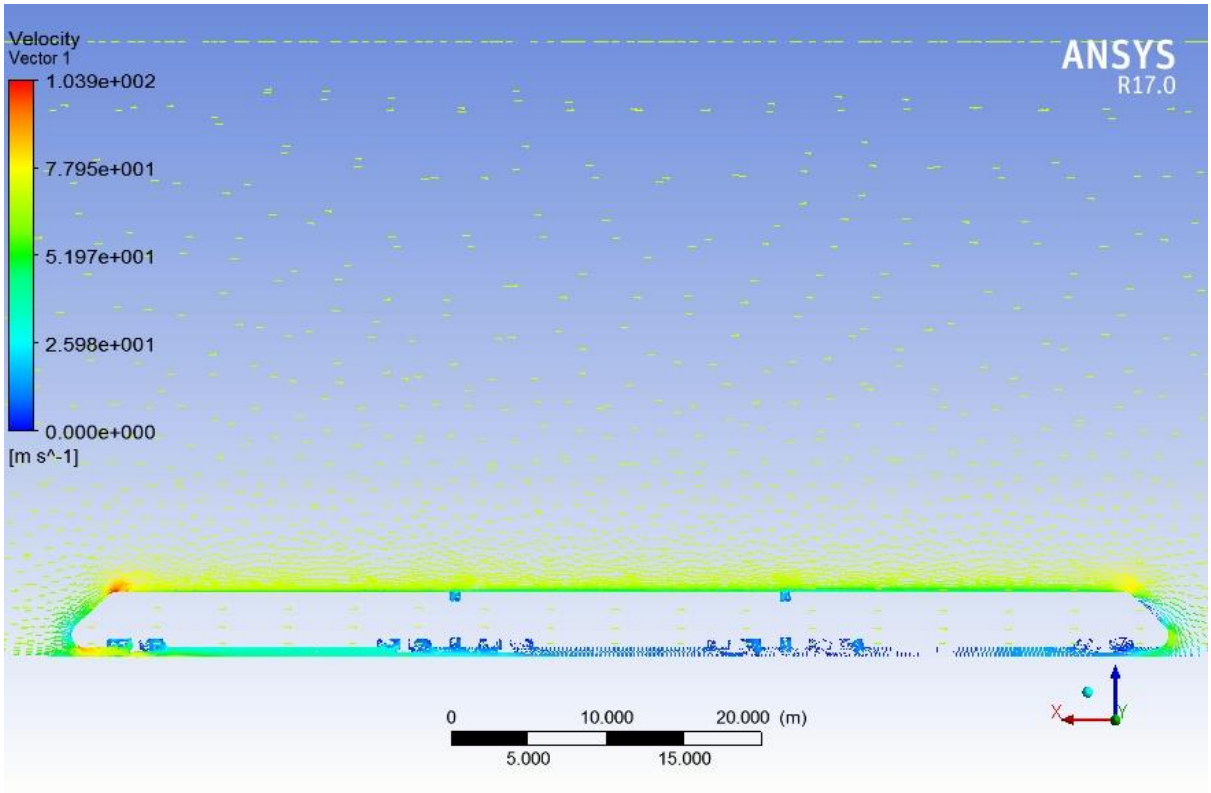

Figure 34: ICE-2 Regional Train Velocity Magnitude Vector Profile (m/s).

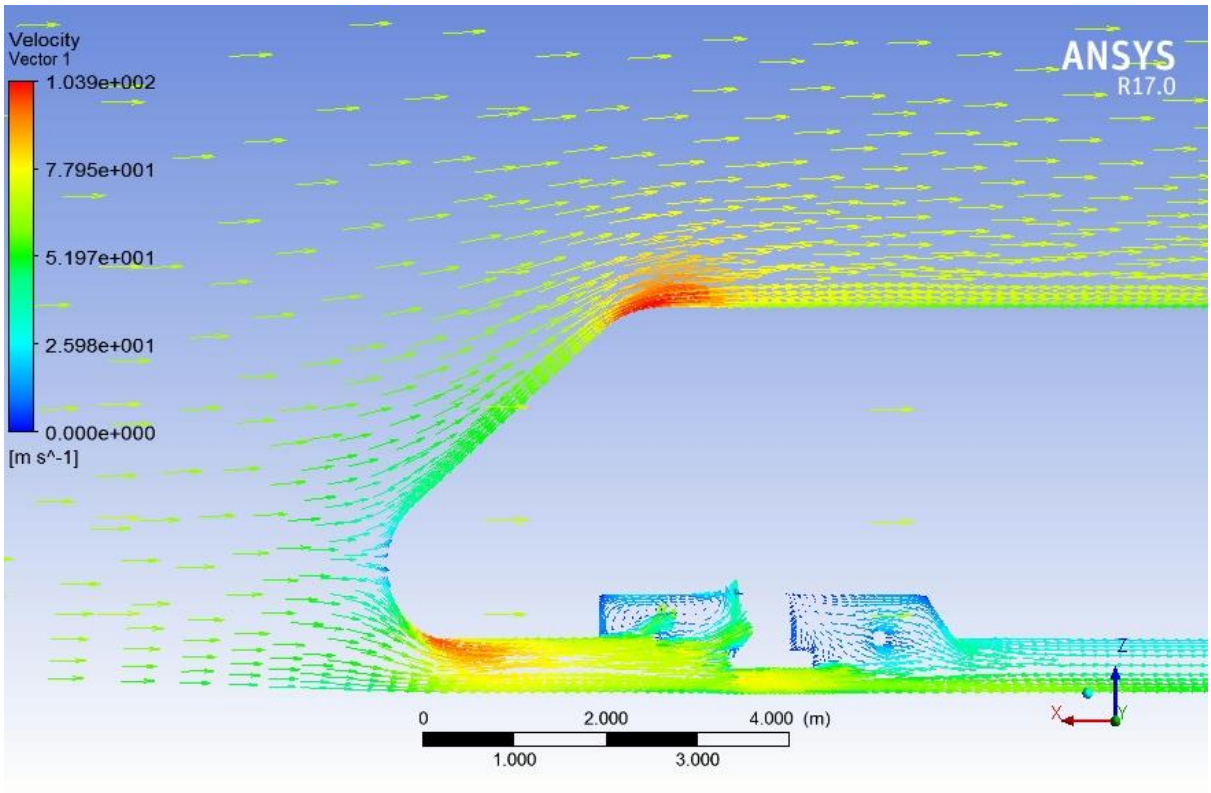

Figure 35: ICE-2 Regional Nose Region Velocity Magnitude Vector Profile (m/s).

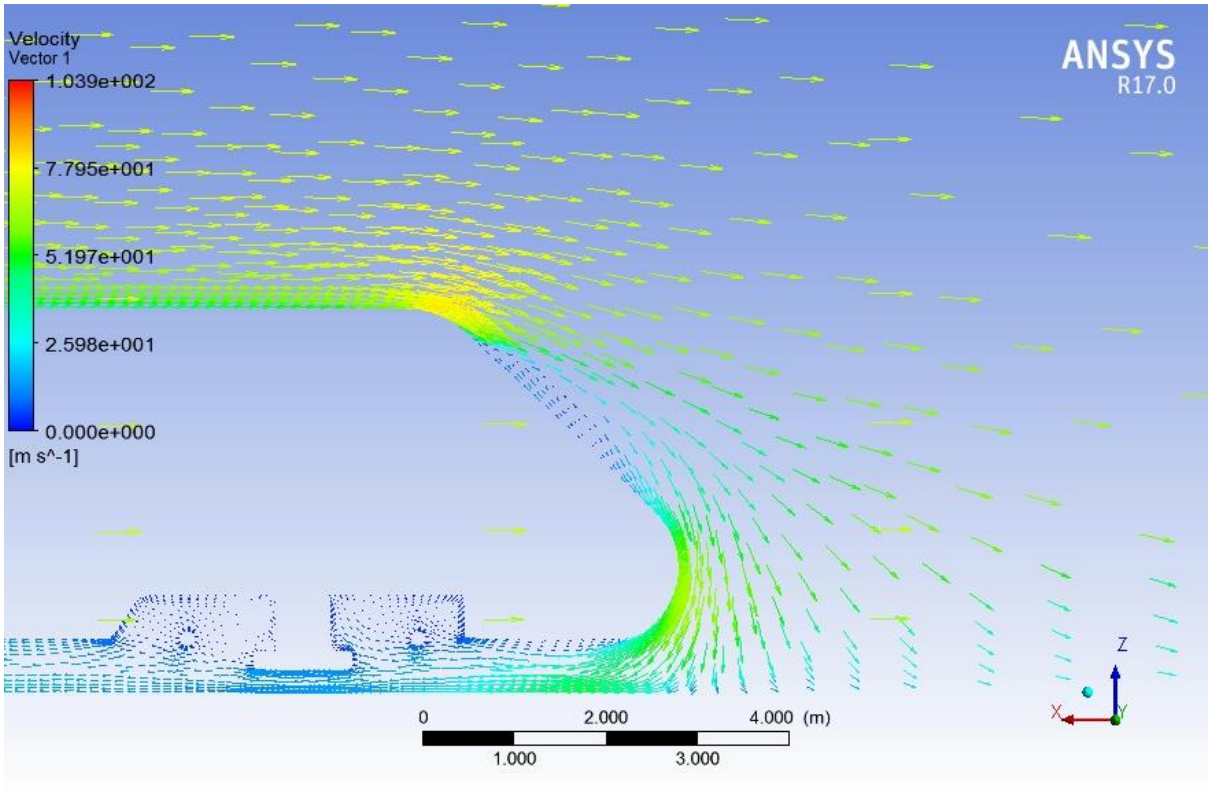

Figure 36: ICE-2 Regional Wake Region Velocity Magnitude Vector Profile (m/s).

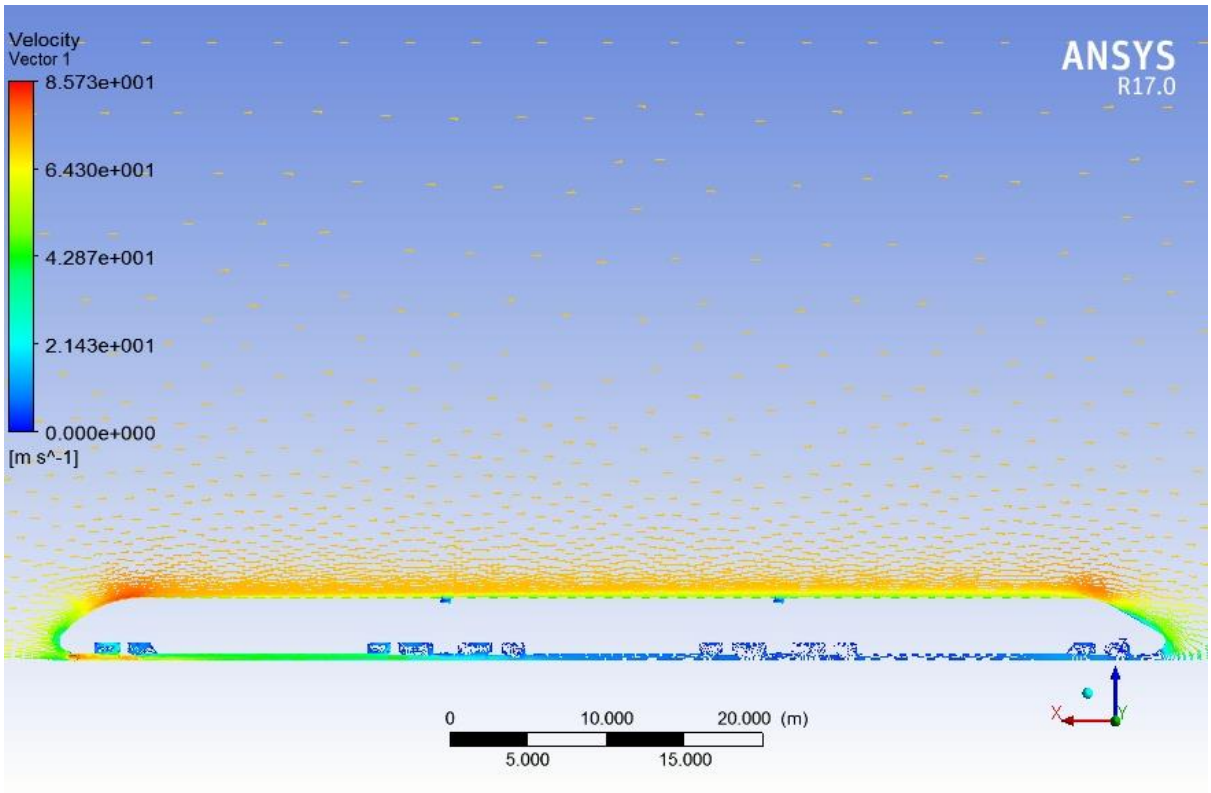

Figure 37: Ethio-HST-250+ Train Velocity Magnitude Vector Profile (m/s).

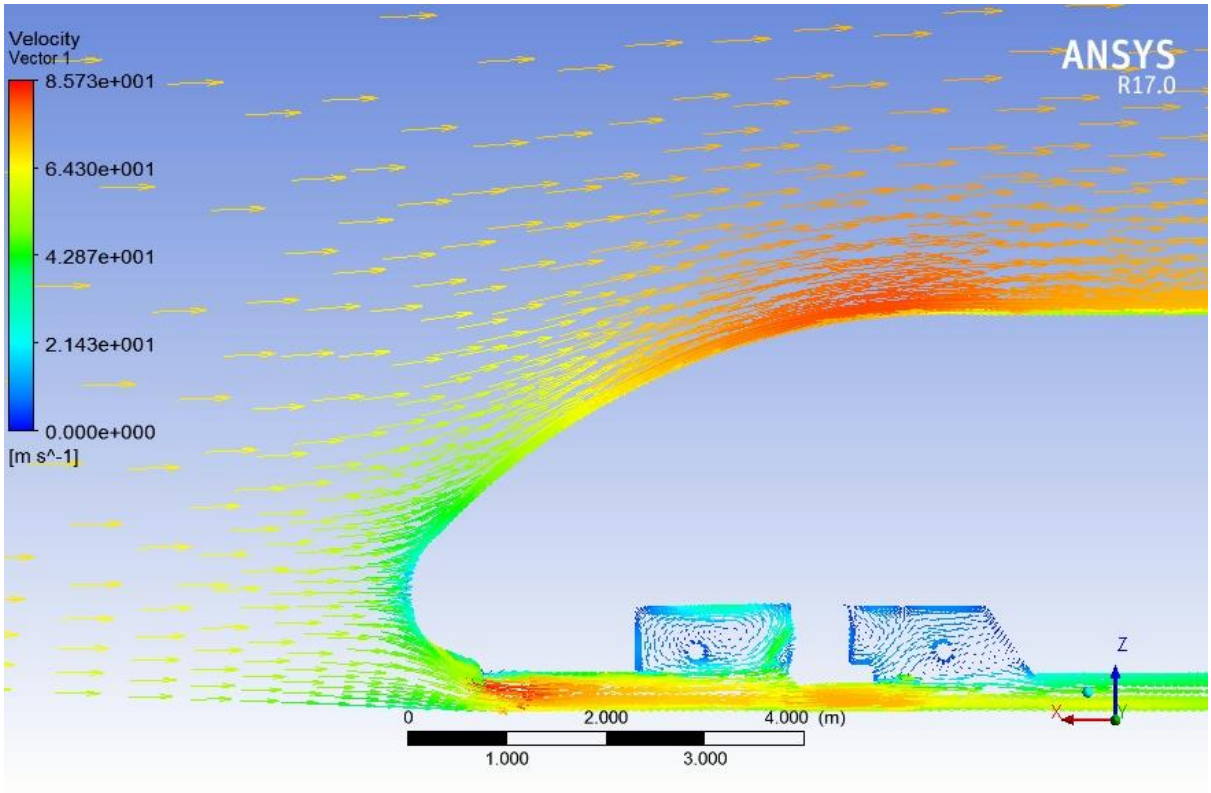

Figure 38: Ethio-HST-250+ Train Nose Region Velocity Magnitude Vector Profile (m/s).

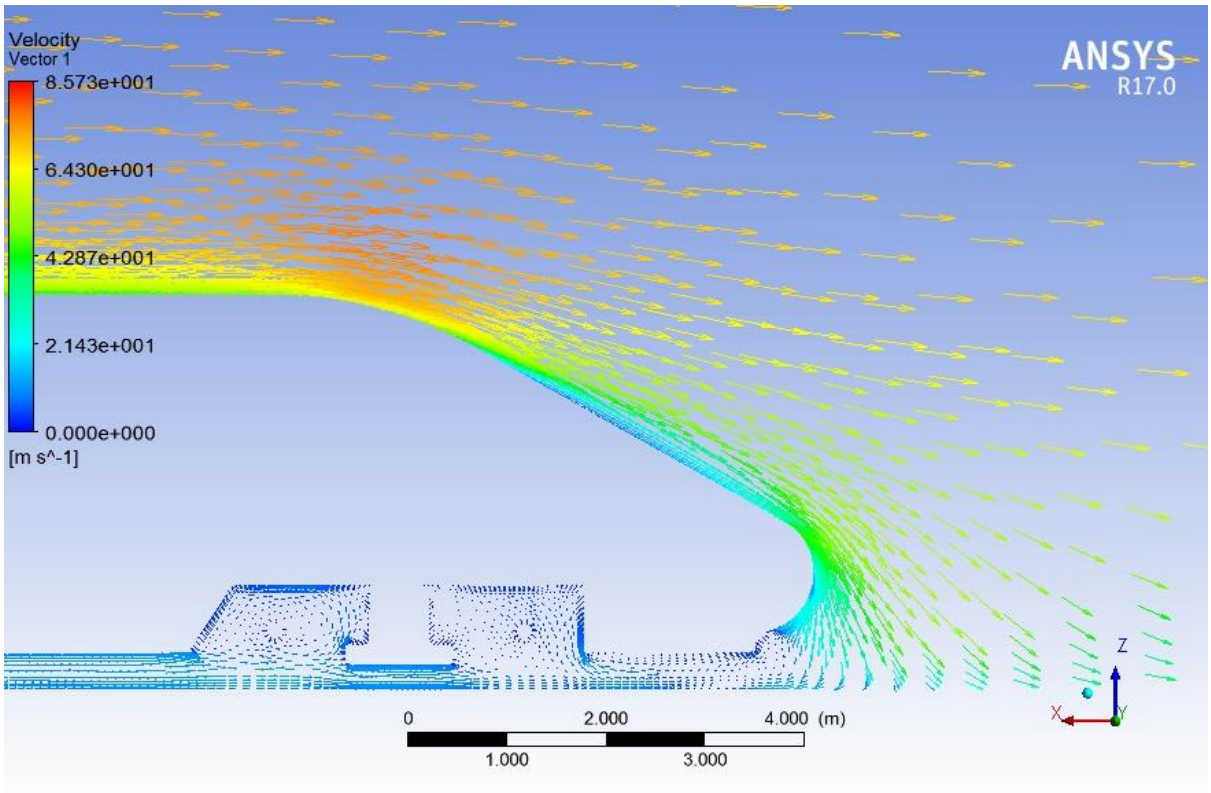

Figure 39: Ethio-HST-250+ Train Wake Region Velocity Magnitude Vector Profile (m/s).

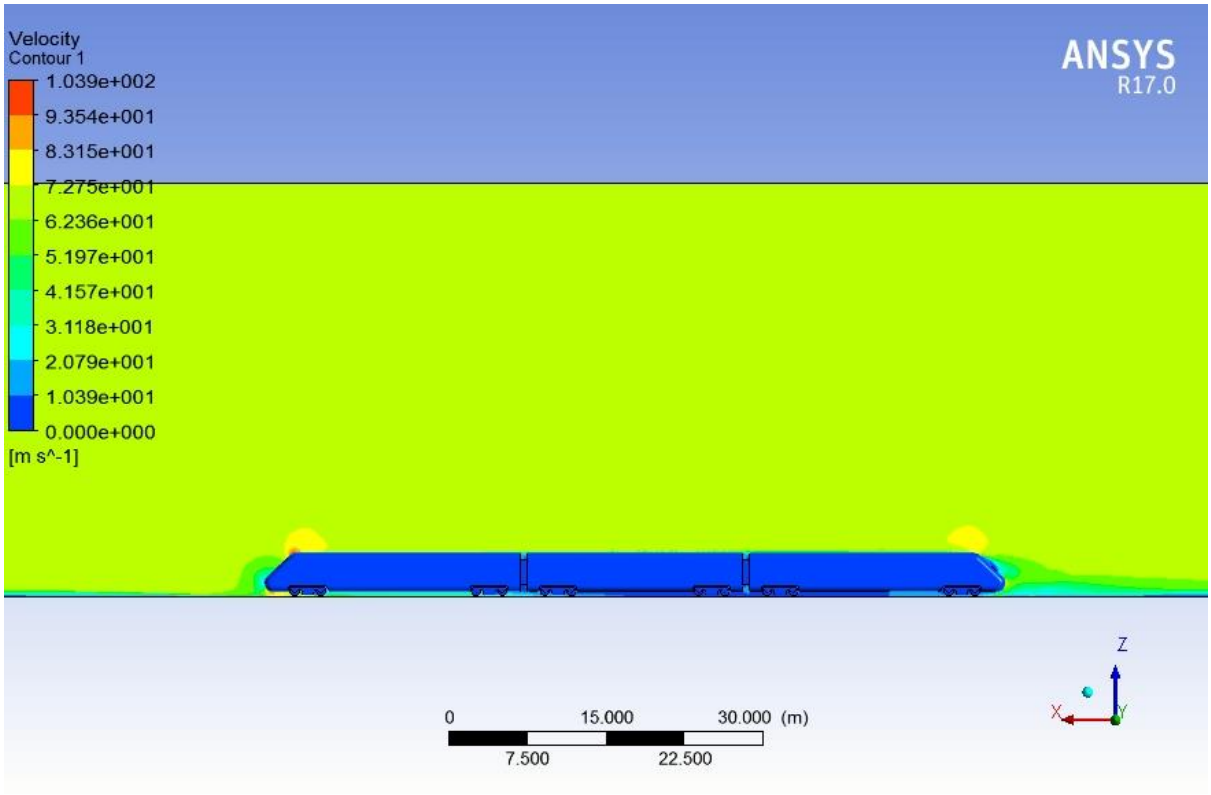

Figure 40: ICE-2 Regional Train Velocity Magnitude Contour Profile (m/s).

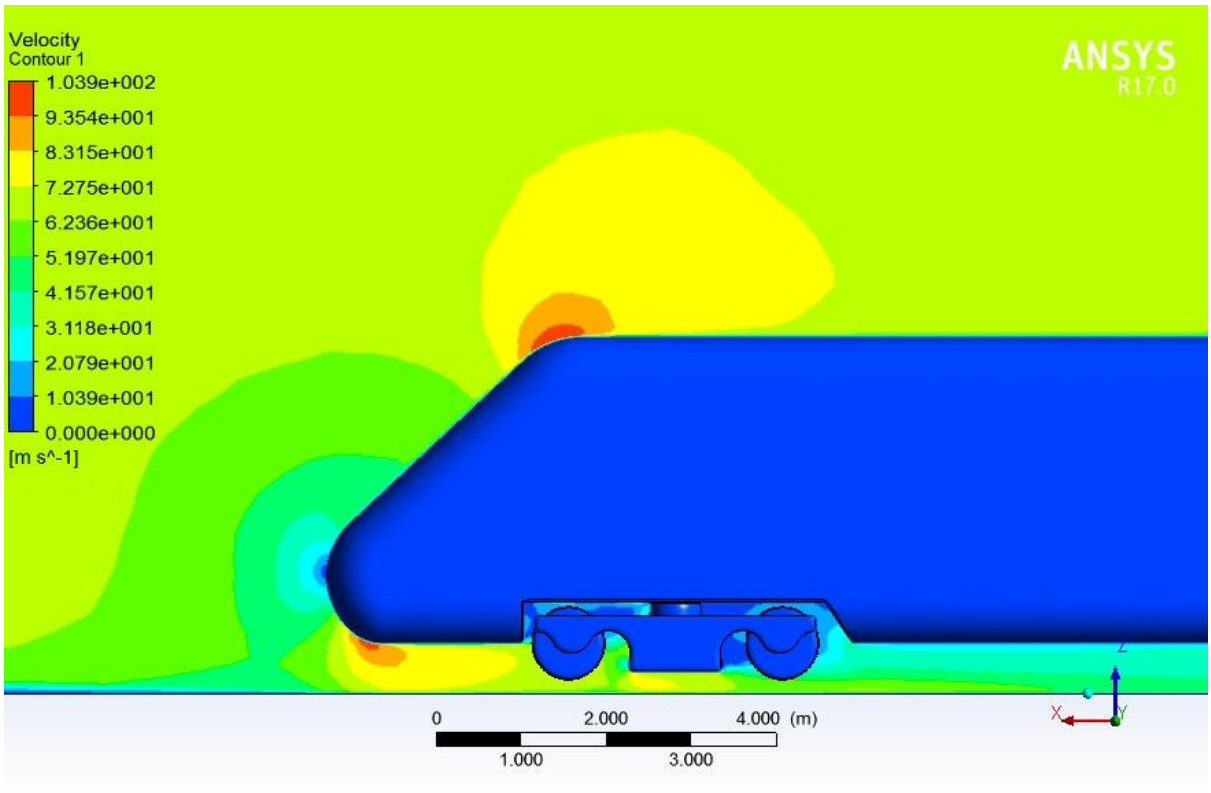

Figure 41: ICE-2 Regional Nose Region Velocity Magnitude Contour Profile (m/s).

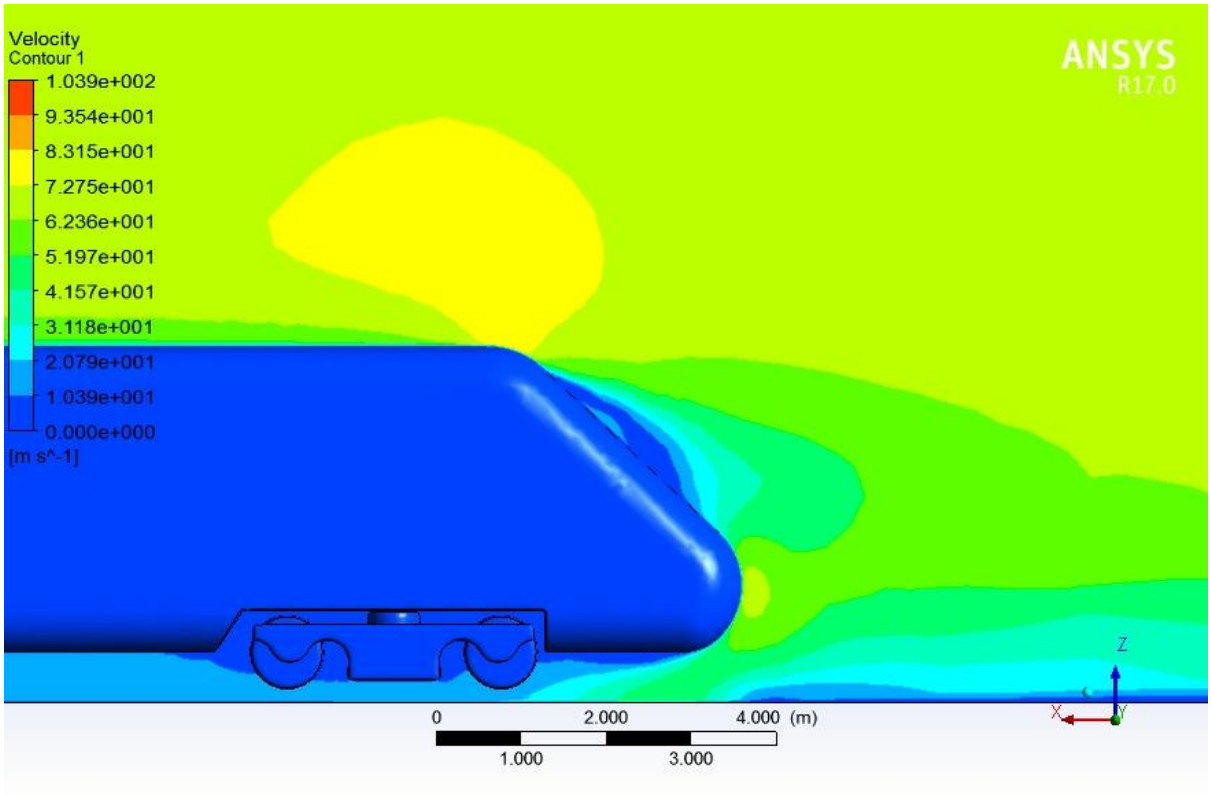

Figure 42: ICE-2 Regional Wake Region Velocity Magnitude Contour Profile (m/s).

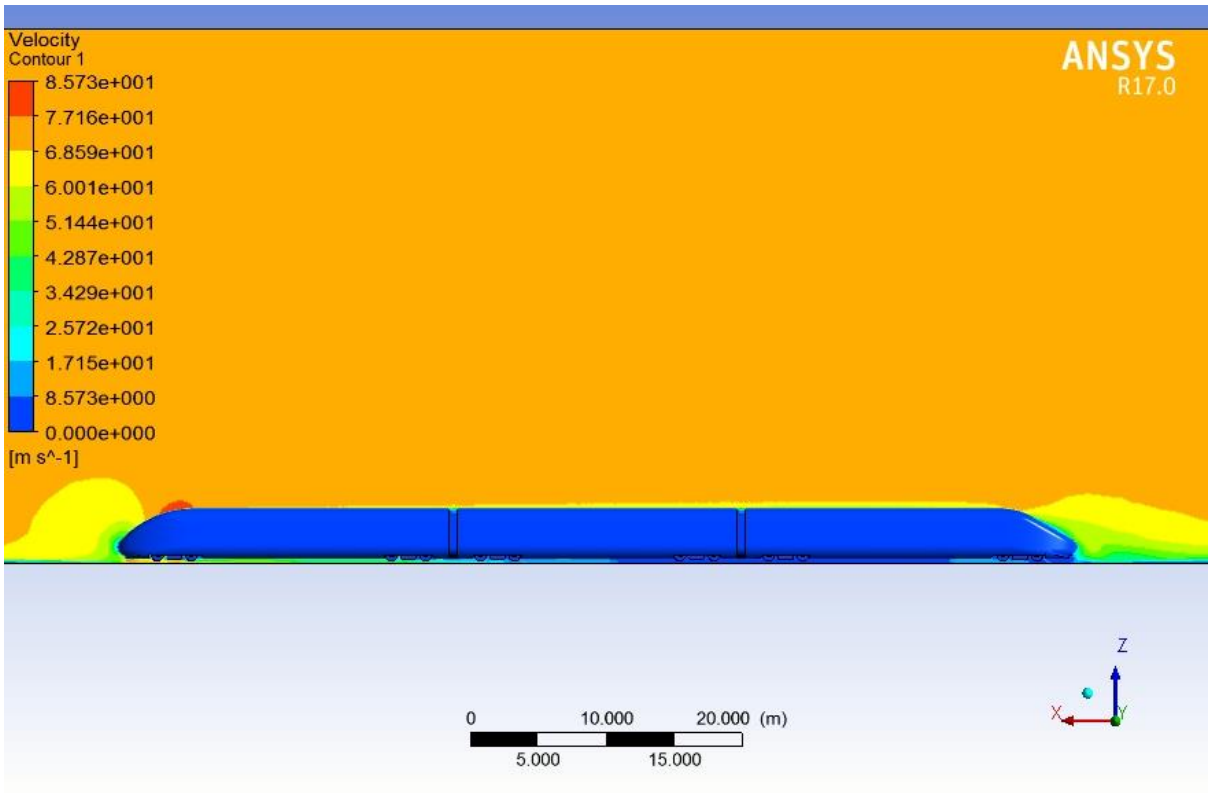

Figure 43: Ethio-HST-250+ Train Velocity Magnitude Contour Profile (m/s).

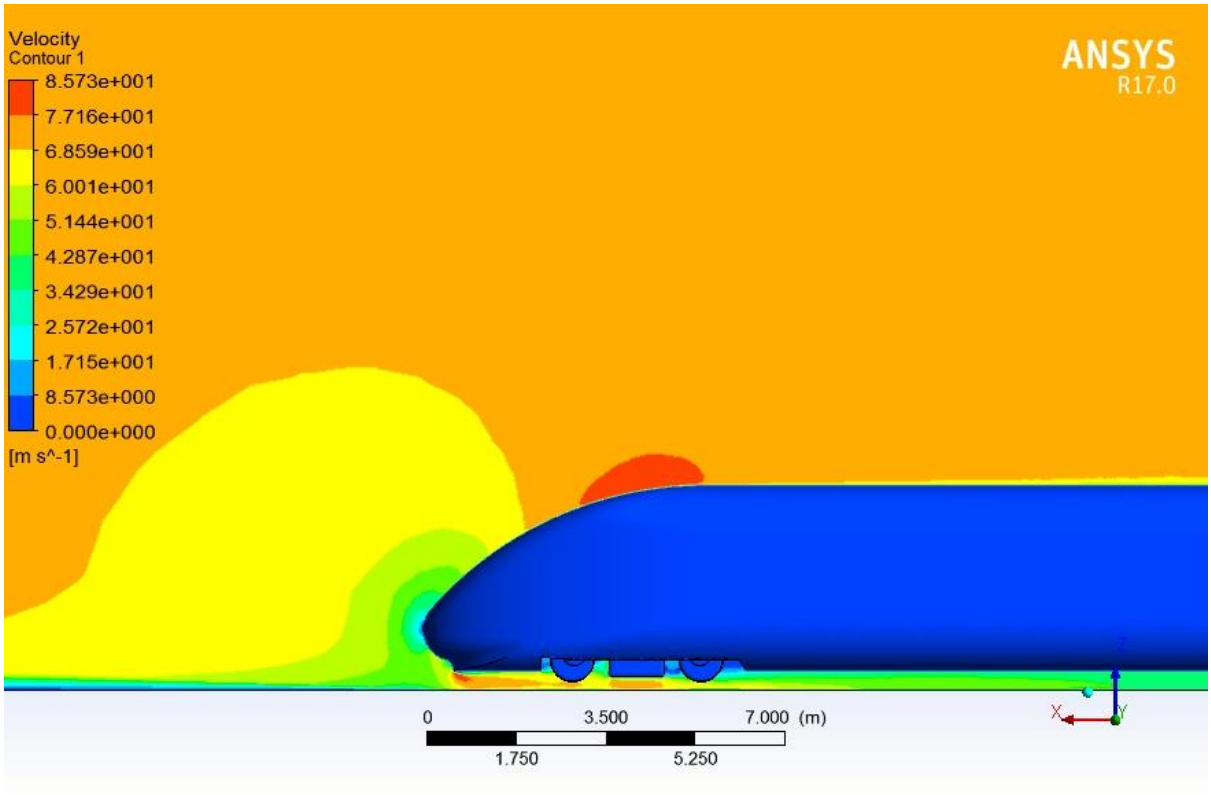

Figure 44: Ethio-HST-250+ Train Nose Region Velocity Magnitude Contour Profile (m/s).

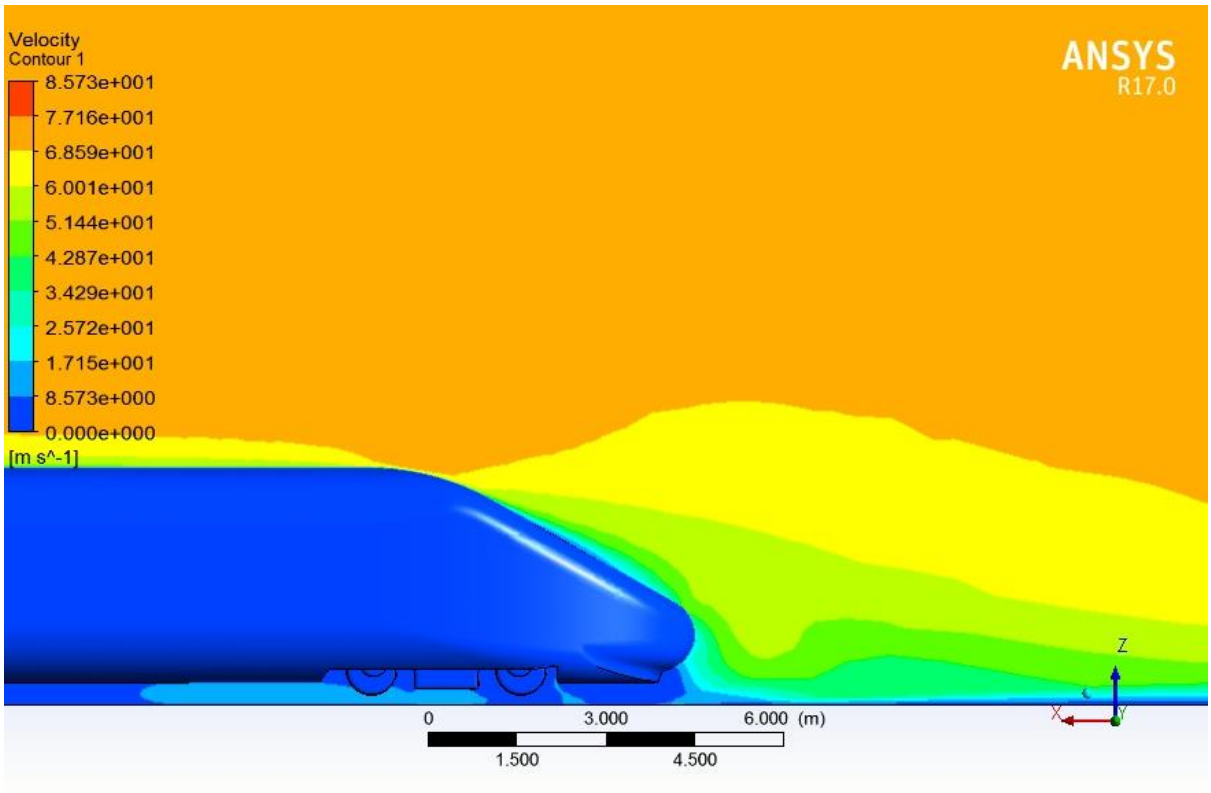

Figure 45: Ethio-HST-250+ Train Wake Region Velocity Magnitude Contour Profile (m/s).

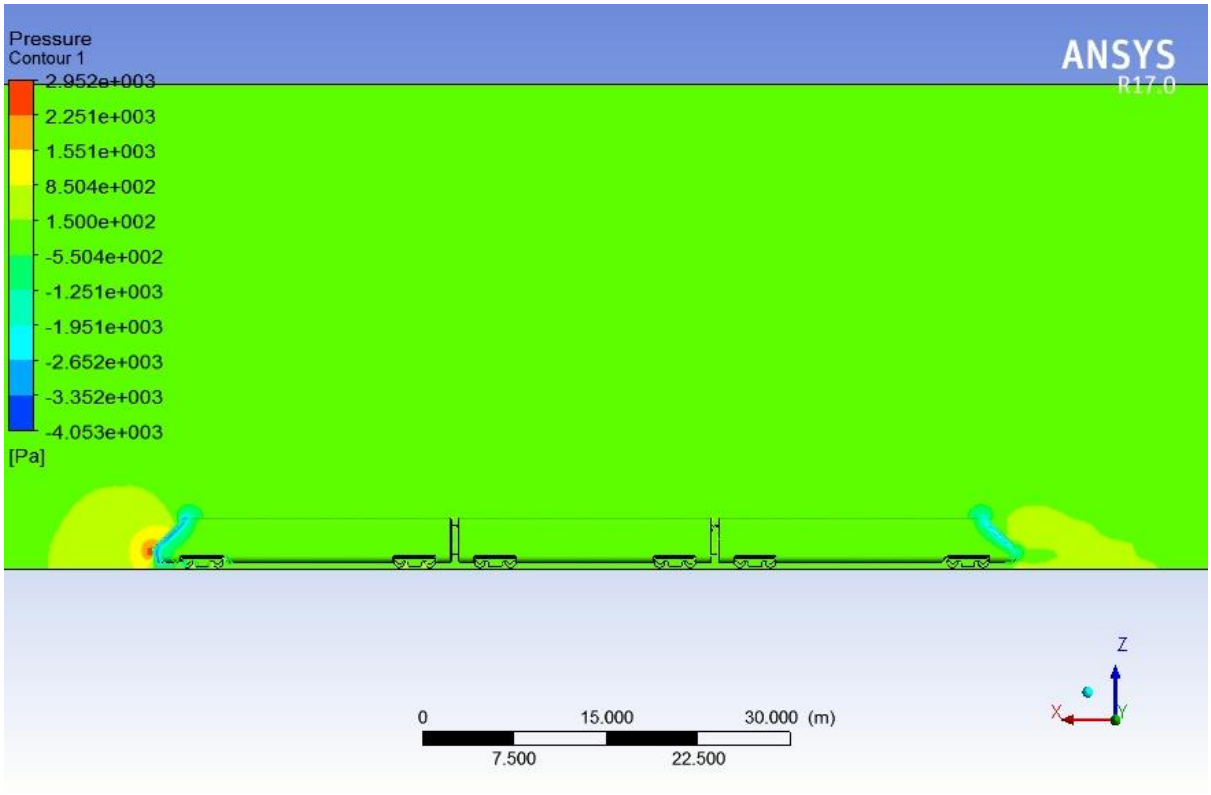

Figure 46: ICE-2 Regional Train Static Pressure Contour (Pascal).

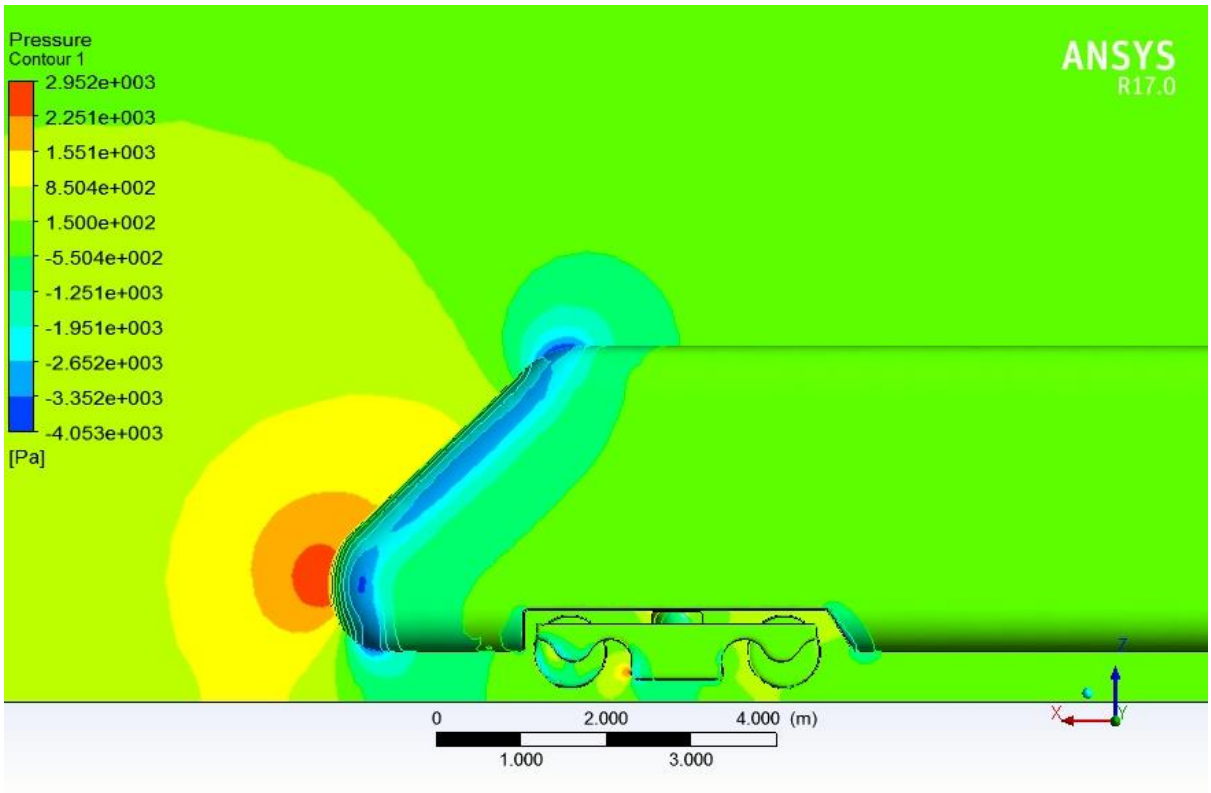

Figure 47: ICE-2 Regional Train Nose Region Static Pressure Contour (Pascal).

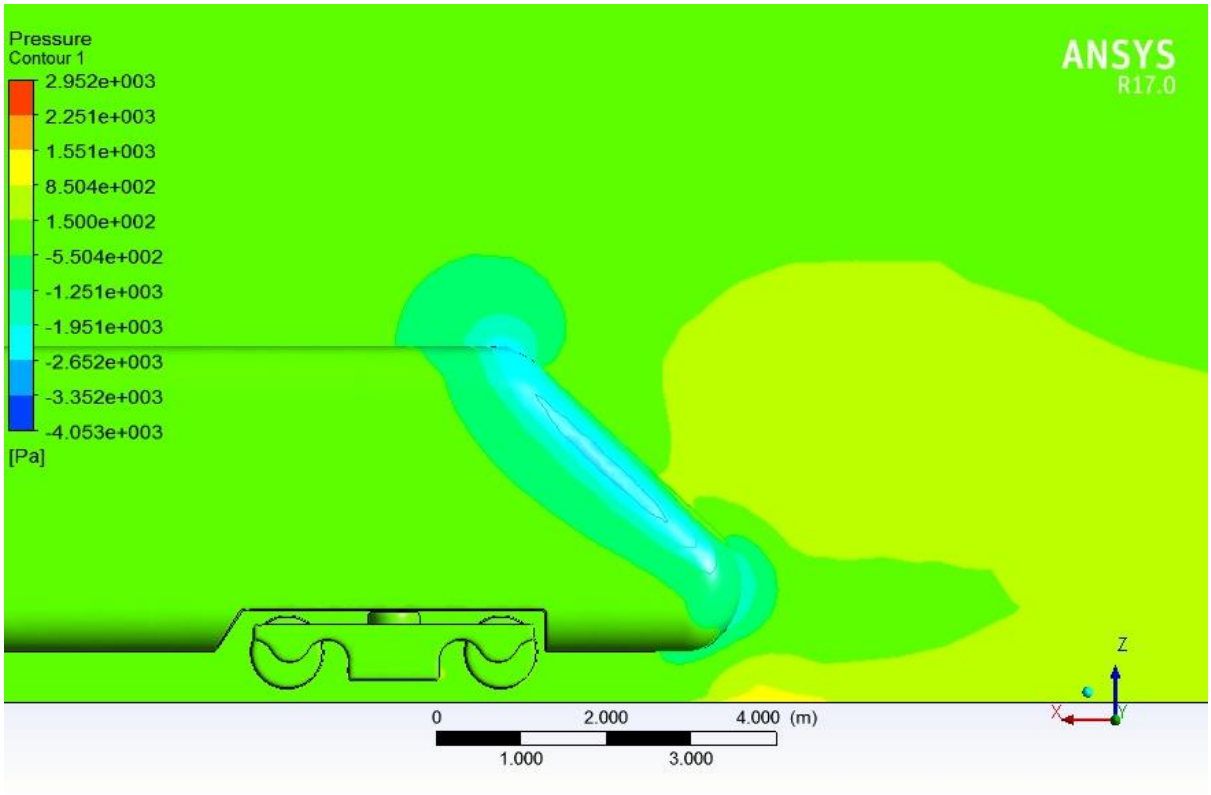

Figure 48: ICE-2 Regional Train Wake Region Static Pressure Contour (Pascal).

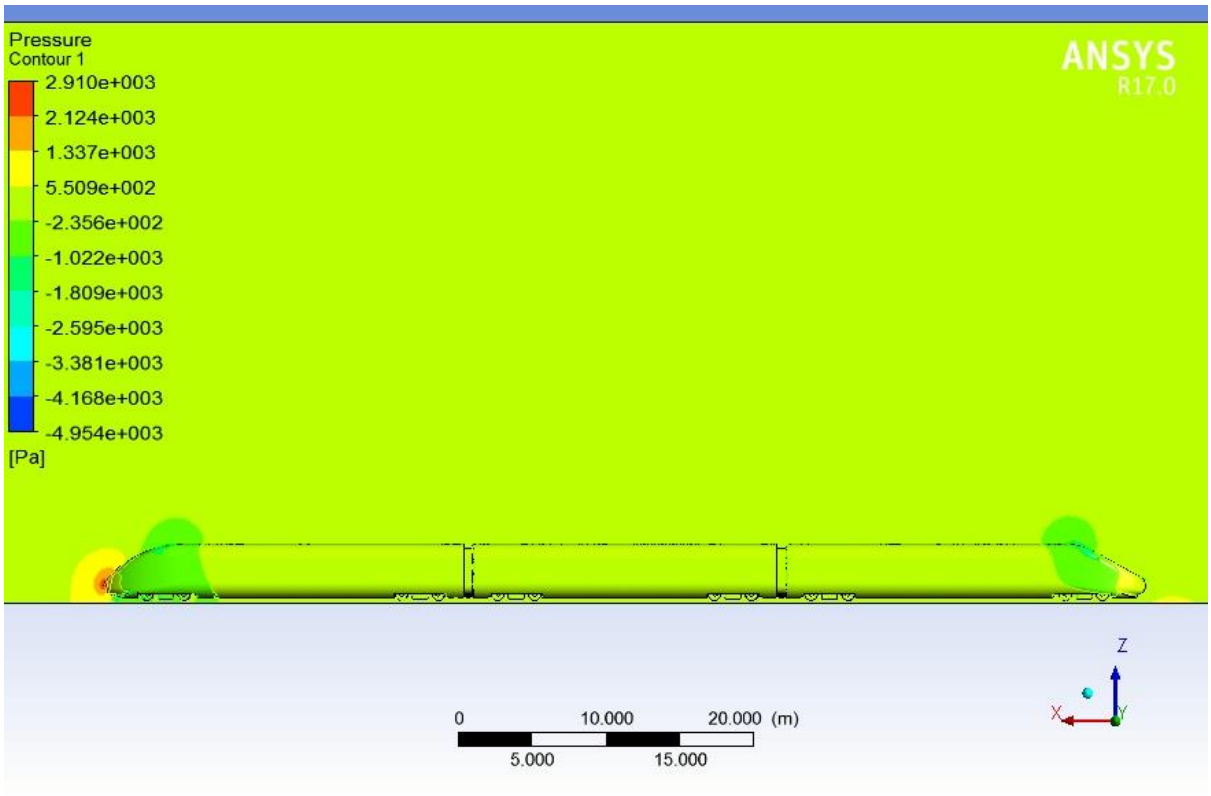

Figure 49: Ethio-HST-250+ Train Static Pressure Contour (Pascal).

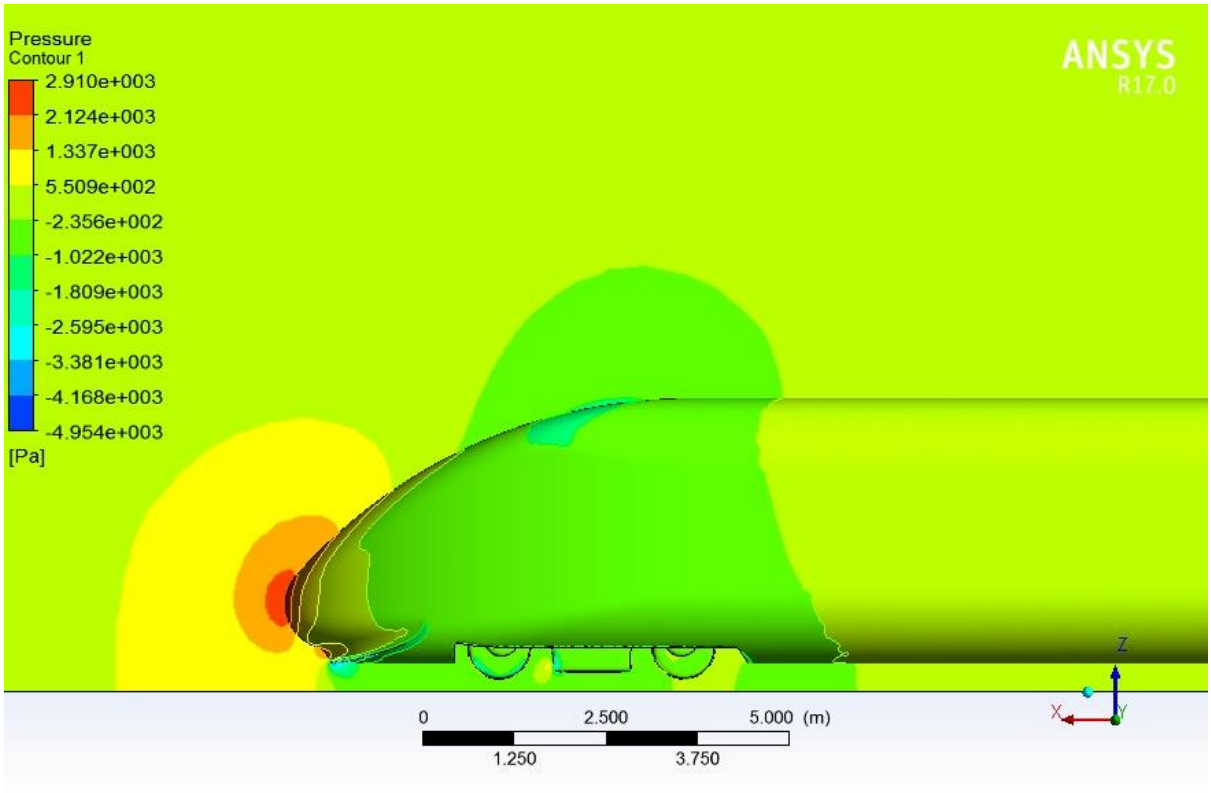

Figure 50: Ethio-HST-250+ Train Nose Region Static Pressure Contour (Pascal).

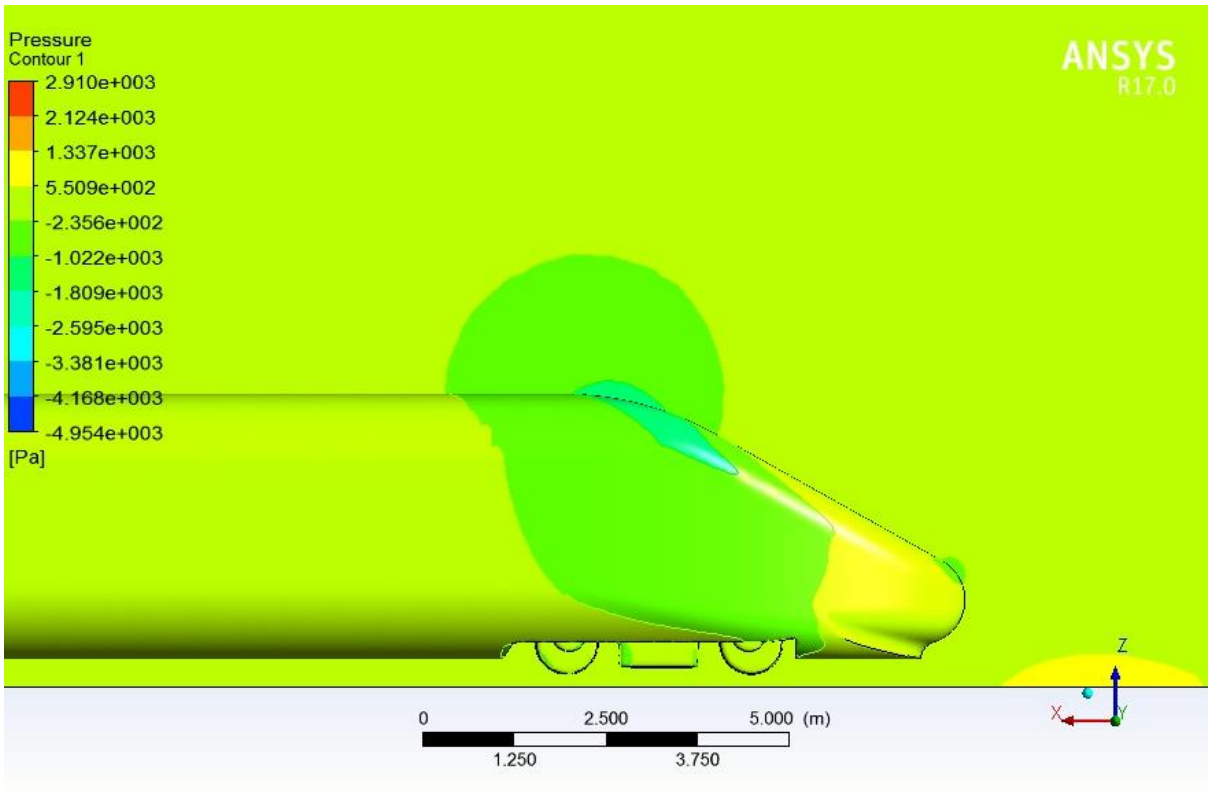

Figure 51: Ethio-HST-250+ Train Wake Region Static Pressure Contour (Pascal).

The plot of velocity magnitude shows; the ICE-2 train have higher value at the tip of the nose head of the train colored by dark red color as the sudden profile change is exists. On the other

most parts of the train model's body parts, the velocity magnitude for the Ethio-HST train is equal or greater than the ICE-2 train. This will cause for aerodynamic drag reduction for the Ethio-HST train with smooth curving profile and will have higher mean velocity magnitude. The ICE-2 train have higher range of maximum velocity magnitude at the sharp corners, but Ethio-HST have higher mean velocity magnitude where at smooth profiles. Actually Ethio-HST have tendency of greater velocity magnitude than ICE-2 for most places of the train model except the places where ICE-2 train having sharp curving (e.g., upper nose tip of the train). Note that, the higher velocity magnitude of ICE-2 train at the upper nose head tip is caused by sudden profile change (being less streamlined). But, Ethio-HST train is more streamlined allover aerodynamically shaped than the ICE-2 train thus the mean velocity magnitude is higher on smooth places and this is proof of the smooth flow and less disturbance.

The pressure magnitude of static pressure contours of the two train models of the above graphs shows, the critical places of the train models where the pressure will be higher at low velocity magnitude. As the velocity vectors and contours shows, where the maximum velocity magnitude is indicated, the ICE-2 train will have higher velocity on short and sharp corners where the compressed air caused by highest pressure of upstream areas of the sharp corner forces to accelerate, then it will also have lowest pressure at there. But, Ethio-HST have smooth and long curving and it will have low pressure over there, thus overall pressure magnitude will be reduced for train having more smooth flow. Note that, at the place of train model where velocity is higher indicating less pressure, and for places with less velocity magnitude will have higher pressure value in general. Thus from the above paragraph, the mean velocity of critical places of described above is higher for Ethio- HST train than ICE-2 train. This will indicate the mean pressure value of ICE-2 train is higher than Ethio-HST train at the similar places of the models.

Generally, the main cause of aerodynamic drag reduction is the frontal blocking nose shape of ICE-2 train is improved by streamlined modified train with consideration of other additional aerodynamic effect reduction techniques employed on the modified train.

The negative pressure value for both pressure coefficient plot and static pressure contour is caused by the value of gauge pressure is set to zero on fluent solver setup under boundary condition of outlet pressure. Thus all pressure values less than atmospheric pressure ($1*10^5$ pa) will be get negative value. If a particular negative pressure value is added with one atmospheric pressure (of gauge pressure) the result will be positive.

The following table gives result summary on major improvements achieved on drag, lift, and moment coefficients. The table is extracted from fluent solver based on symmetric cross sectional reference area report (.txt). Thus, the results of parameters or variables such as drag and lift forces will have half of the whole magnitude for each. Then multiplying by two or doubling is recommended for each variables to consider the whole train model not for the half or the symmetry part the train for final result.

Table 7: Summary of drag, lift, and moment values.

Train model	Drag forces (N) report (F_D) Direction Vector (-1 0 0)			Coefficient of drag (C_D)		
	Pressure	Viscous	Total	Pressure	Viscous	Total
ICE-2	7821.458	1639.4658	9460.9238	0.43627605	0.091448376	0.52772442
Ethio-HST	3377.6635	1539.4358	4917.0993	0.18482192	0.084236181	0.2690581
	Lift forces (N) report (F_L) Direction Vector (0 0 1)			Coefficient of lift (C_L)		
ICE-2	5177.471	33.018799	5210.4898	0.2887961	0.001841768	0.29063787
Ethio-HST	1536.073	18.289208	1554.3623	0.084052174	0.0010007647	0.085052939
	Moments (n-m) (M) Moment Center (-35.3 0 2) Moment Axis (0 1 0)			Coefficient of moment (C_M)		
ICE-2	230517.11	-1178.676	229338.44	12.858101	-0.065745788	12.792355
Ethio-HST	138240.3	-632.4822	137607.82	7.5643524	-0.034608711	7.5297437

As aerodynamic drag is composed of the pressure drag and friction drag, the pressure drag of the train is the force caused by the pressure distributed on the train along the reverse running direction. Friction drag of the train is the sum of shear stress (viscous), which is the reverse direction of train running direction [89]. As mentioned previously, these values are not for full

reference area, instead symmetry computational domain is used. Thus all forces and the symmetric reference area values except the coefficients should be get doubled. Coefficients are remains constant for either full or symmetry (half) of the model without consideration of the forces and reference area of the model.

Note that, the half reference area is calculated by fluent solver under result of projected area. If the simulation is done without symmetry, the projected area will be for the full train cross section. Before the table, optionally the formula for the relationship of required variables given as follows [1], [62], [69], [84].

The friction coefficient C_F,

$$C_F = \frac{\tau}{0.5 * \rho * U^2} ;$$

The pressure coefficient C_P,

$$C_P = \frac{P}{0.5 * \rho * U^2} ;$$

The drag force coefficient C_D,

$$C_D = \frac{F_D}{0.5 * \rho * U^2 * A} ;$$

The Lift Coefficient C_L,

$$C_L = \frac{F_L}{0.5 * \rho * U^2 * A};$$

The Side Force Coefficient C_S,

$$C_S = \frac{F_S}{0.5 * \rho * U^2 * A};$$

Coefficient of Overturning Moment C_{M_x},

$$C_{M_x} = \frac{M_x}{0.5 * \rho * U^2 * A * L} ;$$

Coefficient of Rolling Moment C_{M_y},

$$C_{M_y} = \frac{M_y}{0.5 * \rho * U^2 * A * L};$$

Coefficient of Overturning Moment C_{M_z},

$$C_{M_z} = \frac{M_z}{0.5 * \rho * U^2 * A * L}$$

Where ρ = Air density, U = Air/Train speed, A = Train cross sectional area, and L = represents a fixed reference length, the value of air density, ρ = 1.185kg/m^3, air velocity of U = 70 m/s.

Note that, in addition to the above discussion on the velocity and pressure variation over the two train bodies, the aerodynamic coefficients of blunt and streamlined body flows are different. Drag, in the context of fluid dynamics, refers to forces that act on a solid object in the direction of the relative flow velocity (note that the diagram below shows the drag in the opposite direction to the flow). The aerodynamic forces on a body come primarily from differences in pressure and viscous shearing stresses. Thereby, the drag force on a rigid body surface could be divided into two components, namely frictional drag (viscous drag) and pressure drag (form drag). The net drag force could be decomposed as follows:

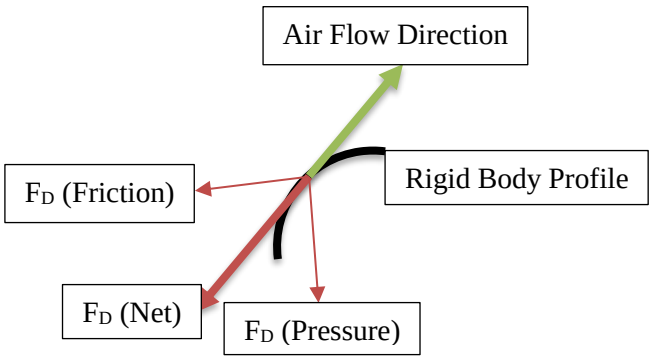

Figure 52: The relationship between air flow direction and drag resistance.

$$C_D = \left(\frac{2F_D}{\rho U^2 A}\right) = C_P + C_F$$

$$= \left(\frac{1}{\rho U^2 A}\right) \oint_S dA(p - p_o)\,(\hat{n}.\hat{\imath}) + \left(\frac{1}{\rho U^2 A}\right) \oint_S dA\,(\hat{t}.\hat{\imath})\tau_w$$

Where: C_P = the pressure drag coefficient, C_F = the friction drag coefficient, $\hat{t}$ = Tangential direction to the surface with area dA, $\hat{n}$ = Normal direction to the surface with area dA, τ_w = the shear Stress acting on the surface dA, p_o = the pressure far away from the surface dA, p =

pressure at surface dA, $\hat{\imath}$ = the unit vector in direction normal to the surface dA, forming a unit vector $d\hat{A}$.

Flow across a body showing the relative impact of drag force to the direction of motion of fluid over the body. This drag force gets divided into frictional drag and pressure drag. The rigid body profile is considered as a streamlined body if friction drag (viscous drag) dominates pressure drag and is considered as bluff body when pressure drag (form drag) dominates friction drag.

Therefore, when the drag is dominated by a frictional component, the body is called a streamlined body; whereas in the case of dominant pressure drag, the body is called a blunt body. Thus, the shape of the body and the angle of attack determine the type of drag. For example, an airfoil is considered as a body with a small angle of attack by the fluid flowing across it. This means that it has attached boundary layers, which produce much less pressure drag.

The wake produced is very small and drag is dominated by the friction component. Therefore, such a body (Ethio-HST) is described as streamlined, whereas for bodies with fluid flow at high angles of attack, boundary layer separation takes place. This mainly occurs due to adverse pressure gradients at the top and rear parts of the train.

Due to this, wake formation takes place, which consequently leads to eddy formation and pressure loss due to pressure drag. In such situations, the rigid body is stalled and has higher pressure drag than friction drag. In this case, the body is described as a blunt body.

A streamlined body looks like a fish (Tuna, Oropesa, etc.) or an airfoil with small angle of attack, whereas a blunt body looks like a brick, a cylinder or an airfoil with high angle of attack. For a given frontal area and velocity, a streamlined body will have lower resistance than a blunt body. Cylinders and spheres are taken as blunt bodies because the drag is dominated by the pressure component in the wake region at high Reynolds number.

To reduce this drag, either the flow separation could be reduced or the surface area in contact with the fluid could be reduced (to reduce friction drag). This reduction is necessary in devices like trains, bus, etc. to avoid vibration and noise production.

Thus, on the above equations, the total aerodynamic drag is the sum of friction and pressure drag components. Trade-off relationship between pressure drag and friction drag means the total drag increase while either of the drag components are fluctuating.

The effect of side force, overturning moment, and rolling moment is not considered as they are canceling each other for open air condition (without crosswind effect consideration). But for cross wind and additional effects their effect will be valuable and concern.

Prandtl (1904) first deduced the relation between velocity gradient and shear stress:

$$\tau_w = \mu \frac{du}{dy}$$

Where; μ = the dynamic viscosity, τ_w = wall shear stress, and u = free stream velocity.

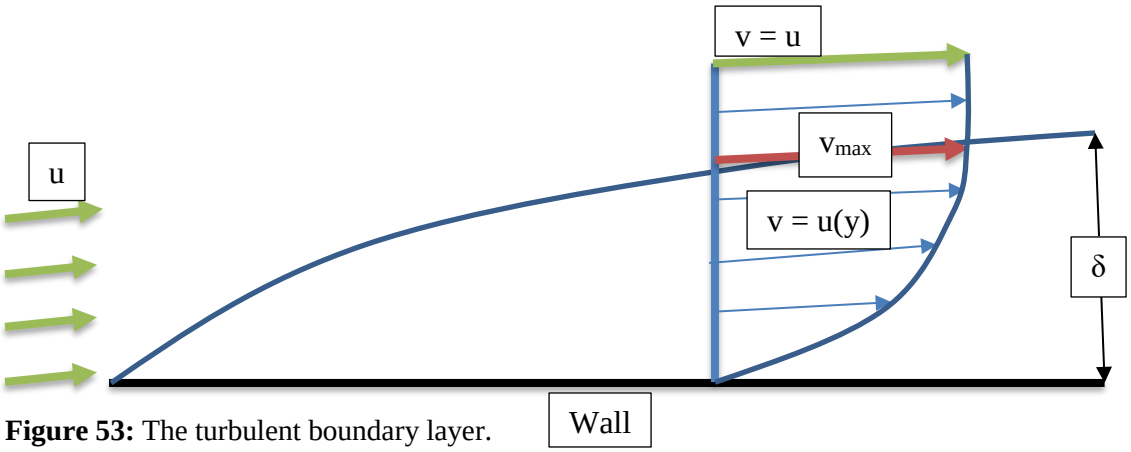

Figure 53: The turbulent boundary layer.

In turbulent flow, the boundary layer is defined as the thin region on the surface of a body in which viscous effects are important. The boundary layer allows the fluid to transition from the free stream velocity u = U to a velocity of zero at the wall. The velocity component normal to the surface is much smaller than the velocity parallel to the surface: v << u. The gradients of the flow across the layer are much greater than the gradients in the flow direction. The boundary layer thickness δ is defined as the distance away from the surface where the velocity reaches maximum from the free-stream velocity and towards the wall as shown the above figure.

To know the value of shear stress τ on the surface of the body, the knowledge of the frictional drag forces opposing the flow or movement of travelling object is needed. Thus, the formula of velocity gradient becomes higher at boundary layer δ, and the shear stress becomes higher at that point. See the following relationship;

$$\tau_w = \mu \frac{du}{dy}, at\ \partial y = \delta\ and\ \partial u = v_{max} \rightarrow \tau_w \cong \mu \frac{v_{max}}{\delta}$$

This equation indicates that the shear stress will increase for high velocity magnitude at specific flow instant. The relationship between the coefficient of drag and the shear stress will be rewritten as follows.

$$C_D = \frac{F_D}{0.5 * \rho * U^2 * A} = C_F + C_P = \frac{\tau_w}{0.5 * \rho * U^2} + \frac{P}{0.5 * \rho * U^2} \; ;$$

The above formula shows the direct relationship between the coefficient of drag and shear stress and pressure. This shows for any place where maximum velocity being higher will lead to higher shear stress and will be cause for coefficient of drag becoming higher. But as discussed above at appoint where shear stress (friction) being higher leads to the reduction of pressure part of the drag. It means, there is tendency of compromising between the shear and the pressure part of the total drag force (total coefficient of drag). With consideration of the above discussions the ICE-2 train will have higher shear stress where maximum velocity is existing than the Ethio-HST train. then overall coefficient of drag will be result with these concepts.

Note that, the ICE-2 train full reference area is 12.350142 m^2 (half reference area of 6.175071 m^2) and the Ethio-HST train full reference area is 12.5895002 m^2 (half reference area of 6.2947501m^2). Projected (reference) area change and percentage for full train (not for symmetry) is calculated bellow.

$$\%\Delta A = \frac{A_{ICE-2} - A_{Ethio-HST}}{A_{ICE-2}} * 100\%$$

$$= \frac{12.350142 \; - 12.5895002}{12.350142} * 100\%$$

$$= \frac{-0.2393582}{12.350142} * 100\%$$

$$= -0.0193810079268724 * 100\%$$

$$= -1.938100792687242\%$$

$$\cong 1.94\%$$

$$\Delta A = A_{ICE-2} - A_{Ethio-HST}$$

$$= 12.350142 \; - 12.5895002$$

$$= -0.2393582$$

$$\cong 0.24 \, m^2$$

The following table will give the relationship of the reference area and other parameters for symmetric and full air domain.

Table 8: Comparisons of parametric values between half (symmetric) and full reference area.

Train models	Parameters	Parameter value (half area)	Parameter value (full area)
ICE-2	F_D	9460.9238 N	18921.8476 N
	C_D	0.52772442	0.52772442
	F_L	5210.4898 N	10420.9796 N
	C_L	0.29063787	0.29063787
	M	229338.44 N-m	458676.88 N-M
	C_M	12.792355	12.792355
Ethio-HST	F_D	4917.0993 N	9834.1986 N
	C_D	0.2690581	0.2690581
	F_L	1554.3623 N	3108.7246 N
	C_L	0.085052939	0.085052939
	M	137607.82 N-m	275215.64 N-m
	C_M	7.5297437	7.5297437

4.1.1 The Amount of Aerodynamic Drag Percentage

The Drag Force, F_D, acts in the direction of the free stream while the Lift Force, F_L, is normal to the free stream. Objects such as airfoils are designed to generate lift. However, for objects such as cars, trains, it is desired to reduce both the lift and the drag since the lift on a car or train reduces the contact force between the wheels and the ground or rails. Typically, the lift and drag are given in terms of the Coefficient of Lift (C_L) and the Coefficient of Drag (C_D) which are dimensionless forms of the Lift and Drag forces [62] as listed on the table under result.

After shape optimization was done the change in aerodynamic drag coefficient of the two models can be calculated in percentage. From this we have calculated decrease in drag coefficient as [62]:

$$\%\Delta C_D = \frac{C_{D,ICE-2} - C_{D,Ethio-HST}}{C_{D,ICE-2}} * 100\%$$

$$= \frac{0.52772442 - 0.2690581}{0.52772442} * 100\%$$

$$= \frac{0.25866632}{0.52772442} * 100\%$$

$$= 0.4901541603854527 * 100\%$$

$$= 49.01541603854527\%$$

$$\cong 49.01\%$$

$$\Delta C_D = C_{D,ICE-2} - C_{D,Ethio-HST}$$

$$= 0.52772442 - 0.2690581$$

$$= 0.25866632$$

$$\cong 0.26$$

In similar way the change in aerodynamic lift coefficient of the two models can be calculated as percentage as follows.

$$\%\Delta C_L = \frac{C_{L,ICE-2} - C_{L,Ethio-HST}}{C_{L,ICE-2}} * 100\%$$

$$= \frac{0.29063787 - 0.085052939}{0.29063787} * 100\%$$

$$= \frac{0.205584931}{0.29063787} * 100\%$$

$$= 0.7073576853560068 * 100\%$$

$$= 70.73576853560068\%$$

$$\cong 70.73\%$$

$$\Delta C_L = C_{L,ICE-2} - C_{L,Ethio-HST}$$

$$= 0.29063787 - 0.085052939$$

$$= 0.205584931$$

$$\cong 0.21$$

Also use for the change in aerodynamic moment coefficient of the two models can be calculated.

$$\%\Delta C_M = \frac{C_{M,ICE-2} - C_{M,Ethio-HST}}{C_{M,ICE-2}} * 100\%$$

$$= \frac{12.792355 - 7.5297437}{12.792355} * 100\%$$

$$= \frac{5.2626113}{12.792355} * 100\%$$

$$= 0.4113872152547361 * 100\%$$

$$= 41.13872152547361\%$$

$$\cong 41.14\%$$

$$\Delta C_M = C_{M,ICE-2} - C_{M,Ethio-HST}$$

$$= 12.792355 - 7.5297437$$

$$= 5.2626113$$

$$= 5.26$$

The change in aerodynamic drag force, lift force, and moment of the two models can be calculated as percentage as the above procedures.

The change in aerodynamic drag force of the two models in percentage:

$$\%\Delta F_D = \frac{F_{D,ICE-2} - F_{D,Ethio-HST}}{F_{D,ICE-2}} * 100\%$$

$$= \frac{18921.8476 \quad - 9834.1986}{18921.8476} * 100\%$$

$$= \frac{9087.649}{18921.8476} * 100\%$$

$$= 0.4802728143735816 * 100\%$$

$$= 48.02728143735816\%$$

$$\cong 48.03\%$$

$$\Delta F_D = F_{D,ICE-2} - F_{D,Ethio-HST}$$

$$= 18921.8476 \quad - 9834.1986$$

$$= 9087.649N$$

$$\cong 9.09\ kN$$

The change in aerodynamic Lift force of the two models in percentage:

$$\%\Delta F_L = \frac{F_{L,ICE-2} - F_{L,Ethio-HST}}{F_{L,ICE-2}} * 100\%$$

$$= \frac{10420.9796 \quad - 3108.7246}{10420.9796} * 100\%$$

$$= \frac{7312.255}{10420.9796} * 100\%$$

$$= 0.7016859528253946 * 100\%$$

$$= 70.16859528253946\%$$

$$\cong 70.17\%$$

$$\Delta F_L = F_{L,ICE-2} - F_{L,Ethio-HST}$$

$$= 10420.9796 \quad - 3108.7246$$

$$= 7312.255\ N$$

$$= 7.31\ kN$$

The change in aerodynamic Moment of the two models in percentage:

$$\%\Delta M = \frac{M_{ICE-2} - M_{Ethio-HST}}{M_{ICE-2}} * 100\%$$

$$= \frac{458676.88 \ - 275215.64}{458676.88} * 100\%$$

$$= \frac{183461.24}{458676.88} * 100\%$$

$$= 0.3999792620896872 * 100\%$$

$$= 39.99792620896872\%$$

$$\cong 40.00\%$$

$$\Delta M = M_{ICE-2} - M_{Ethio-HST}$$

$$= 458676.88 \ - 275215.64$$

$$= 183461.24 \ N - m$$

$$\cong 0.18 * 10^6 \ N - m$$

4.1.2 The Relationship of Aerodynamic Drag and Power Consumption

The relationship between aerodynamic drag resistance and the traction power is too much complex. The assumptions will also get numerous such as mass of train, traction power etc., and because of these parameters other parameters which come next to them will also be a set of guess. Thus the approximate relationship of these two parameters will be discussed using their empirical formula as shown below as also used on Orellano A. (Dr.) [69].

Power = Force * Velocity

P = F * V

To get more exact value using the relationship between drag and that of traction power the use of Davis experience formula discussed in chapter two considering that methods is essential. But for prediction purpose, basic formulas may be used as written above. The estimation or indication traction power will be done without knowing the actual traction power of both train models.

Thus, from the above formula;

P = traction power consumed by the aerodynamic drag.

V = the speed of the train (the wind speed for ANSYS Fluent).

F = the aerodynamic drag resistance force.

From previous relations again, F = F_D, and V = U. with these values at hand it is possible to calculate the traction power using the drag force for each train models or by using only the change in drag force (ΔF_D). To make clear the traction power calculation will be solved on both methods.

First the traction power used by aerodynamics drag force resistance of the ICE-2 Train model is calculated.

$$P_{D_{ICE-2}} = F_{D_{ICE-2}} * U$$

$$= 18921.8476 * 70$$

$$= 1324529.332\ W$$

$$= 1324.529332\ kW$$

$$\cong 1324.53\ kW$$

Next the traction power used by aerodynamics drag force resistance of the Ethio-HST will be computed in similar way.

$$P_{D_{Ethio-HST}} = F_{D_{Ethio-HST}} * U$$

$$= 9834.1986 * 70$$

$$= 688393.902\text{W}$$

$$= 688.393902\ \text{kW}$$

$$\cong 688.40\ \text{kW}$$

The change in power usage in percentage for the two train models can be calculated:

$$\%\Delta P = \frac{P_{D_{ICE-2}} - P_{D_{Ethio-HST}}}{P_{D_{ICE-2}}} * 100\%$$

$$= \frac{1324529.332 - 688393.902}{1324529.332} * 100\%$$

$$= \frac{636135.43}{1324529.332} * 100\%$$

$$= 0.4802728143735816 * 100\%$$

$$= 48.02728143735816\%$$

$$\cong 48.03\ \%$$

$$\Delta P = P_{D_{ICE-2}} - P_{D_{Ethio-HST}}$$

$$= 1324529.332 - 688393.902$$

$$= 636135.43\ W$$

$$= 636.13543\ kW$$

$$\cong 636.13\ kW$$

4.2 Discussions

Outputs variables of the simulation must be validated somewhere under the research thesis. Thus some comparison of these two simulations each other and then the modified model will be evaluated with external HST aerodynamic studies. All the above values come from on the improved aerodynamic shape of the train model. The analytical comparison is described in detail under cost analysis. This subtopic will concern main and general points which need wordy descriptions.

As described analytically under cost analysis, the general aerodynamic worthiness of the new model (Ethio-HST) over ICE-2train is about 50%. This is incredible change which is done on the train body modeling. For more clarification, overviews of some typical parameters are described below in the form of comparison.

The coefficient of aerodynamic drag for ICE-2 train is 0.53 which is less than the value listed under table 1, for similar model called ICE of drag coefficient of 0.69. this indicates the remaining drag coefficient values on the difference or changes of these results are belonging to the effect of pantograph and other extrude parts on the whole train body which are not include or considered under this computation. Also there is difference of reference area and the impact of latest version of CFD software are some causes for this much amount of drag coefficient variation for similar trains. Then with these exceptions, the aerodynamic drag coefficient for the modified train model (Ethio-HST) is 0.27. This will result the change in drag coefficient of 0.26 and in percentage 49.01%. This will result in similar sense for the aerodynamic drag force percentage vales obtained.

The aerodynamic lift coefficient for ICE-2 train is 0.29 and for the Ethio-HST is 0.08 and the percentage of reduction is 70.73% (of $\Delta C_L = 0.21$). This percentage is almost the same for aerodynamic lift force as they obey direct relationship.

The aerodynamic moment coefficient of ICE-2 train is 12.79 and for Ethio-HST is 7.53. Then the percentage of reduction will be 41.14% (of $\Delta C_M = 5.26$). It is pretty much the same for the moment reduction percentage. In similar way, the details of other parameters are summarized under the following table.

Table 9: Summary of the aerodynamic parameters comparison.

Categories	Parameters								
	F_D [kN]	C_D	F_L [kN]	C_L	M [N-m]	C_M	P_D [kW]	E_D [kWh]	A [m^2]
ICE-2	18.92	0.53	10.42	0.29	0.46e+6	12.79	1324.53	1324.53	12.35
Ethio-HST	9.83	0.27	3.11	0.08	0.27e+6	7.53	688.40	688.40	12.59
Change (Δ)	9.09	0.26	7.31	0.21	0.18e+6	5.26	636.13	636.13	0.12
Percentage (%)	48.03	49.01	70.17	70.73	40.00	41.14	48.03	48.03	1.94

These things discussed above, mainly the aerodynamic drag force leads valuable power or energy consumption. From the above analytical result, the power loss by aerodynamic drag force of ICE-train (for Ethio-HST is conserved) of 636.13 Kw.

Generally, the values obtained on the result are less than the value obtained on table 1 of 0.69 for the reference (ICE-2) train. As discussed, the main cause for the reduced value of drag resistance of the result of this study is the pantograph system is not included. In addition to this the crosswind effect need to be considered to get better accurate drag value. Also there is difference on reference area and maybe air property for the ICE trains with C_D of 0.69 and the ICE-2 train simulated on this thesis respectively. And one thing is the accuracy of the CFD software becomes greater for this study, as the version of the CFD software for this research thesis is up to date. The difference on train model length, the degree of train system simplification, mesh quality, numerical method on turbulence model, and other things leads to the variation of simulation results for the same existing train.

5. CHAPTER FIVE: CONCLUSION, RECOMMENDATION, AND FUTURE WORK INDICATIONS

5.1 Conclusions

It is a good measure to reduce the aerodynamic drag by changing the connecting part of the train. The outer wind shields can lower train's air drag by about 15%. Smoothing the underneath structures of the train by using the body mount system or the skirt system can largely reduce the aerodynamic drag. The train with bottom cover can reduce the air resistance by about 50%, compared with the train without bottom plate or apron plate [89]. From results, the reduction of coefficient of aerodynamic drag percentage of 49.01% with change of 0.26 much amount of aerodynamic drag loss is conserved due to the improved design of more aerodynamically shaped train model over ICE-2 train.

This much amount of aerodynamic drag reduction is achieved by implementation of aerodynamic drag resistance reduction methods of aerodynamic shape optimizations techniques such as use of streamlined shape, bottom cover plate, spoiler geometry, different shape of headstock and tailstock, bogie fairing, underbody shape modifying, etc. with the above statements and others written literatures in this thesis.

The reduction of aerodynamic drag leads to save traction power of 636.13 kW. Then the reduction of aerodynamic lift force and moment will result the guarantee or assurance of train stability and safety which resulted by the life force and by pitching effect of the moment. This also reduces probability of derailment phenomenon because of the loose attachment of the rail and the wheel by lift force. The reduction of these main parameters leads to the reduction of passenger discomfort and vibrations.

These all points described above leads to conclude the performance of high speed trains will be increased by reduction of aerodynamic effects. This indicates for ERC and the Government the power of CFD software to save this much amount of power easily without actual building and buying of the model for aerodynamic test.

5.2 Recommendations

The computation performed under this study does not include the pantograph and its basement which assembles over the roof of the train. To get more realistic result the pantograph system

should be included. Even including of the rail system will get the result more real, but in consideration computational cost.

The study also becomes accurate and real if cross wind, tunnel, and other similar effects are considered. The study of including these characters leads to strengthen safety conditions. Under cross wind effect the degree key aerodynamic effects such as side force, overturning moment, and rolling moment will be examined.

The other point is the use of more accurate CFD numerical methods such as LES if computation materials available. Note that, the wish of computing using common computers is not being achieved even for RANS method (recommended for engineering analysis) and the model used for this study may not recommended. Another thing is the experimental evaluation is perfect validation of the CFD result if the experimental equipment and materials are available.

5.3 Future Works Indications

As tried to indicate under the recommendation, the study of high speed passenger trains should be including the following points in addition to the points covered under this steady.

- Cross wind effect,
- Curve effect,
- Uphill and downhill effects,
- Tunnel effect,
- Bridge effect,
- Embankment effect and etc.

These conditions except the cross wind needs to be studied for their specific topography conditions as much as possible. This can help to improve the existing geographical topography.

The other thing which should be recommended is the use of higher order accurate CFD numerical methods with availability of supercomputers and other computing materials. The physical experiment will be more real for laboratory test or even for full scale test. The experiment analysis also need special physical measuring tools, sensors, actuators, equipment, and physical model of train etc. for aerodynamic drag evaluations.

Reference

1. Abel D. "Stability of trains under aerodynamic excitation for Addis Ababa Light Railway Transit." School of Mechanical and Industrial Engineering, Addis Ababa University, Ethiopia (2015).
2. Afshar A. "Evaluation of Liquid Fuel Spray Models for Hybrid RANS/LES and DLES Prediction of Turbulent Reactive Flows." Graduate Department of Aerospace Engineering University of Toronto (2014).
3. Ali M.Z., et al. "Aerodynamics." IOSR Journal of Mechanical and Civil Engineering (IOSR-JMCE), e-ISSN: 2278-1684, p-ISSN: 2320-334X, PP 64-67.
4. Andrés F. Tabares et al. "Critical Sources of Aerodynamic Resistance in a Medium Distance Urban Train: a CFD approach." Revista Científica Guillermo de Ockham, vol. 11, núm. 1, enero junio, 2013, pp. 111-124 Universidad de San Buenaventura Cali, Colombia.
5. Asress M.B., Svorcan J. "Numerical investigation on the aerodynamic characteristics of high-speed train under turbulent crosswind." J. Mod. Transport. (2014) 22(4):225–234, DOI 10.1007/s40534-014-0058-7.
6. Baker C. "A review of train aerodynamics Part 2 – Applications." The Aeronautical Journal (2014), vol 118, no. 1202.
7. Baker C., et al. "Aerodynamic pressures around high-speed trains: the transition from unconfined to enclosed spaces" Proceedings of the Institution of Mechanical Engineers Part F Journal of Rail and Rapid Transit (2013), vol 227, no. 6, pp. 609-622., DOI: 10.1177/0954409713494947.
8. Baker C., et al. "Cross-wind effects on road and rail vehicles." Cross-wind effects on road and rail vehicles, Vehicle System Dynamics: International Journal of Vehicle Mechanics and Mobility (2009), 47:8, 983-1022, DOI: 10.1080/00423110903078794.
9. Bosquet R., et al. "Model of High-Speed Train Energy Consumption." World Academy of Science, Engineering and Technology, Vol: 7, no-6, 2013-06-22.
10. Bouferrouk A., et al. "Calculation of the crosswind displacement of pantographs." BBAA VI International Colloquium on: Bluff Bodies Aerodynamics & Applications Milano, Italy, July, 20-24 2008.
11. Bouferrouk A., et al. "CFD Simulations of Crosswind Impinging on a High Speed Train Model." 18th Australasian Fluid Mechanics Conference, Launceston, Australia, 3-7 December 2012.

12. Bourquin V., et al. "Aerodynamic Effects in Railway Tunnels as Speed is increased." Swiss Federal Institute of Technology, Laboratory of Fluid Mechanics, EPFLLMF, CH-1015 Lausanne, Switzerland.
13. Browand F., et al. "The Aerodynamics of Heavy Vehicles II Trucks, Buses, and Trains." Springer Science & Business Media, Sep 30, 2008.
14. Cabot W. and Moin P. "Approximate Wall Boundary Conditions in the Large-Eddy Simulation of High Reynolds Number Flow." Flow, Turbulence and Combustion 63: 269–291, 1999.
15. Ceyrowsky T., et al. "Unsteady RANS simulations of flows around a simplified car body." Euromech Colloquium 509, Vehicle Aerodynamics, External Aerodynamics of Railway Vehicles, Trucks, Buses and Cars, Berlin, Germany, March 24–25, 2009.
16. Cheli F., et al. "Train shape optimization to improve cross-wind behavior." Euromech Colloquium 509, Vehicle Aerodynamics, External Aerodynamics of Railway Vehicles, Trucks, Buses and Cars, Berlin, Germany, March 24–25, 2009.
17. Cheli F., et al. "Wind tunnel tests on heavy road vehicles: cross wind induced loads." Euromech Colloquium 509, Vehicle Aerodynamics, External Aerodynamics of Railway Vehicles, Trucks, Buses and Cars, Berlin, Germany, March 24–25, 2009.
18. Chen R., et al. "A Parallel Domain Decomposition Method for 3D Unsteady Incompressible Flows at High Reynolds Number." Chinese Academy of Sciences, J Sci Comput (2014) 58:275–289, DOI 10.1007/s10915-013-9732-x.
19. Chen R.L., et al. "Analysis theory of random energy of train derailment in wind." Science China Physics, Mechanics & Astronomy, April (2010) Vol.53 No.4: 751–757, DOI: 10.1007/s11433-010-0158-2.
20. Chen R.L., et al. "Numerical study on the restriction speed of train passing curved rail in cross wind." Science in China Series E: Technological Sciences | Jul. 2009 | vol. 52 | no. 7 | 2037-2047, DOI: 10.1007/s11431-009-0202-5.
21. Chen X., et al. "Aerodynamic simulation of evacuated tube maglev trains with different streamlined designs." Journal of Modern Transportation, Volume 20, Number 2, June 2012, Page 115-120, DOI: 10.1007/BF03325788.
22. Cho H., et al. "Aerodynamics of Heavy Vehicles." Annu. Rev. Fluid Mech. 2014. Vol-46:441–68.
23. Diedrichs B. "Aerodynamic calculations of crosswind stability of a High-speed train using control volumes of arbitrary polyhedral shape." BBAA VI International Colloquium on: Bluff Bodies Aerodynamics & Applications Milano, Italy, July, 20-24 2008.

24. Diedrichs B. "Unsteady aerodynamic crosswind stablity of a high speed train subjected to gusts of various rates." Euromech Colloquium 509, Vehicle Aerodynamics, External Aerodynamics of Railway Vehicles, Trucks, Buses and Cars, Berlin, Germany, March 24–25, 2009.
25. Euromech Colloquium 509, Vehicle Aerodynamics, External Aerodynamics of Railway Vehicles, Trucks, Buses and Cars, Berlin, Germany, March 24–25, 2009.
26. Favre T. and Efraimsson G. "An Assessment of Detached-Eddy Simulations of Unsteady Crosswind Aerodynamics of Road Vehicles." Flow Turbulence Combust (2011) 87:133–163, DOI 10.1007/s10494-011-9333-4.
27. Ghani O.A., "Design optimization of aerodynamic drag at the rear of generic passenger cars using NURBS representation." Faculty of Engineering and Applied Science, University of Ontario Institute of Technology (2013).
28. Gilbert T. "Aerodynamic effects of high speed trains in Confined spaces." School of Civil Engineering, University of Birmingham (2013).
29. Gilbert T., et al. "Aerodynamics of high-speed trains in confined spaces." The Seventh International Colloquium on Bluff Body Aerodynamics and Applications (BBAA7) Shanghai, China; September 2-6, 2012.
30. Gillespie T.D. "Fundamentals of Vehicle Dynamics." Society of Automotive Engineers, Inc. 400, Commonwealth Drive, Warrendale, PA 15096-0001.
31. Givoni M. "Development and Impact of the Modern High-speed Train: A Review." Transport Reviews, Vol. 26, No. 5, 593–611, September 2006.
32. Gourvish T. "The High Speed Rail Revolution: History and Prospects." High speed two (hs2).
33. Guillou F. "CFD Study of the Flow around a High-Speed Train." Kungliga Tekniska Högskolan, Stockholm, Aeronautical and Vehicle Engineering Department.
34. Heckmann A., et al. "Considerations on active control of crosswind stability of railway vehicles." Vehicle System Dynamics: International Journal of Vehicle Mechanics and Mobility, 2014, Vol. 52, No. 6, 759–775, DOI: 10.1080/00423114.2014.901539.
35. Heine Ch. and Matschke G. "The Influence of the Nose Shape of High Speed Trains on the Aerodynamic Coefficients." Deutsche Bahn AG, Research and Technology Centre, Voelckerstrasse 5, D-80939 Munich, Germany.
36. Herbst A., et al. "Aerodynamik." Royal institute of technology, www.gronataget.com
37. Herbst A., et al. "Front Shape and Slipstream for Wide Body Trains at Higher Speeds." KTH Railway Group, Publication 1402, ISBN 978-91-7595-057-0.

38. Herbst A.H., et al. "Shape optimization in train aerodynamics." Euromech Colloquium 509, Vehicle Aerodynamics, External Aerodynamics of Railway Vehicles, Trucks, Buses and Cars, Berlin, Germany, March 24–25, 2009.
39. Hillina A. "Analysis of aerodynamic brakes in mainline of Ethiopia Railway Corporation." School of Mechanical and Industrial Engineering, Addis Ababa University, Ethiopia (2015).
40. Hoefener L., et al. "Wind tunnel experiments of a high speed train exposed to cross wind on ground and bridge configurations." Euromech Colloquium 509, Vehicle Aerodynamics, External Aerodynamics of Railway Vehicles, Trucks, Buses and Cars, Berlin, Germany, March 24–25, 2009.
41. Hopkins T., et al. "Maglift Monorail, a High-Performance, Low-Cost, and Low-Risk Solution for High-Speed Ground Transportation." Presented to the High Speed Ground Transportation Association 1999 Annual Conference Seattle, June 6-9, 1999. 1-11. Print.
42. Hucho W.H. "Important gaps in the science of car aerodynamics." Euromech Colloquium 509, Vehicle Aerodynamics, External Aerodynamics of Railway Vehicles, Trucks, Buses and Cars, Berlin, Germany, March 24–25, 2009.
43. Hucho W.H., Sovran G. "Aerodynamics of road Vehicles." Annu. Rev. Fluid Mech. 1993.25:485-537.
44. Jang Y.J. "An investigation of higher-order closures in the computation of the flow around a generic car." Journal of Mechanical Science and Technology 22 (2008) 1019~1029, DOI 10.1007/s12206-008-0205-3.
45. Jönsson M., et al. "PIV investigation of the flow field underneath a generic high-speed train configuration." Euromech Colloquium 509, Vehicle Aerodynamics, External Aerodynamics of Railway Vehicles, Trucks, Buses and Cars, Berlin, Germany, March 24–25, 2009.
46. Jönsson M. "Numerical Investigation of the Flow underneath a Train and the Effect of Design Changes." Luleå University of Technology, MSc Programmers in Engineering, Mechanical Engineering, Division of Fluid Mechanics, 2007:079 CIV - ISSN: 1402-1617 - ISRN: LTU-EX--07/079—SE.
47. Kametani Y., Ukagata K. "Direct numerical simulations of spatially developing turbulent boundary layer for skin friction drag reduction by wall surface heating or cooling." Journal of Turbulence (2012), 13, N34, DOI: 10.1080/14685248.2012.710750.

48. Khayrullina A., et al. "CFD simulation of train aerodynamics: train-induced wind conditions at an Underground Railroad passenger platform." Journal of Wind Engineering & Industrial Aerodynamics, January 2015.
49. Kim T., Yun S. "Aerodynamic drag reduction of 3D train model using dielectric barrier dis-charge plasma actuators." International Symposium on Plasma Chemistry (ISPC 21) (2013) Cairns Convention Centre, Queensland, Australia.
50. Kong F.G., Wang J. "The Numerical Simulation of Aerodynamic Noise Generated by CRH3 Train's Head Surface." Open Journal of Applied Sciences, 2015, 5, 501-508, DOI: 10.4236/ojapps.2015.58049.
51. Krajnovic S., et al. "Shape optimization of a bus for crosswind stability." Euromech Colloquium 509, Vehicle Aerodynamics, External Aerodynamics of Railway Vehicles, Trucks, Buses and Cars, Berlin, Germany, March 24–25, 2009.
52. Krajnović S. "Improvement of aerodynamic properties of high-speed trains by shape optimization and flow control." Chalmers University of Technology, Department of Applied Mechanics, SE-412 96 Gothenburg, Sweden.
53. Ku Y.C., et al. "Multi-Objective Optimization of High-Speed Train Nose Shape Using the Vehicle Modeling Function." 48th AIAA Aerospace Sciences Meeting Including the New Horizons Forum and Aerospace Exposition, 4 - 7 January 2010, Orlando, Florida, AIAA 2010-1501.
54. Kwon H.B, Hong J.S. "Aerodynamic Drag Reduction on High-performance EMU Train by Streamlined Shape Modification." Journal of The Korean Society for Railway (2013), Vol.16, No.3, pp.169-174. ISSN 1738-6225(Print), DOI: 10.7782/JKSR.2013.16.3.169.
55. Lanfrit M. "Best practice guidelines for handling Automotive External Aerodynamics with FLUENT." Version 1.2, (Feb 9th 2005), Fluent Deutschland GmbH Birkenweg 14a 64295 Darmstadt/Germany.
56. Lee H.W., Kwon H.B. "Analysis of the Effects of SD Plasma on Aerodynamic Drag Reduction of a High-speed Train." J Electr Eng Technol Vol. 9, No.? 742-? 2014.
57. Li T., et al. "An improved algorithm for fluid-structure interaction of high-speed trains under crosswind." Journal of Modern Transportation, Volume 19, Number 2, June 2011, Page 75-81, DOI: 10.1007/BF03325743.
58. Liu T.H., Zhang J. "Effect of landform on aerodynamic performance of high-speed trains in cutting under cross wind." J. Cent. South Univ. (2013) 20: 830-836, DOI: 10.1007/s11771-013-1554-3.

59. Liu Y., et al. "Large Eddy Simulation of the flow around a train passing a stationary freight wagon." The Seventh International Colloquium on Bluff Body Aerodynamics and Applications (BBAA7), Shanghai, China; September 2-6, 2012.
60. Li Y.F., et al. "Aerodynamic drag analysis of double-deck container vehicles with different structures." J. Cent. South Univ. Technol. (2011) 18: 1311−1315 DOI: 10.1007/s11771−011−0838−8.
61. Lorriaux E., et al. "Aerodynamic optimization of railway motor coaches." Laboratoire de Mécanique et d'Energétique, Université de Valenciennes, FRANCE.
62. Mamo N. "Aerodynamic characteristics and aerodynamic shape optimization of Ethiopian national train, case study on Addis Ababa Dire Dawa passenger train." School of Mechanical and Industrial Engineering, Addis Ababa University, Ethiopia (2014).
63. Mancini G. "Effects of experimental bogie fairings on the aerodynamic drag of the ETR 500 high speed train." FS – Trenitalia – Unità Tecnologie Materiale Rotabile, Sperimentazione – Viale S. Lavagnini 58 – 50129 Firenze – Italy.
64. Martins A.M.C. "Boundary layer control in high speed trains." Mechanical Engineering Department, Instituto Superior Técnico, UTL, Lisbon, Portugal.
65. Mazyan W.I. "Numerical Simulations of Drag-Reducing Devices for Ground Vehicles." Sharjah, United Arab Emirates January 2013.
66. McCallen R., et al "The Aerodynamics of Heavy Vehicles: Trucks, Buses, and Trains." Volume 1, Springer Science & Business Media, Sep 1, 2004.
67. McCallen R., et al. "The Aerodynamics of Heavy Vehicles: Trucks, Buses, and Trains." Springer Science & Business Media, Jul 30, 2013.
68. Ni Y.Q., Ye X.W. "Proceedings of the 1st International Workshop on High-Speed and Intercity Railways." Volume 2, Springer Science & Business Media, Feb 13, 2012.
69. Orellano A. (Dr.) "Aerodynamics of high speed trains." Stockholm, KTH, 2010, Germany.
70. Orellano A., Schober M. "Aerodynamic Performance of a Typical High-Speed Train." Proceedings of the 4th WSEAS International Conference on Fluid Mechanics and Aerodynamics, Elounda, Greece, August 21-23, 2006 (pp18-25).
71. Paniagua J.M., et al. "Aerodynamic Optimization of the ICE 2 High-Speed Train Nose using a Genetic Algorithm and Metamodels." Ministry of Science and Technology.
72. Paniagua J.M. "Aerodynamic optimization of the nose shape of a high speed train." Polytechnic university of Madrid (2014).
73. Paniagua J.M., et al. "Aerodynamic Optimization of the Nose Shape of a Train Using the Adjoint Method." Journal of Applied Fluid Mechanics, Vol. 8, No. 3, pp. 601- 612, 2015.

74. Paniagua J.M., et al. "Multi-objective Aerodynamic Optimization of High-speed Trains in Tunnels." Dpto. Ingenier´ıa Energ´etica y Fluidomec´anica, Universidad Polit´ecnica de Madrid, C/Jos´e, Guti´errez Abascal 2, 28006 Madrid, Spain.
75. Parab A.et al. "Aerodynamic Analysis of a Car Model using Fluent- Ansys 14.5." International Journal on Recent Technologies in Mechanical and Electrical Engineering (IJRMEE) ISSN: 2349-7947 Volume: 1 Issue: 4, 007– 013.
76. Paul J.C., et al. "Application of CFD to Rail Car and Locomotive Aerodynamics." Airflow Sciences Corporation, 12190 Hubbard Street, Livonia, MI 48150, USA.
77. Paz C., et al. "CFD assessment of the effect of windblown sand on a high-speed train." ECCOMAS Thematic Conference on Multibody Dynamics, June 29 - July 2, 2015, Barcelona, Catalonia, Spain.
78. Pii L, et al. "A full scale simulation of a high speed train for slipstream prediction." Transport Research Arena (2014): 1-10. TRA. Web. 10 Jul. 2015.
79. Raghunathan R.S., et al. "Aerodynamics of high-speed railway train." Progress in Aerospace Sciences 38 (2002) 469–514.
80. Rocchi D., et al. "Design of ansaldobreda high speed trains according to the TSI crosswind requirements." Politecnico di Milano, Milano, Italy.
81. Schetz J.A. "Aerodynamics of high-speed trains." Annu. Rev. Fluid Mech. 2001. 33:371–414.
82. Sebesan I., et al. "Experimental analysis for aerodynamic drag of the electric locomotives." INCAS BULLETIN, Volume 5, Issue 3/ 2013, DOI: 10.13111/2066-8201.2013.5.3.11.
83. Shao, et al. "Aerodynamic modeling and stability analysis of a high-speed train under strong rain and crosswind conditions." J Zhejiang Univ-Sci A (Appl Phys & Eng) 2011 12(12):964-970, DOI: 10.1631/jzus. A11GT001.
84. Shuanbao Y., et al. "Optimization design for aerodynamic elements of high speed trains." Computers & Fluids 95 (2014) 56–73, DOI: 10.1016/j.compfluid.2014.02.018.
85. Singh J., Randhawa J.S. "CFD Analysis of Aerodynamic Drag Reduction of Automobile Car - A Review." International Journal of Science and Research (IJSR), Volume 3 Issue 6, June 2014, ID: 02014156.
86. Spanos P. D., et al. "A nonlinear model for top fuel dragster dynamic performance assessment, Vehicle System Dynamics." International Journal of Vehicle Mechanics and Mobility (2012), 50:2, 281-297, DOI: 10.1080/00423114.2011.583666.

87. Stanewsky E. "Drag Reduction by Shock and Boundary Layer Control: Results of the Project EUROSHOCK II." Supported by the European Union 1996-1999. Springer Science & Business Media, Apr 24, 2002.
88. Thompson J. "Basic High-Speed Train Tunnel Configuration." Technical Memorandum, TM 2.4.2, California High-Speed Train Project (2010).
89. Tian H.Q. "Formation mechanism of aerodynamic drag of high-speed train and some reduction measures." J. Cent. South Univ. Technol. (2009) 16: 0166−0171, DOI: 10.1007/s11771−009−0028−0.
90. Tian H.Q., et al. "Flow structure around high-speed train in open air." J. Cent. South Univ. (2015) 22: 747−752, DOI: 10.1007/s11771-015-2578-7.
91. Tan Runhua, et al. "Interactive Training Model of TRIZ for Mechanical Engineers in China." Chinese Journal of Mechanical Engineering (2014) Vol. 27, No. 2, DOI: 10.3901/CJME.2014.02.240.
92. Vytla V.V., et al. "Multi Objective Aerodynamic Shape Optimization of High Speed Train Nose Using Adaptive Surrogate Model." 28th AIAA Applied Aerodynamics Conference, 28 June - 1 July 2010, Chicago, Illinois, AIAA 2010-4383.
93. Wang H., et al. "Performance evaluation of air distribution systems in three different China railway high-speed train cabins using numerical simulation." BUILD SIMUL (2014) Vol. 7, No. 6: 629–638, DOI 10.1007/s12273-014-0168-5.
94. Wang L., et al. "Control method of unfavorable speed interval for high-speed trains." Journal of Modern Transportation, Volume 20, Number 3, September 2012, Page 153-159, DOI: 10.1007/BF03325793.
95. Wang X.P., et al. "Primary Study of Aerodynamic Performance Evaluation and Optimization of the High-Speed Train." AIP Conference Proceedings 1376, 178 (2011); DOI: 10.1063/1.3651869.
96. Wang Y.W., et al. "Aerodynamic simulation of high-speed trains based on the Lattice Boltzmann Method (LBM)." Sci China Ser E-Tech Sci | Jun. 2008 | vol. 51 | no. 6 | 773-783, DOI: 10.1007/s11431-008-0063-3.
97. Werning B.S."A synopsis of aerodynamic and aero-acoustic Research for modern high-speed trains" European Congress on Computational Methods in Applied Sciences and Engineering, ECCOMAS 2000, Barcelona, 11-14 September 2000.
98. Xiong H.B., et al. "Numerical study on the aerodynamic performance and safe running of high-speed trains in sandstorms." Journal of Zhejiang University-SCIENCE A (Applied Physics & Engineering) (2011) 12(12): 971-978.

99. Yang G.W., et al. "Aerodynamic design for China new high-speed trains." Sci China Tech Sci, 2012, 55: 1923-1928, DOI: 10.1007/s11431- 012-4863-0.

100. Yang X., et al. "Preliminary study on streamlined design of longitudinal profile of high-speed train head shape." Procedia - Social and Behavioral Sciences 96 (2013) 1469 – 1476.

101. Yan Z., et al. "A Scalable Numerical Method for Simulating Flows around High-Speed Train under Crosswind Conditions." Shenzhen Institutes of Advanced Technology, Chinese Academy of Sciences, Shenzhen 518055, P.R. China, (2013), Commun. Comput. Phys. DOI: 10.4208/cicp.150313.070513s.

102. Yao S.B., et al. "Multi-objective optimization of the streamlined head of high-speed trains based on the Kriging model." Sci China Tech Sci, 2012, Vol.55 No.12: 3495-3509, DOI: 10.1007/s11431-012-5038.

103. Yao S.B., et al. "Numerical study on wake characteristics of high-speed trains." Acta Mechanica Sinica (2013) 29(6):811–822, DOI: 10.1007/s10409-013-0077-3.

104. Yao S.B., et al "Three-dimensional aerodynamic optimization design of high-speed train nose based on GA-GRNN." Sci China Tech Sci, 2012, 55: 3118-3130, DOI: 10.1007/s11431-012-4934-2.

105. Yu M.G., et al. "Multi-objective optimization design method of the high-speed train head." Journal of Zhejiang University-SCIENCE A (Applied Physics & Engineering), 2013 14(9):631-641.

106. Zhang J., et al. "Identification of key design parameters of high-speed train for optimal design." Int J Adv Manuf Technol (2014) 73:251–265, DOI 10.1007/s00170-014-5822-7.

107. Zhang W., et al. "A review of vehicle system dynamics in the development of high-speed trains in China." Southwest Jiaotong University, Chengdu, China, Springer-Verlag Berlin Heidelberg 2013, Int. J. Dynam. Control (2013) 1:81–97, DOI 10.1007/s40435-013-0005-1.

108. Zhuang Y., Lu X. "Numerical investigation on the aerodynamics of a simplified high-speed train under crosswinds." Theoretical and Applied Mechanics Letters 5 (2015) 181–186.

Appendix

The following figures and tables are supportive materials used on this thesis.

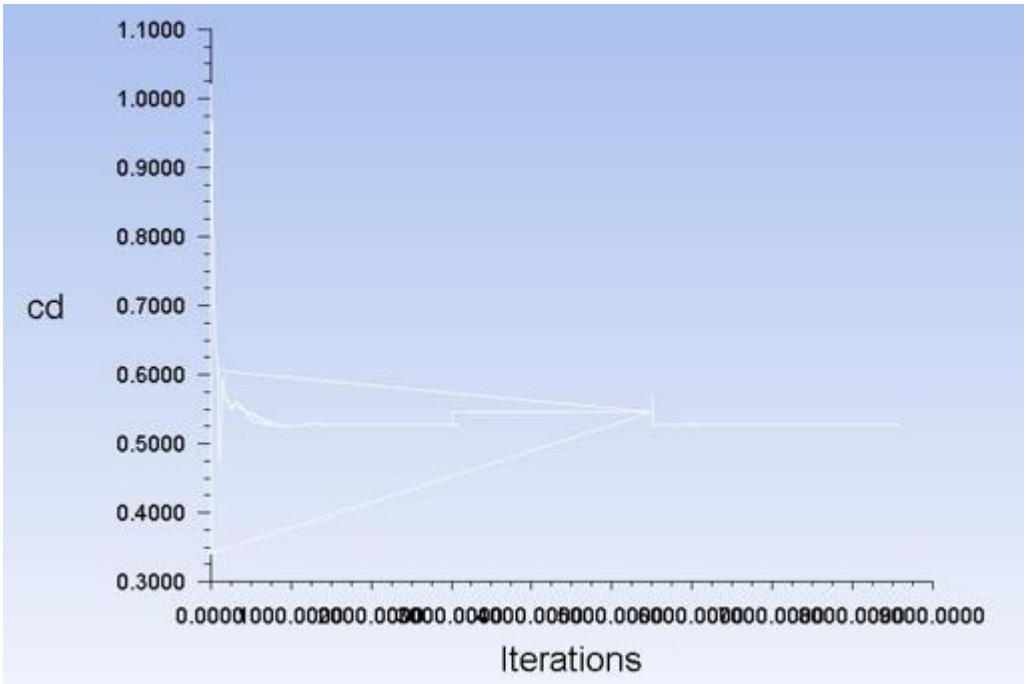

Figure 54: Coefficient of drag force convergence history of ICE-2 Regional Train.

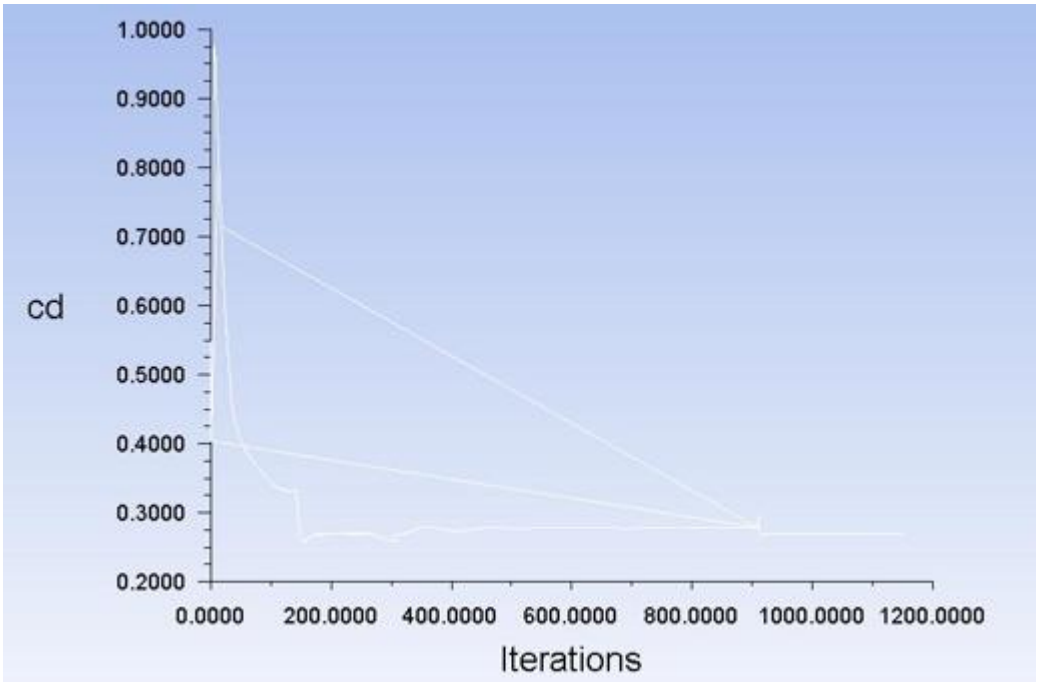

Figure 55: Coefficient of drag force convergence history of Ethio-HST Train.

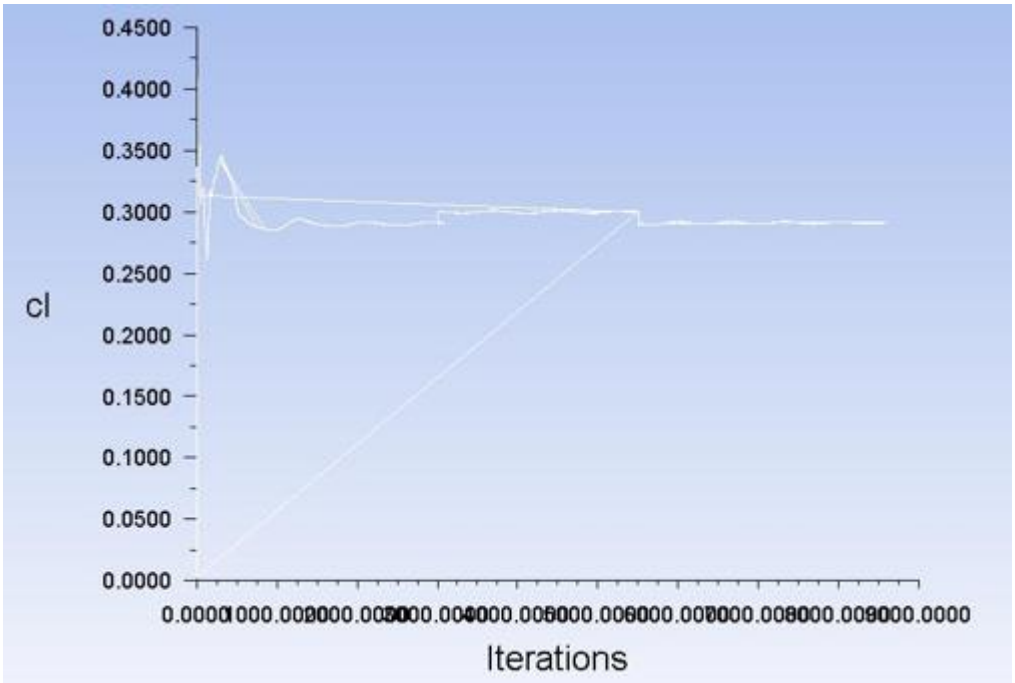

Figure 56: Coefficient of lift force convergence history of ICE-2 Regional Train.

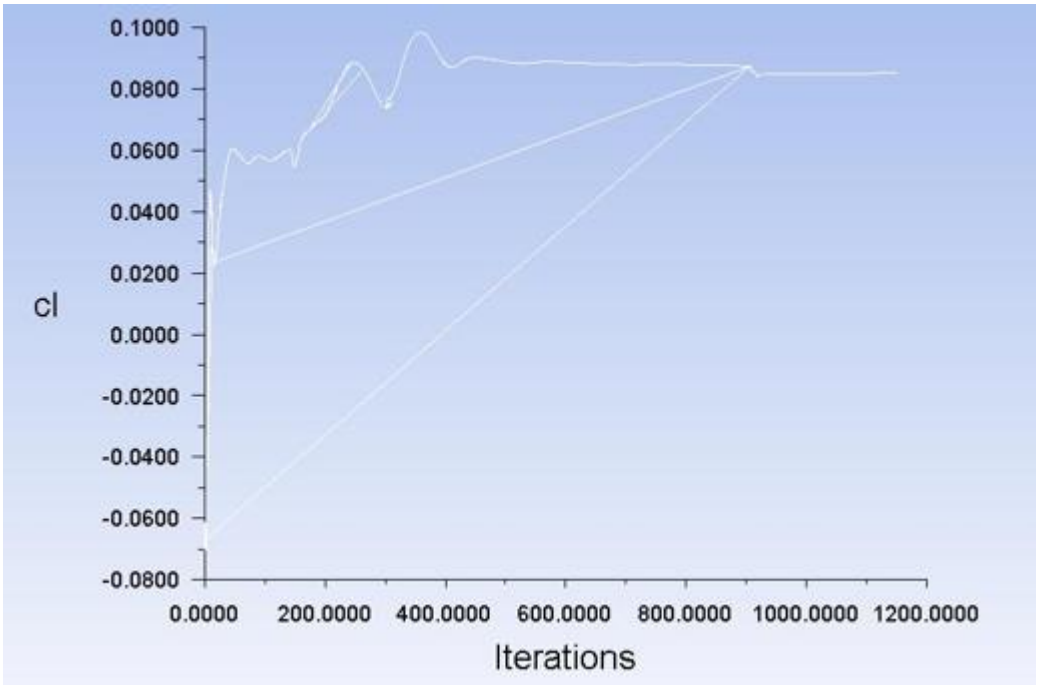

Figure 57: Coefficient of lift force convergence history of Ethio-HST Train.

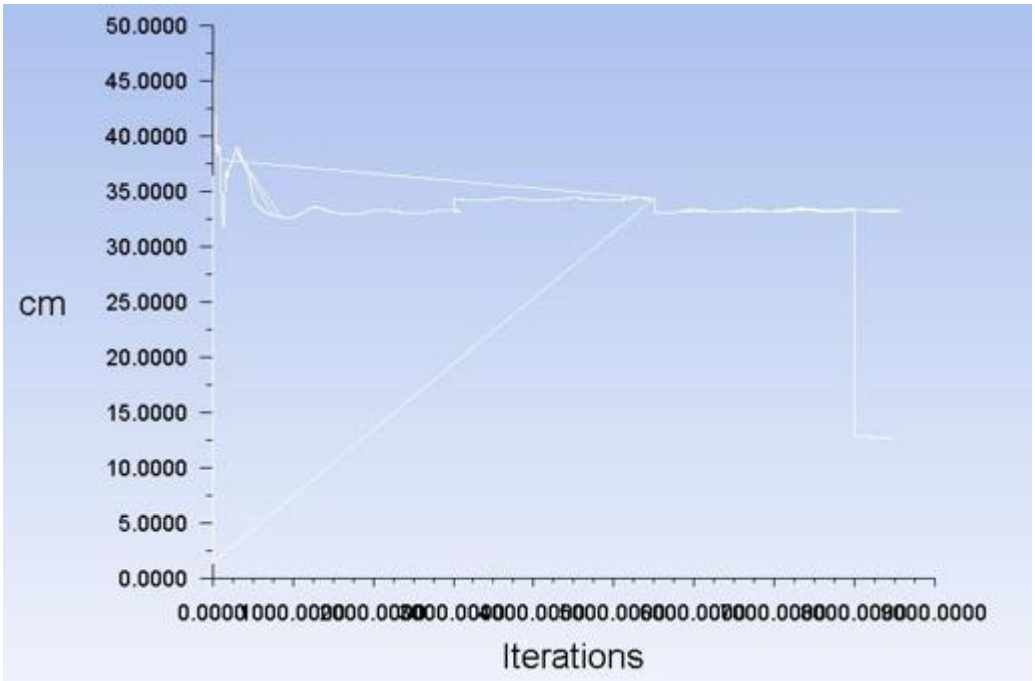

Figure 58: Coefficient of moment convergence history of ICE-2 Regional Train.

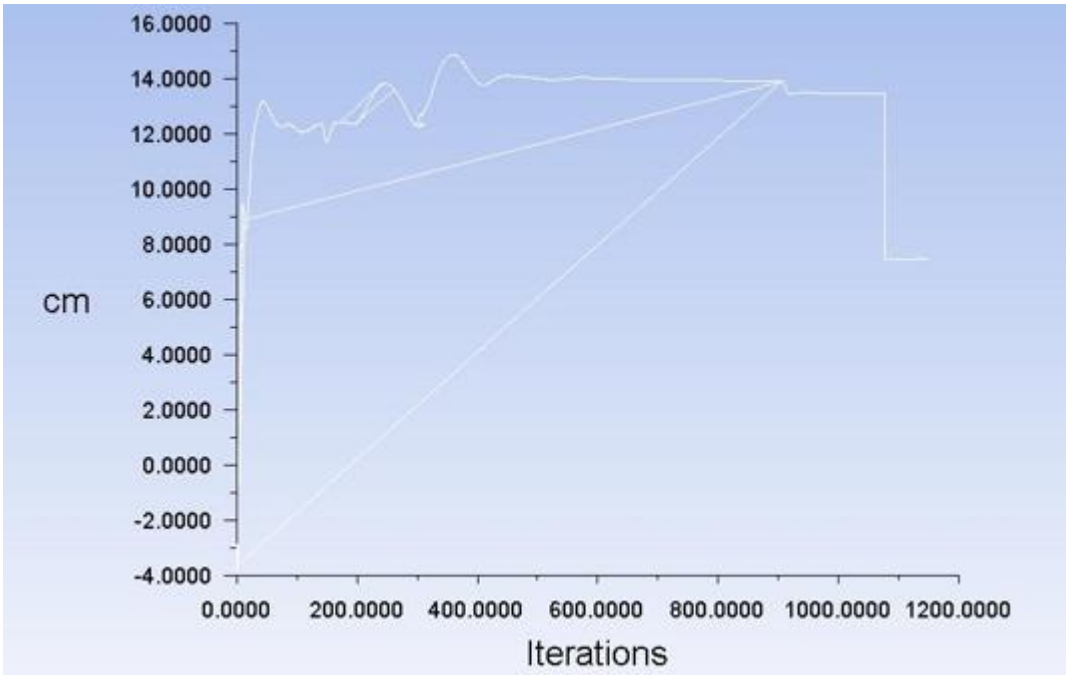

Figure 59: Coefficient of moment convergence history of Ethio-HST Train.

The coefficient graphs shown above indicates the coefficients are normally converged after making zigzag line at air property of 15°c. Then after, the property of air is assigned at 25°c, the graph goes from the staring iteration and comes (converges) faster with straight lines.

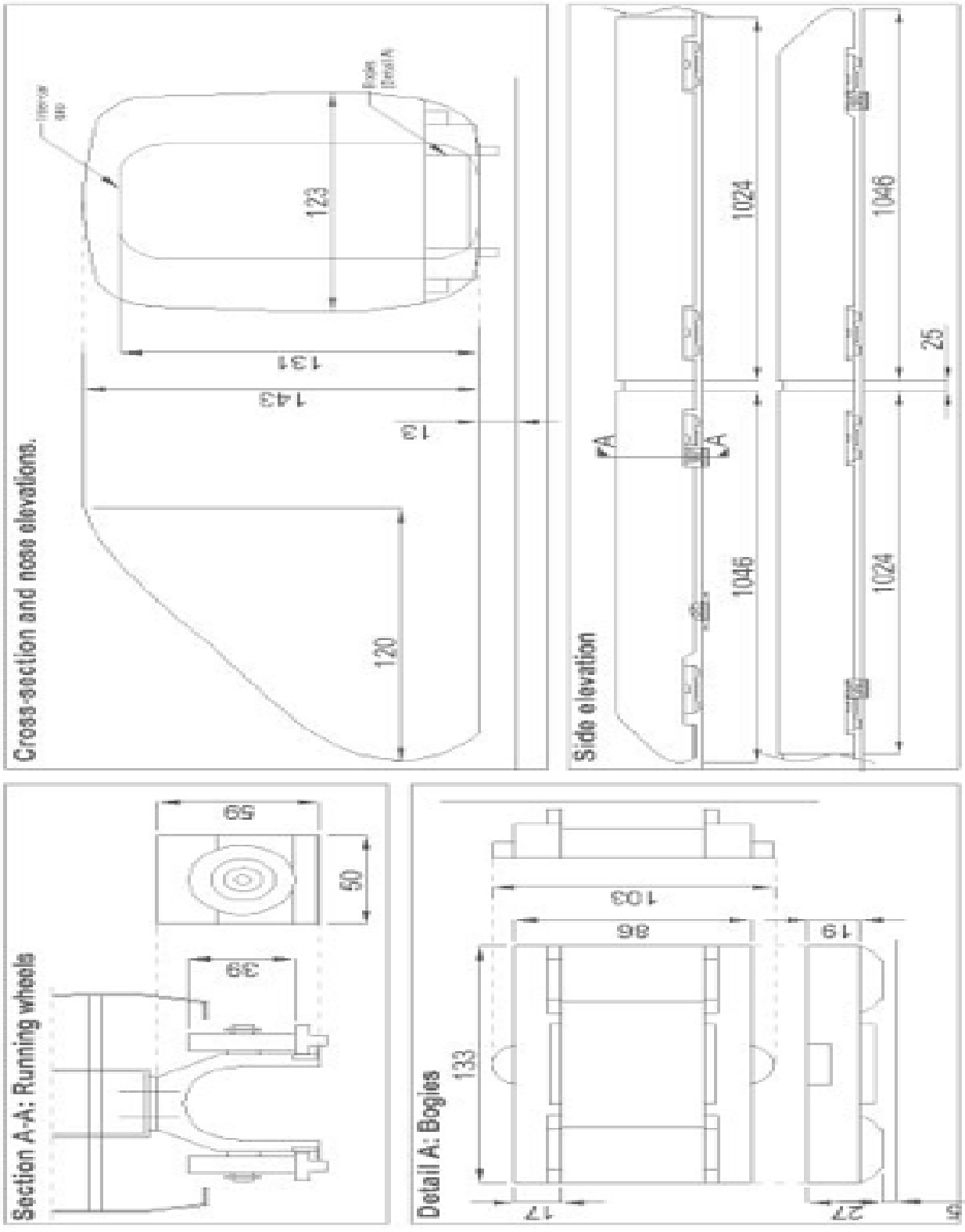

Figure 60: Key Dimension of ICE-2 model shown in mm (scale: 1/25) [28].

Figure 61: ICE-2 Regional Train real Photograph of an ICE2 train [28], [48].

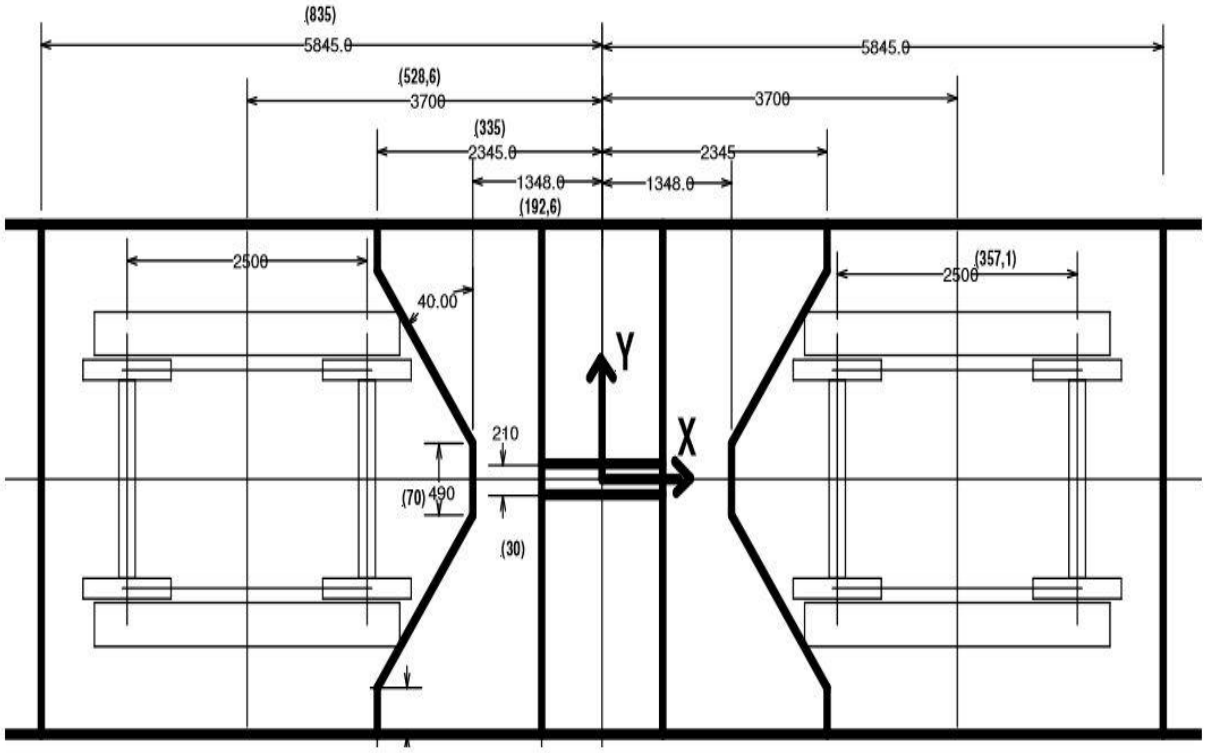

Figure 62: The improved geometry of under body [46].

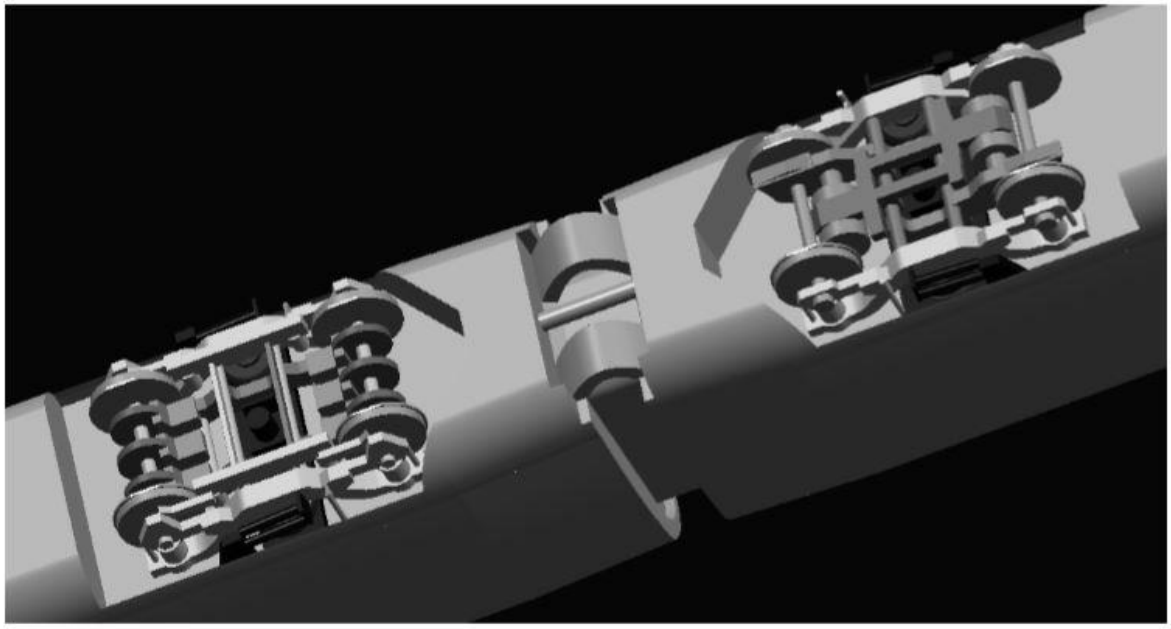

Figure 63: The underbelly of the ICE 3 CAD-model [46].

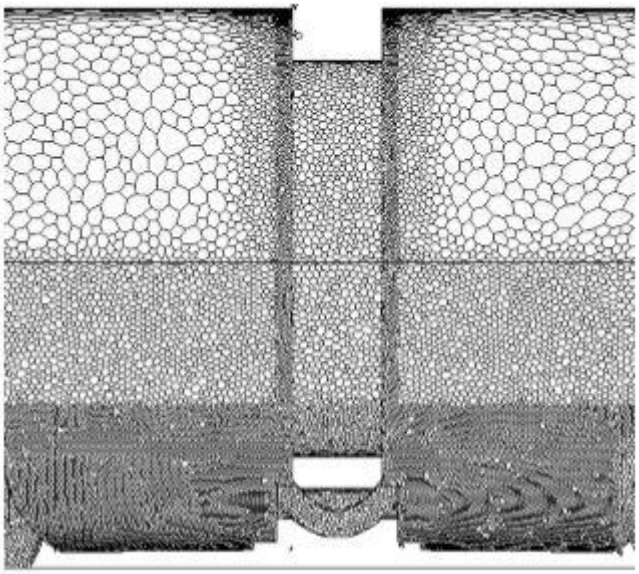

Figure 64: Side view of underbelly of the ICE 3 CAD-model [46].

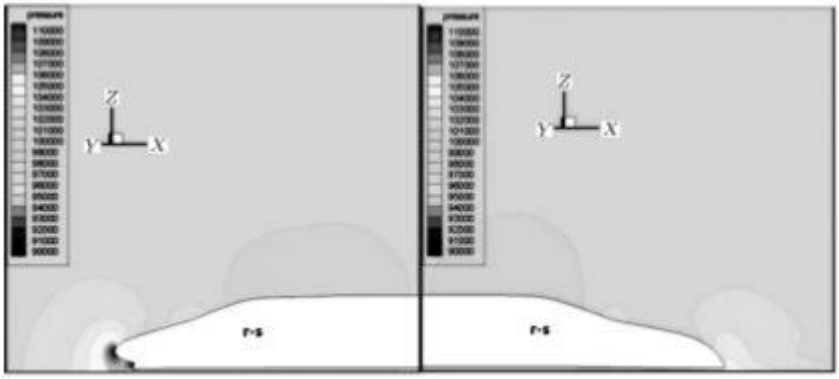

Figure 65: Rocket head and Sword tail profiles [95].

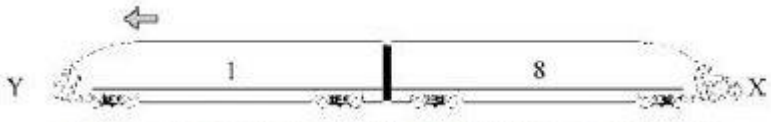

Figure 66: Improved CRH with new structured headstock and tailstock [91].

Figure 67: Train with bogie fairings [63].

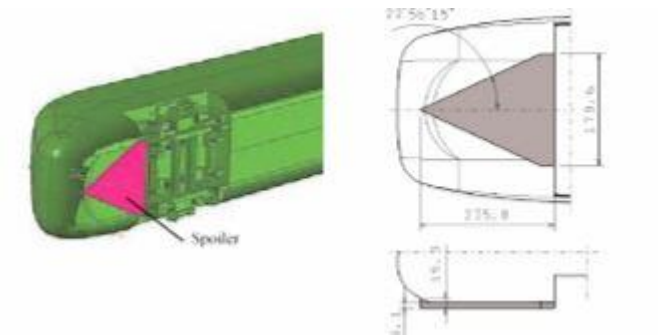

Figure 68: Use of spoiler underbody [70].

Table 10: Distribution of aerodynamic forces of the CRH380A train [102].

Train part	Original shape		Optimal shape		Original shape	Optimal shape
	pressure	shear	pressure	shear	tail *Cl*	tail *Cl*
Nose	**0.0147**	0.0145	**0.0115**	0.0145	–	–
Nose-down	**0.0353**	0.0023	**0.0308**	0.0023	–	–
Head-body	0.0000	0.0207	0.0000	0.0209	–	–
Head-down	0.0102	0.0026	0.0097	0.0025	–	–
Bogie1	0.0322	0.0011	0.0331	0.0012	–	–
Bogie2	0.0075	0.0004	0.0081	0.0004	–	–
Shield-1	**−0.0332**	0.0001	**−0.0343**	0.0001	–	–
Middle-body	0.0000	0.0320	0.0000	0.0325	–	–
Middle-down	0.0113	0.0022	0.0122	0.0023	–	–
Bogie3	0.0087	0.0004	0.0091	0.0004	–	–
Bogie4	0.0053	0.0002	0.0043	0.0002	–	–
Shield-2	**0.0485**	0.0002	**0.0496**	0.0002	–	–
Shield-3	**−0.0279**	0.0001	**−0.0287**	0.0001	–	–
Tail-body	0.0000	0.0180	0.0000	0.0182	0.0833	0.0832
Tail-down	0.0042	0.0011	0.0057	0.0011	−0.1194	−0.1187
Wake	**0.0433**	0.0107	**0.0391**	0.0106	**0.1896**	**0.1813**
Wake-down	**0.0081**	0.0008	**0.0046**	0.0007	−0.0899	−0.0890
Bogie5	0.0042	0.0003	0.0047	0.0003	−0.0061	−0.0059
Bogie6	0.0043	0.0002	0.0035	0.0002	−0.0062	−0.0061
Shield-4	**0.0423**	0.0002	**0.0432**	0.0002	−0.0147	−0.0154
Total	**0.2143**	**0.1081**	**0.2062**	**0.1089**	**0.0366**	**0.0294**

Table 11: Total aerodynamic drag coefficient of TGV running at 260 km/h [79].

Components of traveling drag		Drag coefficient (15°C, 1013 mbar)		Total drag		
				Drag in 260 km/h		Power in 260 km/h (kW)
		N/(km/h)^2	(%)	N	(%)	
Aerodynamic component	Drag of train	0.04595	80	3106	62.5	2243
	Equipments on train roof	0.00965	17	652	13.1	471
	Total aerodynamic components	0.05560	97	3758	75.6	2714
	Disk brake	0.00170	3	115	2.3	83
	Total	0.05730	100	3873	77.9	2797
Rolling drag (train 407 ton)	$BV = 3.256V$			847	17.1	612
	$A = 250$			250	5.0	181
Total drag $D = A + BV + CV^2$				4970	100.0	3590